INFRARED IMAGING FOR DAMAGE DETECTION IN CONCRETE STRUCTURES

A Thesis Submitted in Fulfillment of the Requirement for the Award of the Degree of

MASTER OF ENGINEERING

In

Structure Engineering

Submitted By

RITIKA SINGLA

Roll No. 801624023

Under Supervision of

Dr. SHRUTI SHARMA
Associate Professor
Civil Engineering Department
TIET Patiala

Dr. SANDEEP K. SHARMA
Associate Professor
Mechanical Engineering Department
TIET Patiala

CIVIL ENGINEERING DEPARTMENT

THAPAR INSTITUTE OF ENGINEERING & TECHNOLOGY
(A DEEMED TO BE UNIVERSITY), PATIALA, PUNJAB

JUNE, 2018

DECLARATION

I, **RITIKA SINGLA** hereby declare that the work presented in this thesis entitled **INFRARED IMAGING FOR DAMAGE DETECTION IN CONCRETE STRUCTURES** in the fulfillment of the requirement for the award of degree of **Master of Engineering** submitted at **CIVIL ENGINEERING DEPARTMENT (CED)**, Thapar Institute of Engineering & Technology (Deemed to be University), Patiala is an authentic record of work carried out under the supervision of **Dr. SHRUTI SHARMA** Associate Professor, Civil Engineering Department, and **Dr. SANDEEP SHARMA** Associate Professor, Mechanical Engineering Department, TIET, Patiala from **JULY 2017 to JULY 2018**. The matter presented in this has not been submitted either in part or full to any other university or institute for the award of any other degree.

Date..22/8/18.....

Ritika Singla
Ritika Singla
801624023

Shruti Sharma 22/8/2018
Dr. SHRUTI SHARMA
Associate Professor
CED, TIET
Patiala, Punjab

Sandeep
Dr. SANDEEP SHARMA
Associate Professor
MED, TIET
Patiala, Punjab

Date:..22/8/18.....

ACKNOWLEDGEMENT

This acknowledgement is intended to be thanks giving to all those people who have been involved directly or indirectly with my thesis work.

First of all, a special debt of gratitude is owned to my supervisor, Dr. Shruti Sharma, Associate Professor, Civil Engineering Department, Thapar Institute of Engineering and Technology for her gracious efforts and keen pursuits, which has remained as a valuable asset for the successful completion of research work. Her dynamism and diligent enthusiasm has been highly instrumental in keeping my spirit high. The flawless and forthright suggestions blended with an innate intelligence application have crowned my task as a success.

I would also like to thank Dr. Sandeep Sharma, associate Professor MED, Thapar Institute of Engineering and Technology. The inputs provided by him, his interest and critical appraisal during the entire research is invaluable.

I also like to offer my sincere thanks to all faculty members, teaching and non-teaching staff of Civil Engineering Department, and Staff of Central Library, TIET, Patiala for their assistance. I am extremely thankful to Sh. Varinder Kumar, Sh. Ram Simran and all other laboratory colleagues for helping me carry out my experimental work.

Above all, I thank my parents whose love and affectionate blessing have been a constant source of inspiration in making this manuscript a reality. A special thanks to my sisters Ashima and Anamika for their patience and constant support throughout this research work.

RITIKA
(801624023)

ABSTRACT

Deterioration of the structures occurs due to various factors like aging, climatic conditions, etc. Degradation of concrete structures is a widespread problem worldwide. In order to prevent imminent degradation of structures, proper maintenance and periodic inspections are imperative. Traditionally, condition of the structure has been monitored visually, non-destructive evaluating (NDE) technologies have also been evolving and they are expected to be utilized effectively for the management and inspection of civil structures. One of the various NDE techniques is the image based technology. In this research image-based technology using Infrared Thermography (IRT) is introduced and implemented.

In order to explore and enhance the usability of infrared thermography technique, experiments on various construction materials like bricks, interlocking tiles, steel rods, cement mortar cubes, cement concrete cubes were conducted. Delamination detection on the concrete structures was also performed. The results are quite promising and are helpful in detecting defects like cracks, voids, delaminations, etc. as the IR camera can capture the temperature difference between sound and defective areas. However, there are many challenges in using IRT for inspection but it can be overcome by combining it with other techniques like ultrasonic emission, acoustic emission and finite element method. Hence, infrared thermography technique is an excellent technology for assessing the concrete structures in a practical way.

TABLE OF CONTENTS

LIST OF TABLES

LIST OF FIGURES

CHAPTER 1

INTRODUCTION

1.1 GENERAL

Material deteriorates during service life with cracks and delaminations due to extreme exposure condition such as high temperature, repeated loading, environmental and weather conditions. The cracks can also be generated due to corrosion of reinforcement. Sometimes due to lack of compaction, air voids and delaminations in concrete exists during the construction process. These cracks and delaminations are detrimental to the service life of the structures. To evaluate and inspect structure from damaging development of Non-Destructive Evaluation (NDE) technique or Non-Destructive Testing (NDT) is required. Non-destructive testing (NDT) refers to quality control inspecting and evaluating methods that can be employed to assess the specimens of materials without impeding its future usefulness. The most commonly used NDT methods are liquid penetration, eddy-current, magnetic-particle, radiographic, ultrasonic, and visual testing. Conventionally, qualified engineers enacted visual inspections and hammer sounding or chain drag to monitor the structures but these methods are time-consuming and require substantial labor and experience and also possess great threat to the person performing them. Inspection of the structures using images is one of the most innovative technologies to make up for these negative points.

Thermography means 'writing with heat'. Infrared thermography (IRT) can be described as the science of acquisition and investigation of data from non contact thermal imaging devices. The infrared radiations emitted by objects which are not visible to the human eye are translated into temperature and are shown as thermal images. When the temperature of the material builds up, amid the day time when the sun and surrounding condition are warming the material, the surface zone over the defect heats up rapidly than the surface zone when the material is undamaged. During the day time these defects can be identified as '*hot spots*' on the surface of the material, corresponding to the undamaged material. Contrary to this during night time, when temperature of the air falls and the materials is cooling, the surface region over the defect cools faster than the undamaged material. Therefore, during night time those regions appear as '*cold spots*' relative to the undamaged material. **Figure 1.1** explains this phenomenon **[1]**. Hence, it can be said that Infrared Thermography (IRT) is an image based technology which is used to evaluate the surface

temperature of the materials or objects using an infrared camera which controls and gather infrared radiations produced by the surface, change over them into electric signal and creates a pixelated image, colour intensity of which shows the body's surface temperature distribution.

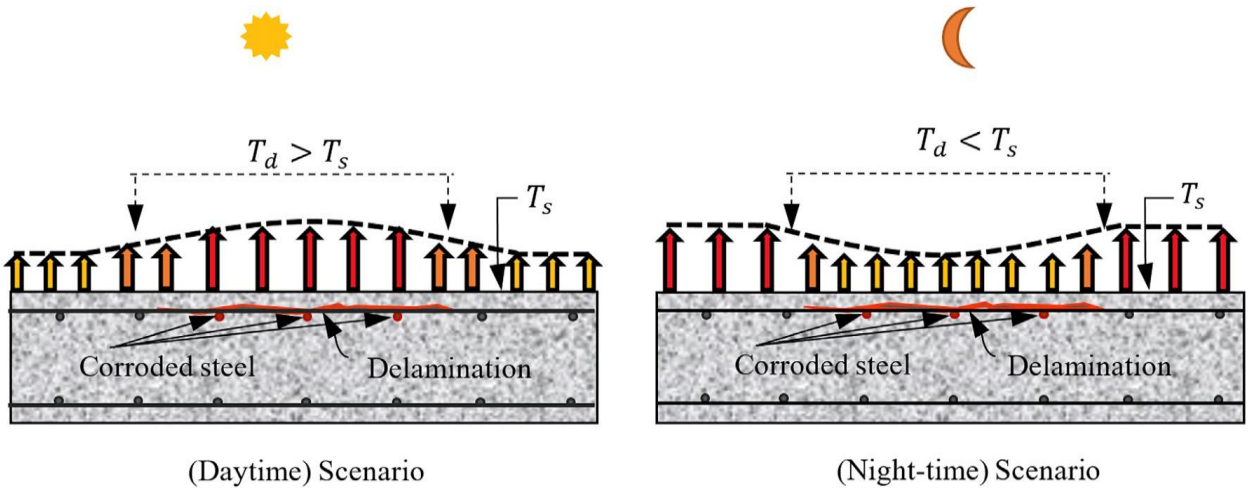

Figure 1.1: Schematic Diagram showing Hot Spot and Cold Spot in Bridge Deck [1].

With the use of thermography large areas can be examined and recorded in a short time period enabling fast overview about the reinforcement position, presence of voids and delaminations, the presence and distribution of moisture and about other geometrical parameters. Concisely, IRT provides an advantage of being able to spot such invisible deteriorations such as delaminations and voids with reasonable precision. IRT also helps avoid the time and expense of gaining the immediate access to the materials surface to conduct traditional tests. Meanwhile Infrared thermography technology has some limitations. IR technique is capable of detecting only those defects which have measurable change in thermal properties. Also, it has ability to detect the subsurface defects at limited thickness.

NDE techniques in general are characterized as active or passive, surface or volumetric **[2].**

Active techniques are those in which considerable amount of energy in some form is imparted to the test specimens or objects and corresponding change in output energy are studied to assess the presence of defects. Eddy currents, radiography, thermography are some examples of this technique.

Passive techniques monitor the test object or specimen in its normal state or under the influence of typical environmental factor without imparting energy to the object. The reaction of the test

object to its ambient environment or operating condition is considered for detecting the defects. Acoustic Emission, leak test and visual inspection are some examples of passive thermography.

Surface methods typically detect flaws or damage at the surface of the material. Eddy currents and penetrants are good examples.

Volumetric methods are used to detect subsurface defects located within the volume of the material. Radiography and ultrasonic techniques are good examples.

IRT has characteristics of both the surface technique and the volumetric technique, in that it measures the effect on the surface of a defect within the volume of the material.

IRT can also be used to inspect objects or materials both in active and passive state. Monitoring of the deck of the bridge or road surface under the ambient environmental conditions is the good example of passive infrared thermography.

1.2 BACKGROUND

When an object is heated, its temperature increases due to absorption of heat energy. Exchange of heat between the object and its neighboring is a dynamic process including convection, conduction and radiation. Radiation of heat might be seen as the generation of electromagnetic waves comprising of a huge range of wavelengths. Wavelengths of the infrared radiations lies between 0.9 to 14μm and is put in electromagnetic spectrum amongst the visible waves and microwaves. From the NDT standpoint, IRT depends on the concept that the movement of heat transfer in any substance is affected by the change in thermal properties of the substance, particularly those caused by the subsurface imperfections. Infrared radiation emitted by the objects surface after the absorption of heat is noticed by an infrared camera. Difference in the surface temperature due to any deformity would thus be identified from the thermal images **[3]**.

Thermal diffusivity of the materials used in the construction process like bricks, tiles, plaster, mortar and concrete is low as compared to the materials used for strengthening of these construction materials i.e. steel bars and fiber reinforced composites. Due to this reason building materials like bricks, tiles, plaster, mortar and concrete require large heating and measuring time for their thermal evaluation. But it is not possible to inspect the large rock like specimens because the distribution of heat is non-uniform. The use of active infrared technique in structural designing has been considered very less as compared to the other fields inspite of the fact that

structure of these building materials is non-homogeneous and includes voids, cracks and delaminations.

1.3 OBJECTIVE OF THE WORK

The main objective of this work was to evaluate the applicability of InfraRed Thermography (IRT) in civil engineering structures.

The primary objective of this research work is to check the effectiveness of InfraRed Thermographic technique. In order to explore and enhance the usability of InfraRed Thermography (IRT) technique, to detect various kinds of defects, cracks, etc in various construction materials like bricks, interlocking tiles, steel rods, cement mortar cubes, cement concrete cubes tests were conducted.

1. To monitor the surface defects in concrete.
2. To monitor the mechanical cracks (tension and compression) in interlocking tile, bricks, cement mortar and cement concrete.
3. To evaluate the sensitivity of IRT for defect detection at different cover depth in concrete.
4. To investigate the effectiveness of IRT for detecting flaws in GFRP laminates bonded to concrete (Delamination).
5. To monitor simulated and actual corrosion defects in rebar in concrete

1.4 FORMAT OF THE THESIS

The main objective of this study is to monitor the efficiency of infrared thermography method to estimate the various kinds of defects.

The thesis is divided into five chapters.

1st Chapter gives the general discussion about structure health and its monitoring.

2nd Chapter deals with the basic information about infrared thermography technique as NDT method and also presents the thorough review of literature work on this technique.

3rd Chapter presents the experimental programme in which all the tests, procedures and measures to be followed are explained in detail.

4th Chapter deals with the results and discussions where findings in the experimental programme are explained in detailed.

6th Chapter deals with the conclusions.

CHAPTER 2

INFRARED THERMOGRAPHIC (IRT) TECHNIQUE AND REVIEW

2.1 INTRODUCTION AND CONCEPT

InfraRed Thermography (IRT) is defined as the science devoted to the acquisition and handling of thermal data from non-contact measuring instruments. InfraRed camera gathers infrared radiation, which is a type of electromagnetic radiation the wavelength of which is longer than that of visible light. Any object, whose temperature is above absolute zero i.e. T > 0K releases infrared radiation. The human eye is not capable to see this type of radiation. Thus, this information is acquired and processed by infrared measuring devices **[4]**.

Devices measuring infrared radiation transmitted by an object and convert it into an electric impulse and display it as thermal image or thermogram. Thermal images are visuals that displays of the quantum of infrared energy that the object in view transmit, emit and reflects. To get a specific and precise temperature of an object is very difficult due to numerous sources of the infrared energy. A thermal imaging camera performs calculations to translate the information and create an image **[5]**. However the image is an estimation of the temperature at which the object is working, in actual the camera uses various sources of data on the basis of the areas neighbouring it to know that value rather than investigating the actual temperature **(Figure 2.1)**.

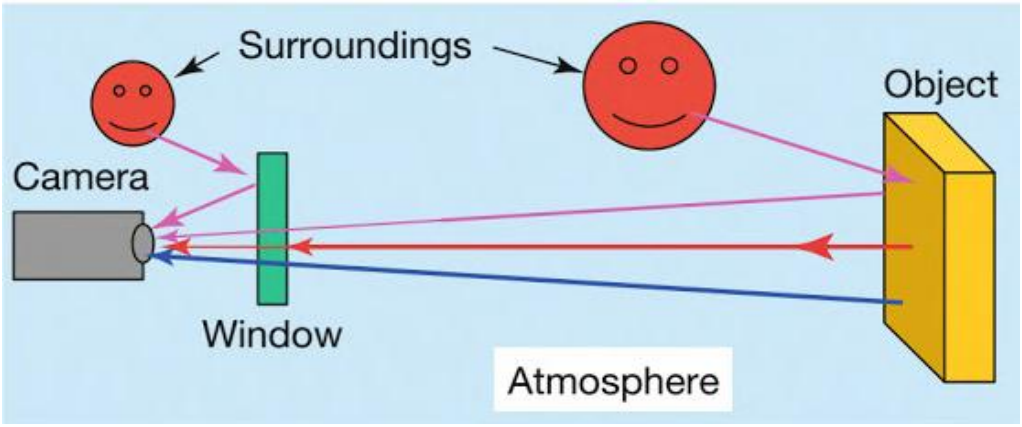

Figure 2.1: Various signal contribution entering an IR camera due to external influences. [6]

The formula clears the above phenomenon much effectively:

Incident Radiant Energy = Emitted Radiant Energy + Transmitted Radiant Energy + Reflected Radiant Energy

where:

Incident Radiant Energy is the radiant energy image profile when seen from a thermal imaging camera; *Emitted Radiant Energy* is normally what is required to be estimated; *Transmitted Radiant Energy* is the radiant energy that passes through the subject from a distant thermal source; *Reflected Radiant Energy* is the measure of radiant energy that reflects off the surface of the object from a distant thermal source.

2.2 HISTORY AND BACKGROUND

This discovery was made by a chance by Sir William Herschel, an astronomer, around 1800 while he was looking for advanced optical filter materials to lessen the radiance of sun's image in telescope throughout solar observation. He was amazed to locate that some of the coloured glass samples, placed in the telescopes to less the radiance of solar radiation, passed some more heat while some passed little heat. He used conventional mercury thermometer with blackened bulb to compute the temperature from violet to red along the spectrum of light rays and found that there was increase temperature from violet colour to red colour along this spectrum and maximal increase in temperature was observed in zone of no sunlight behind the red colour of spectrum. He named this phenomenon as '*dark heat'* and '*invisible rays'* and called that part of the electromagnetic spectrum as 'thermometrical spectrum'. The name infrared i.e. behind red part was given substantially later.

The first heat picture was captured by Sir John Herschel in 1840. He named the thermal image taken on the paper as thermography **[7]**.

In 1880 with the invention of the bolometer, the sensitivity of device improved further which comprised of a blackened platinum strip attached to one arm of Wheatstone bridge circuit exposed to infrared radiation.

It was in 1950s during wartimes when thermal imaging instruments were made accessible for security purpose. Earlier, the devices were unwieldy with oscilloscope and camera with weight exceeding 400N besides a generator set to supply power. The devices used now-a-days weigh less than 10N and are inclusive of battery and are available with wide range of options to suit many applications. The sensitivity of devices is better than 0.05°C with a temperature range of material exceeding to 250°C **[7].**

2.3 PRINCIPLE

The principle of infrared thermography depends on the fact that anybody having temperature above absolute zero (-273.15°C) emits electromagnetic radiation. There is relationship between the surface of an object and spectral composition and the intensity of the radiations emitted by that object. The temperature of an object can be determined in a non-contact way by determining the intensity of radiation. The energy from a heated object radiates at various levels over the electromagnetic spectrum. Mostly, it is the energy emitted at infrared wavelengths which is used to decide the temperature of the object. **Figure 2.2** shows varied forms of emitted energy in the electromagnetic spectrum incorporating X-rays, UV rays, Infrared rays and Radio waves. All these energies are emitted in the form of wave and travel with the speed of light. The main difference in all these rays is that their wavelength which corresponds to frequency of emitted rays. The spectral region with the wavelength from 0.78 µm to 1mm is usually called infrared.

A small part of IR spectrum is used for InfraRed imaging of any object. It is shown in **Figure 2.3** in an expanded view. Generally three spectral ranges are characterized for thermography: the long-wave (LW) region from 8 to 14µm, the mid-wave (MW) region from around 3 to 5 µm, and the short-wave (SW) region from around 0.8 to 1.7 µm. For these three ranges of wavelengths commercial cameras are available **[6]**.

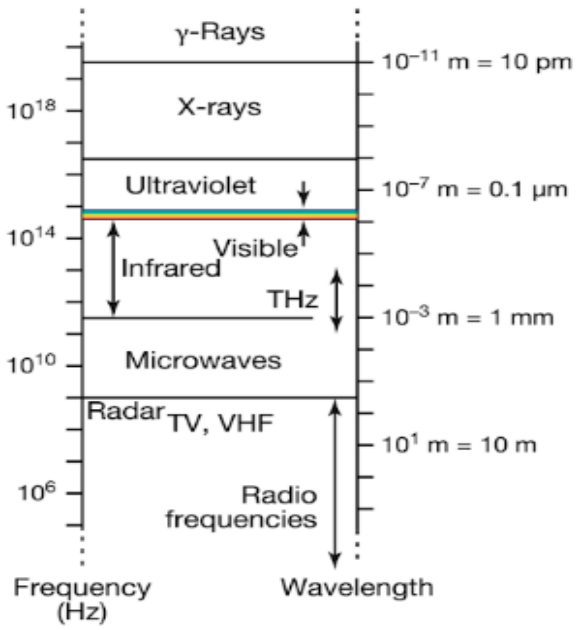

Figure 2.2: Electromagnetic Spectrum as function of wavelength [6]

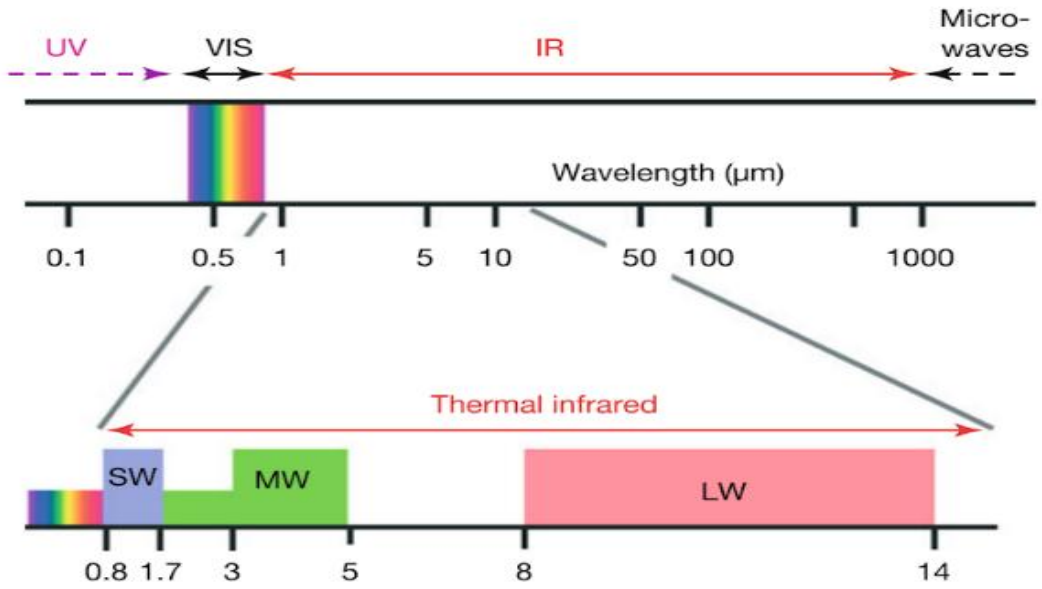

Figure 2.3: Expanded view of spectral region of IR [6]

The emittance at each wavelength of an objects surface is dependent on its temperature and spectral emissivity. For a blackbody, the spectral emittance is given by the Planck's equation. For governing thermal emission Planck's law is one of the most important laws. Planck's law describes for a given temperature the dispersion of emitted energy as a component of the wavelength. As explained by Kirchhoff's law, once the energy is absorbed it is emitted to the environment, which states that at equilibrium the radiation emitted must be equal to the radiation absorbed **[7]**.

The spectral radiance $E_{\lambda, b}$, the power irradiated by a black body per unit of solid angle, **[7]**

$$E_{\lambda,b} = \frac{2hc^2}{\lambda^5(1 - \exp\frac{hc}{\lambda KT})} \quad \ldots\ldots\ldots (2.1)$$

h- Planck's constant ($6.63\times 10^{-34} Js$)

c- Velocity of light (3×10^{8}m/s)

K- Boltzmann's constant (1.318×10^{-23}(J/K))

ƛ - Wavelength of emitted radiation (μm)

T- Temperature of the blackbody

The Planck's formula is plotted in **Figure 2.4** for several discrete temperatures varying from range 200-6000K. For each plot, a group of curves is obtained, $E_{\lambda, b}$ goes to zero for ƛ=0 and

then increase fastly to a maximum value and then again decreases towards zero for a wavelength with very long values **[27]**.

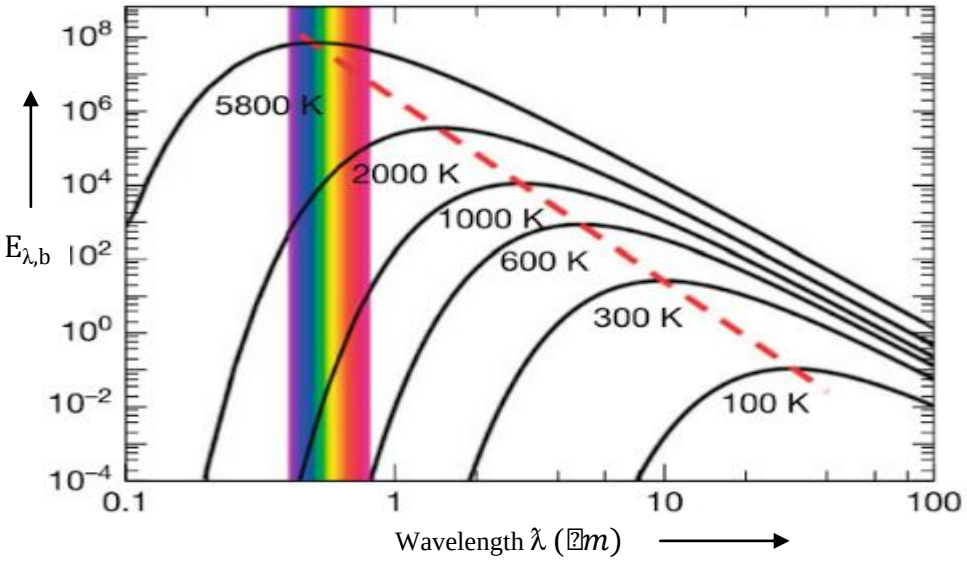

Figure 2.4: Distribution of emissive power with wavelength [24]

It can be seen from **Figure 2.4** the higher the temperature, the shorter is the wavelength at which the maximum occurs.

By differentiating the Planck's law with respect to λ and by finding the maximum radiation intensity the *Wien's Displacement Law* is obtained **[7]**.

$$\lambda_{max} = \frac{d_w}{T} \qquad \ldots\ldots\ldots (2.2)$$

d_w=Wien's displacement constant (approx 2898)

By integrating the Planck's law over the entire spectrum (λ= 0-∞) the total hemispherical radiation intensity i.e. *Stefan Boltzmann Law* is obtained **(2.3) [7]**

$$E_{\lambda,b} = \sigma T^4 \qquad \ldots\ldots\ldots (2.3)$$

σ = Stefan Boltzmann's constant ($5.67\times10^{-8}\ W/m^2K^4$)

In the case of real objects whose absorbance is limited, only some part of the energy will be radiated from the surface. This fraction of the blackbody spectral radiance is given by the property of the surface called the emissivity **[8]**.

$$E_{\lambda,T} = \varepsilon E_{\lambda,\,b}(\lambda, T) \qquad \ldots\ \ldots\ \ldots\ (2.4)$$

Emissivity (ε) of any object depends upon λ, T, angle from which object is viewed and its surface condition like roughness, formation of oxide layers, presence of physical and chemical contamination.

.Generally the value of emissivity lies between 0 and 1 as factor obtained after comparing the object's radiance to the blackbody radiance.

Temperature Measurement- If there is a temperature change on the surface of an object then there is a time delay before the effect of this change occurs below where a defect such as a void occurs. The more extended this time delay before the temperature changes, the more would be the depth of the defect underneath the surface. Normally any object deeper than 10 cm will only appear after a significant period of time (>1 hr) after the temperature change has happened.

An infrared thermographic technique determines the temperature of surface only, but the surface temperature of concrete mass depends on three factors: (i) layout of subsurface, (ii) the surface condition, and (ii) the environment. The effect of sub surface concrete configuration is of more interest for study of NDT **[7]**.

The configuration of subsurface effects are based on the assumption that heat flow at varying rates from hotter to cooler parts depending on the insulating effects of the substance in which it flows. Different building materials have distinctive thermal conductivities. For instance, an void created by *honeycombing* or *delaminations* caused by corrosion has smaller value of thermal conductivity than that the solid and non homogeneous concrete surrounding it.

Thermal energy can be transferred from warmer to cooler regions in three **[9]**:

i. *Conduction:* It happens when two objects at different temperature come in contact with each other. Flow of heat takes place from hotter to cooler objects until they both acquire the similar temperature. It is the motion of heat through a material by the collision of particles. At the place of contact of two objects, the molecules of the hotter (faster) object collide with molecules of the cooler (slower) object. On collision, the faster moving particles impart some of their energy to the particle moving at slower rate. As the slower particles of the cooler object gain some thermal energy they start colliding with other particles of it. This activity goes on till heat energy from the hotter object spreads uniformly in the cooler object.

ii. *Convection:* It is the best and effective and efficient approach to transmit heat in gases and liquids. Convection happens when hotter areas of a gas or liquid rise to cooler areas in the gas or liquid. During this, cooler gas or liquid replaces the hotter areas of gas or liquid which have ascended higher. This cyclic continuous circulation process results in heat transference to cooler regions.

iii. *Radiation:* Both conduction and convection require material to exchange heat. Radiation is a technique of heat exchange that does not depend on connection between the source of heat and the heated object. As an example, we feel the heat under the sun despite of the fact that we are not touching it. Heat can be radiated through void space by thermal radiation. Radiations are emitted by object when electrons in the high atomic level fall down to lower energy levels. The lost energy is radiated as electromagnetic radiation.

This heat mechanism is explained in **Figure 2.5**

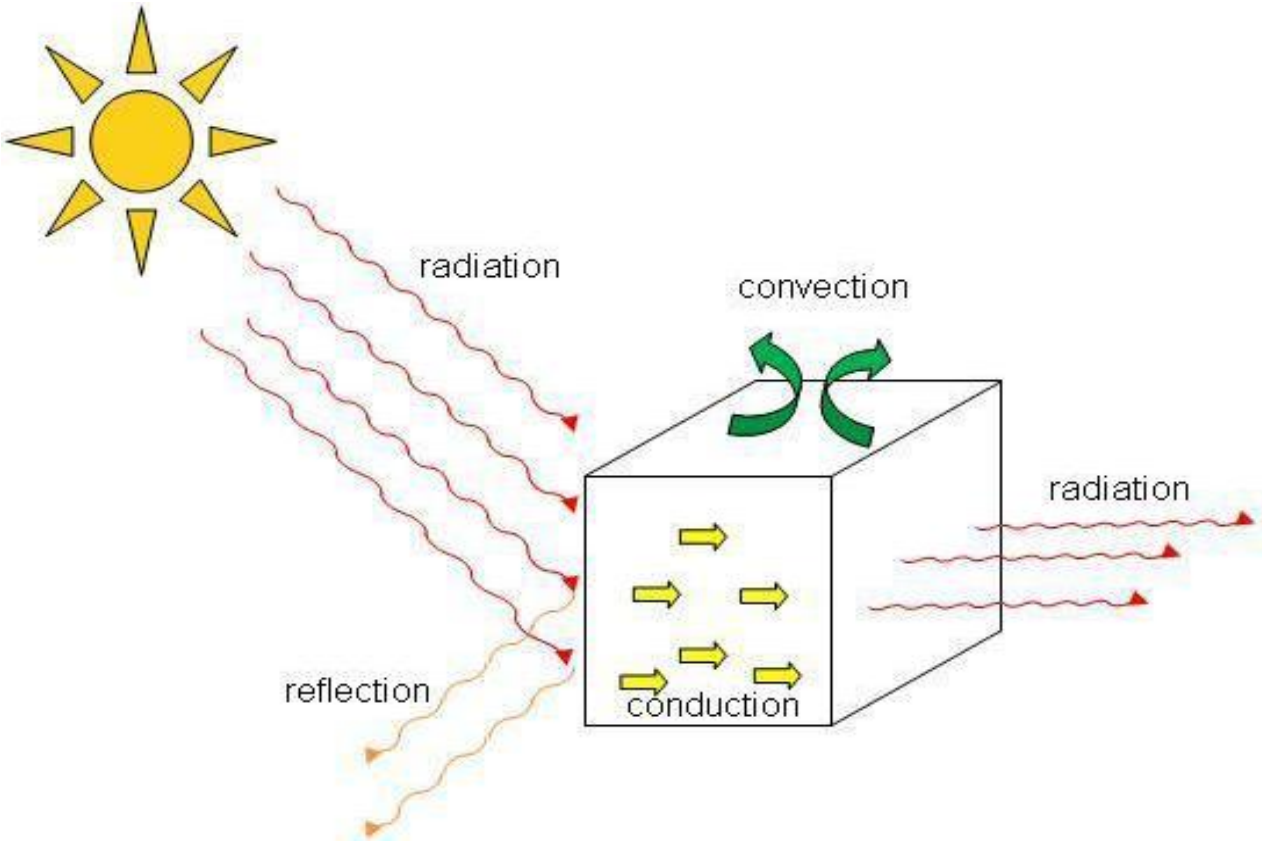

Figure 2.5: Heat transfer properties for concrete specimen [10].

Healthy concrete must have the minimum resistance to the heat conduction and effect of convection and radiation should be nominal. However there are various unusual things associated with poor quality of concrete such as voids and low density. Thermal conductivity of

the concrete decreases due to the presence of these anomalies as these tends to reduce energy conduction properties of the object without increasing the effects of convection.

In order to have constant flow of heat energy, a source of heat must be there. As testing of concrete involve large areas, the heat source applied to provide the heat energy concrete must be able to give a uniform distribution of heat with the minimal cost. Both these necessities are satisfied by sun. Heat energy is supplied normally to test specimen by enabling the sun to warm the regions of concrete surface under test **[7]**. During night-time, this process is inversed with the warm ground acting as the source of heat. The concrete areas which are not accessible to sunlight, another way is to utilize the heat storage ability of the earth to draw heat for the concrete under test. The important consideration in order to use infrared thermography is that, heat should be flowing through the concrete without concerning about the direction of flow. Various heating and cooling sources as a tool for active infrared thermography are given in **Table 2.1**

Table 2.1: Direct heating and cooling sources for active infrared thermography [11].

Heating Unit	Sources
Radiation Unit	Infrared radiator, Flash light, Halogen lamp, Laser, Sunlight, Propane gas with electrolyte oven, Oven
Convection Unit	Fan heater
Contact Unit	Heating mat, Cold pack, Cooling and heating with peltier unit

The second important parameter to be considered when using IRT is to evaluate temperature differences due to presence of voids and delaminations on the surface of test specimen. Out of the three ways to transmit the thermal energy, radiation is the most effective process and it is measured in terms of emissivity of the object which is a material property. The emissivity value for the rough and dark surface is high and that of smooth and shiny surface is low. As an example emissivity value of rough concrete is 0.95 and that of shiny copper is 0.05 **[7]**. In actual terms, when infrared thermography is used to scan the large areas of concrete, the originator must know about various surface textures that can be created on the surface by things as rubber tire tracks, oil spots, broom textured spots, or loose sand and dirt.

The third factors that affect the thermal measurements of a concrete surface are the environment that surrounds that surface.

Various parameters affect the surface temperature measurements **[7]**:

i. *Solar radiation*: Tests ought to be performed amid day or night time when the presence or absence of solar radiation would initiate the most prompt warming or cooling of the concrete surfaces.

ii. *Cloud cover*: Infrared radiation will be reflected by the clouds, showing the heat exchange method to the sky. Therefore, if the tests are to be performed during night-time then cloud-cover should not be there to allow the most efficient system from transmission of energy from the concrete.

iii. *Ambient temperature:* Temperature must have a minimal effect on the accuracy of the testing as it is one of the most important considerations in the prompt heating or cooling of the object's surface. This variable will affect the timeframe during which measurements for high contrast temperature measurements can be made.

iv. *Wind speed*: A high blow of wind tends to reduce the surface temperature as they have distinct cooling effect. Thermal images should be captured when speed of wind is less than 25 km/h.

v. *Surface moisture*: Presence of moisture diffuses the heat from surface and obscure difference and hence the subsurface deformities of the substance. Tests must not be executed on concrete during stagnate water or snow.

A large concrete specimen having both sound and defected areas with cracks, delaminations, voids is selected for the purpose of experimentation after locating for absolute environment conditions for the test purpose. Different kinds of deformities will show a different temperature profile depending on all the environmental conditions. For an example, if the test is performed during night, most deformities will be between 0.1° and 5°C cooler depending on the configuration of the concrete surrounding it. Contrary to this, the same test performed during day will show damaged areas hotter than the healthy concrete.

2.4 TYPES OF INFRARED THERMOGRAPHY

IRT is broadly classified into two kinds, the passive thermography and the active thermography. The passive thermography approach is used to test those materials and structures which are normally at distinct temperature than environmental temperature but in active thermography approach, there is a need of an external stimulus to initiate thermal differences.

1) Passive thermography- In numerous procedures temperature is an imperative parameter to survey appropriate task and passive thermography goes for those measurements. Critical applications of this approach are in production, detection, pharmaceutical, detection of gas, building thermal proficiency overview programs, predictive maintenance, medicine, fire forest, road traffic monitoring, farming and science, and most importantly in nondestructive testing (NDT). In every application, an irregular temperature profile indicates an issue to dealt with.

2) Active Thermography- active infrared thermographic approach determines the dynamic temperature changes. In this, an external stimulus is needed to create a thermal change between the object and framework. Knowing the attributes of this external stimulus i.e. the time and temperature when and what is applied enable quantitative evaluation such as the thickness of a detected void.

Active thermography is divided into many parts depending on simulation methods. The popular methods of active thermography are pulse thermography, lock-in thermography, step-heating and vibrothermography

2.5 THERMOGRAPHIC INSTRUMENT

In order to evaluate and test the subsurface irregularities in concrete we need a sensitive contact thermometer. However, multiples of readings would have to be taken at the same time even on a small test area in order to figure the irregularity accurately and precisely. As this is not possible practically to evaluate such large areas of surfaces of concrete effectively, accurately and quickly there is a need to high resolution devices. This requirement to quickly and efficiently inspect the concrete surface can be fulfilled by Infrared Thermographic Instruments. Infrared camera covers the large area and the subsequent data is presented in the form of thermal images demonstrating the zones the zones of varying temperatures represented by different tones of grey in a white and black image or by different colour palettes in a colour image.

There are two types of infrared cameras available **[12]**:

i. *Focal Plane Array (FPA) Cameras*: They depend on two kinds of detector arrays: photonic cooled detectors (PCD) and uncooled micro-bolometers. Cooled detectors have matrix size of (320H × 240V, 640H × 512V). A cooled detector has a semiconductor material placed in a vacuum-sealed cell and is cooled using cryogenic coolers which is necessary for its operation. depending of the type of semi-conductor used cooled detectors operate at the temperatures range varying from 4 K to just below room temperature. The camera with cooled detector needs few minutes to cool

down before it can be used to start working again. Normally, rotary Stirling engine cryocoolers is used cooling system. Materials used for cooled infrared detection incorporate photodetectors based on a wide variety of semiconductors with. Uncooled thermal detectors use a sensor which works at surroundings temperature. All the modern uncooled cameras use sensors that work by the change of current, resistance or voltage when heated through infrared radiation. Uncooled infrared cameras smaller and less costly than cooled cameras because its sensors can be balanced to an operating temperature by reducing the noise in image's background as well as these cameras do not require cryogenic coolers to cool them to low temperature. Uncooled detectors are depends on ferroelectric and pyroelectric materials or microbolometer technology. However, the image quality and resolution of the uncooled detectors is lower than that of cooled detectors. This may be due to difference in the manufacturing process of both the detector.

ii. Single active element scanner cameras- in these cameras the image is scanned mechanically by a single detector.

Working of Thermographic Cameras

Working process of the infrared cameras is described below:

i. A special lens (germanium lens in this study) focuses the infrared rays emitted by the objects in view.
ii. This concentrated ray of light is examined by a phased array of detector infrared device. The detector creates a comprehensive temperature pattern referred as a thermogram. The detector array just takes around about one-thirtieth of a second to get the temperature information to create a thermogram.
iii. The thermogram made by the detector is converted into electric signals.
iv. The signals are directed to the processing unit, which is a circuit board with a special chip that converts the information from the detector elements into data for the display.
v. The display receives the information from signal processing unit, where it shows different colours after determining the intensity of the infrared emission. The integration of all the signals creates the image.

InfraRed Thermographic equipments are fabricated by many manufacturers. The equipment made by different manufacturers has different specifications which should be compared before

buying it. Three main manufacturers of thermography equipments AGEMA, Inframetrics and FLIR have merged recently.

In this research work, FLIR T540 camera shown in **Figure 2.9** with specification and features as detailed below in **Table 2.2** was used**.**

Table 2.2: Specifications of FLIR T540 [13]

Specification	
IR Resolution	464×348 (161,472 pixels)
Object Temperature Range	-20°C to 120°C 0°C to 650°C (On calibration) 300°C to 1500°C (On calibration)
Digital Zoom	1-6x continuous
Detector Type and Pitch	Uncooled Microbolometer (Focal Plane Array), 17µm
Thermal Sensitivity	<0.03°C @ 30°C (42° lens)
Spectral Range	7.5-14 µm
Display for Image Representation	4” , 640×480 pixels touchscreen LCD with auto rotation
Accuracy	±2°C (±3.6°F) or ±2% of reading

Figure 2.6: Infrared Thermographic Camera (FLIR T540) [13]

2.6 ADVANTAGES OF INFRARED THERMOGRAPHY

Advantages of InfraRed Thermography are:

i. Non-contact technology-the instrument used in this technique is not in contact with the heat source. It is an effective way to measure the temperature of extremely hot objects safely like acids.
ii. Two-dimensional thermal image- helps in distinguishing the possible areas of target.
iii. IRT is in real time- enables high speed imaging of the stationary objects and the acquisition of the faster moving objects also.
iv. Easy interpretation of results: as the results from this technique are in image format, these images can be processed to extract detailed information
v. Security of personnel- as compared to X-ray imaging there are no harmful radiations.
vi. Non-invasive technique- in no way target is affected.
vii. Fast inspection rate- desired size of specimen (upto few meter squares) can be easily inspected in no time
viii. Wide span of applications

2.7 APPLICATIONS

There are various fields in which infrared thermography are used. Some of them are given below:

i. *Electrical Equipment*: IRT is used for non-destructive testing of electrical equipments. The problems such as loose connections, breakdown of capacitor, unbalancing of loads, poor connections, overheating and overloading can be detected. The problems of the loose connections, poor contacts, blocked cooling passages and overheated bushings in transformers can also be detected using this method. There is wide scope of infrared applications in manufacturing electrical components.

ii. *Boilers and Steam Systems*: Inspection of breakdown of insulation is the most common application in this field. It is used to detect leakage of hot gases. For steam systems, a most usual application of infrared thermography is to check joint, valve leakage and tap malfunction. Infrared inspection is also be used to check on the effectiveness of the insulation. Inspection of the leaks in the underground can also be checked using this technique.

iii. *Mechanical Equipment*: In mechanical industry IRT is used as NDT technique. It is used to detect blockage in radiator tubes and air coolers, air leaks and monitoring of the heat exchanger. For fans, pumps, compressors and blowers, InfraRed Thermography is used to detect overheated bearings and increased discharge temperatures. Broken and defective valves detection. It is a quick and cost effective technique to inspect large manufacturing plants.

iv. *Surveillance and Security*: this technique helps in probing and rescue, night operations and enemy identification. InfraRed technology with the use of infrared sensors provides security in homes. In many other fields, security applications for InfraRed Thermography are growing rapidly. InfraRed cameras are also used at some airports to check the body temperature of the passengers due to the outbreak of the threats of various viruses like Ebola virus.

v. *Medical and Veterinary*: In medical field InfraRed Thermography is used to detect arthritis, cancer and circulation issues. It enables the doctors to locate skeletal and muscular problems. Infrared technology is also used by veterinary doctors to fit horses with saddles.

vi. *Other Applications*: IRT can detect increase in moisture in bearings and temperatures buildup in industries. To ascertain inadequate insulation and liquid levels in storage tanks, this technology can be used. It is used to detect the insulation breakdown for ovens and furnaces. IRT is also used to detect generation of gas in the landfills, which is not visible to the human eye. Particulate plumes and subsurface combustion can also be discovered with this method.

2.8 LITERATURE REVIEW

Maierhofer et al. (2002) [15]: In this experimental research two concrete test specimens of size 1.5 x 1.5 x 0.5m^3one containing 8 voids of different sizes and depths of polystyrene blocks and other covered with carbon fiber reinforced laminates were investigated and analyzed. The cooling period of structure after heating with infrared radiator of power 2400W for different heating durations varying from 5 to 60 minutes were analyzed to detect voids and delaminations. The results were compared with simulations and semi-empirical models were developed for the analysis of data. From the thermal images and analytical results it was conclude that results upto a depth of 10cm defects could be located effectively.

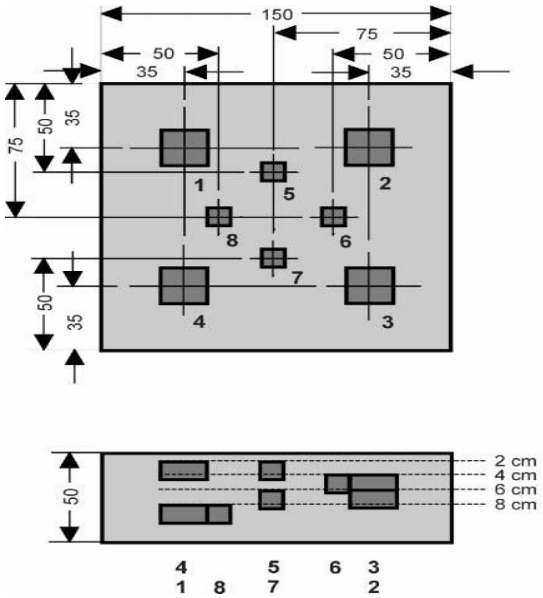

Figure2.7: Concrete specimen with voids [15]

Figure 2.8: Experimental Setup [15]

Two thermal images after heating the specimens 10 minutes at 9 and 58 minutes during cooling stage were captured.

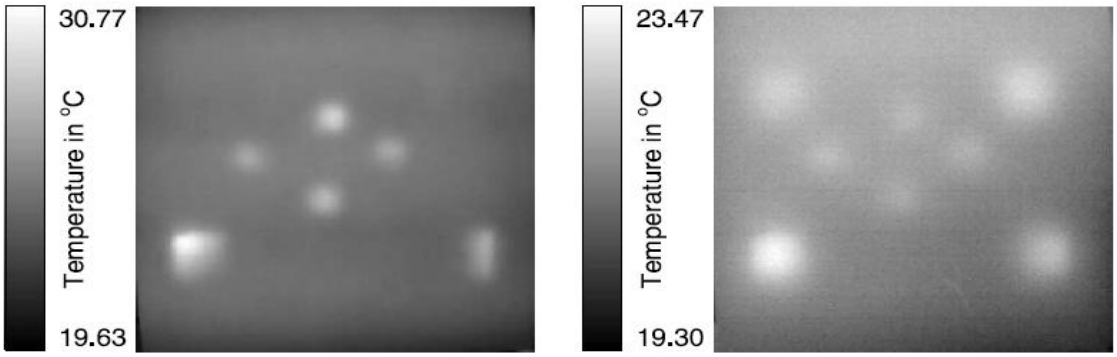

Figure2.9: Thermograms recorded after a heating time of 10 min at the first specimen; left: cooling down time 9 min; right: cooling down time 58 minutes [25]

The results showed that shallow voids gave a good contrast after short cooling period time while deeper voids were seen after long waiting.

Clark et al. (2003) [16]: The research was focused on to investigate the non-domestic structures of UK to identify the delaminations underside the deck of concrete bridge and to examine the internal state of a masonry bridge. For concrete bridge, the survey was done on the bridge in Northamptonshire in UK. From thermal images it was possible to detect delaminated areas as they represented different color bands.

For masonry structure, a single span of 3.6 m, brick arched of Kilbucho Bridge with a low rise was chosen and from thermal images areas with moisture contents were located and it was also possible to locate bricks in the bridge as bricks were of light colour then stones. It was concluded that weather had as major effect on structures.

Chung et al. (2006) [17] studied the amount of corrosion in the rebar for different levels of corrosion (0 to 30%). The motive of this research was to develop a method to measure the level of corrosion in rebar by gathering the thermal data. A total of 45 test specimens were casted with varying concrete cover and level of corrosion. After 28 days of curing, the steel was corroded by electrochemical acceleration test. At the interval of 10 sec. thermal images were captured. Taking in consideration the loss of heat through concrete depth input current was adjusted. For letting the reinforcing steel to get cool for 180 seconds current supply was stopped. Thermal images were taken during this complete process.

Figure2.10 shows thermographic image obtained after processing them in a visualization program.

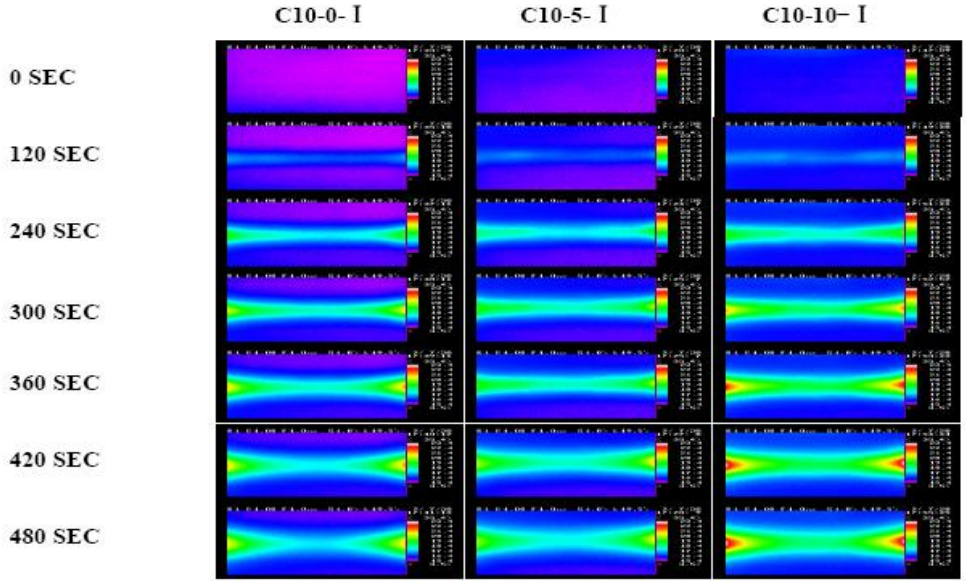

Figure2.10: Infrared thermographic image [17]

From the results it was concluded that the higher the temperature the more is the level of corrosion.

Galietti et al (2007) [18]: This paper presented the contextual analysis of concrete structures reinforced by GFRP with 16 inserted defects. Impulsive heating was used to heat the specimen and thermal images were analyzed. Different neural networks (NN) were also studied. There was

an advantage of using NN, once it was completely prepared after proper training there was no need to explicate it. This was presented by the incorrect investigation of the single layer GFRP acquired by the NN trained with CFRP specimens. Additionally, the untrained instances of two defects in the meantime had been wrongly explicated. Therefore, it was concluded that the implemented NN gave acceptable results but yet this system required use of ultrasonic wave system.

Barreira et al (2007) [19] evaluated the building materials to survey the utilization of thermography to perform some experiments. Some sensible studies were done with LFC's equipments to evaluate how results were affected by emissivity, colour, sensitivity and ecological conditions. For these studies eight identical cellular samples with emissivity 0.62, 0.85, 0.91, 0.92 were casted. The samples were inserted in water accompanied by drying period. The test was done under constant condition in two climatic cells with different relative humidity and temperature.

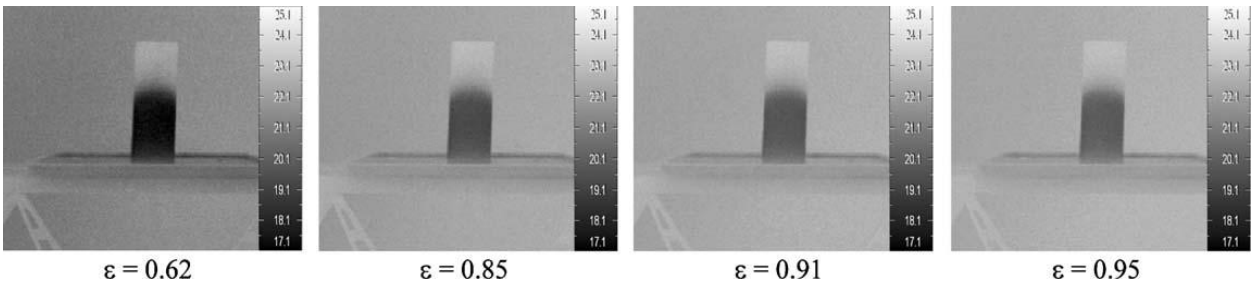

Figure2.11: Thermograms of a cellular concrete specimen after 168 h of absorption obtained with different emissivities [19]

From thermal images it was reported that for qualitative studies emissivity values were not important and environmental conditions influenced the thermal images captured at same time. It was also stated that reflectivity becomes important for the material with low reflectivity as it is reciprocal to emissivity for opaque objects. Also colour had a great effect when temperature difference was largely pronounced.

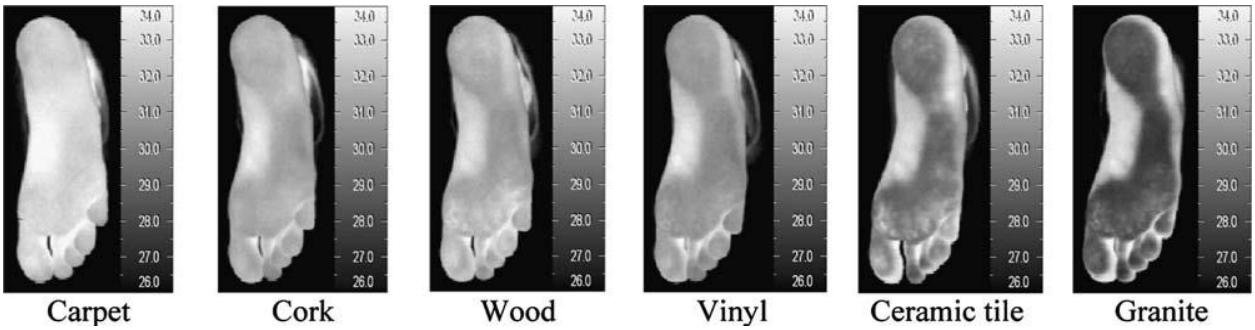

Figure 2.12: Thermograms after 1 min of contact [19]

Comfort of inner floor coating by differentiating six different flooring materials was also studied. From the results of thermal images it was concluded that material with high thermal diffusivity created more perturbance in the first contact and induced lower apparent foot temperature.

Aggelis et al. (2010) [20]: Two methods- thermography and ultrasound methods were used for an identification of subsurface crack that occurred due to the corrosion of steel reinforcement and the peculiarities that those inhomogeneities forced on the temperature field. The steel fiber reinforced concrete (SFRC) specimens of size 100 × 100 × 400mm were subjected to bending at four points. The four point bending resulted in noticeable cracks moving from the bottom side to top side. Due the steel fibers the prisms were not dissociated in parts and fracture was abrupted before reaching to the top side (compression side).

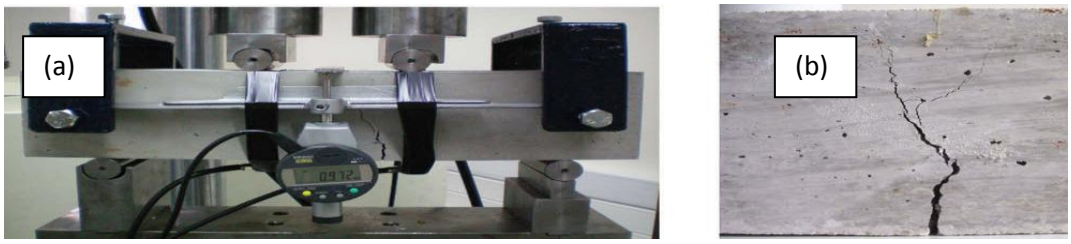

Figure 2.13: Experimental setup for four-point bending and (b) typical crack in SFRC [20]

An infrared camera (FLIR T360) was utilized to take images to that side of the specimen at cooling period after heating the sample in an oven for 3 hours at 90°C. The prismatic specimens were also analyzed by one-sided elastic waves estimation by the method of resonant acoustic emission sensors with a specified goal to measure the impact of the crack on the basis of wave parameters. The particular elastic wave problem was also modeled numerically.

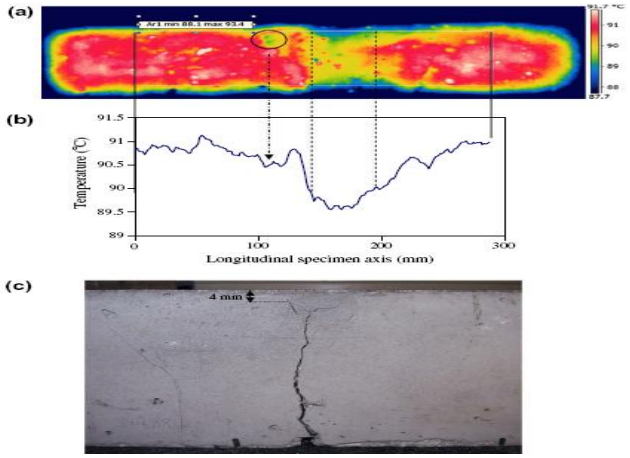

Figure 2.14: Thermograph of a specimen with 2 mm center deflection, (b) average temperature for the axis of specimen and (c) side view of the specimen [20].

From results it was concluded that for huge cracks, the thermal marks on the surface of specimen were effectively recognized on the thermogram but for smaller cracks a basic approach based on

averaging the temperature on the selected points of vertical lines of crack location to generate the mesh leads for identification of damaged area.

Lai et al. (2010) [21]: In this research, two types of defects were highlighted namely delaminations and flaws. They have defined the limit for quantitative estimation for sizes of these anomalies inside the externally reinforced CFRP on to a concrete surface as the embedded deformities tended to decrease the bond strength and durability. The specimens were placed in water bath with temperature varying between 40-60°C to simulate the aggressive environment. The sizes of the CFRP defects and delaminations were dictated by (i) quantitative infrared thermography (ii) preparing of visual pictures after opening up the CFRP by direct shear. Test results showed that apparent size of defects determined by quantitative IRT were in good agreement (88% precision) with actual defect sizes evaluated by the image processing technique. From the impact of exposure of the concrete specimens to high water temperatures on the defect sizes it was presented that for the actual entrapped air voids, these imperfections displayed small change but the glued layer demonstrated noteworthy deterioration because of high water temperature.

Taillade et al. (2011) [22]: They compared two interdependent techniques- shearography (the concept of interferometer with a video split) and pulse simulated infrared thermography for detection and characterization of depth and width of the adhesive delaminations of externally glued and reinforced FRP on surface of concrete structure. Initially, finite element method was used to perform the feasibility study of both methods. After that laboratory test on externally strengthened concrete slab of 400 × 300 mm^2 by three layers of FRP with the 1mm thick middle layer of glue was applied. PTFE discs were used to create debonds at the concrete and FRP interface by supplanting the epoxy.

Aggelis et al. (2010) [23]: Two methods- thermography and ultrasound methods were used for identification of subsurface crack that occurred due to the corrosion of steel reinforcement and the peculiarities that those inhomogeneities force on the temperature field. The steel fiber reinforced concrete (SFRC) specimens of size 100 × 100 × 400mm were subjected to bending at four points. The four point bending resulted in noticeable cracks moving from the bottom side to top side. Due to the steel fibers the prisms were not dissociated in parts and fracture was abrupted before reaching to the top side (compression side). An infrared camera (FLIR T360) was utilized to take images to that side of the specimen at cooling period after heating the sample in an oven for 3 hours at 60°C (more close to realistic state of structure under sunlight). These

test conditions were similar to its preliminary study in which sample was heated at 90°C. Another important feature of this study was that fractures produced in the specimen due to deflection under middle span enabled the formation of cracks with different lengths. Therefore, this study enabled crack detection as well as depth to crack estimation.

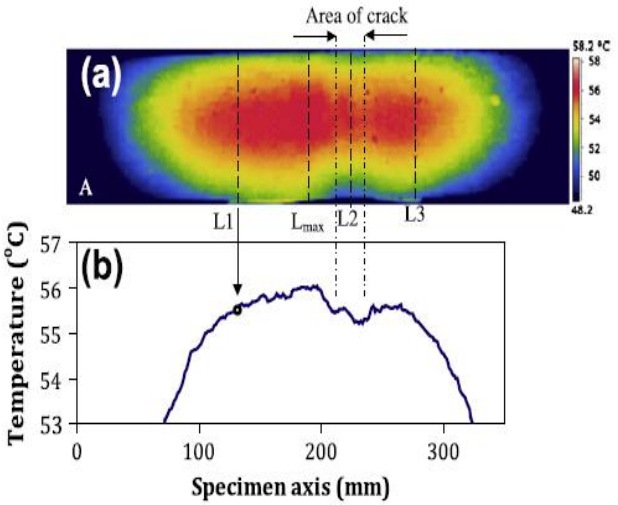

Figure 2.15: Thermograph of the specimen with mid-span deflection 3 mm and (b) average temperature along the specimen's axis [23]

From the thermographs it was revealed the presence of vertical cracks in the subsurface limited to depth of 11mm. The results from simulations and experimental wave parameter showed a very good correlation.

Beak et al. (2012) [24]: This paper represented the employment of the integration of heat induction technique and infrared thermography for nondestructive monitoring of corrosion in rebar in concrete specimens. Two different kinds of test specimens were manufactured including five exposed rebars of 12inch length & 3/8 inch dia with three levels of corrosion (0%, 16.6%, 28.6%) with and without rust and six concrete blocks of size 9.5" x 2.5" x 4.5" with one embedded rebar at the cover depth of 1 and 1.5 inch and three levels of corrosion (0%, 5%, 30%).

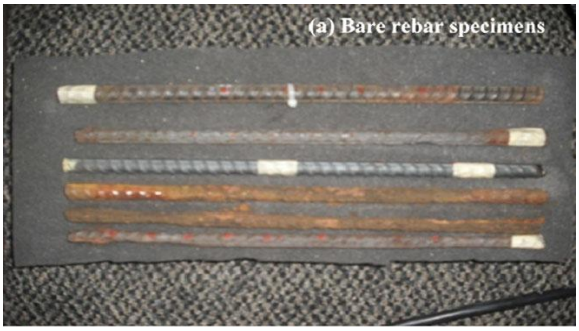

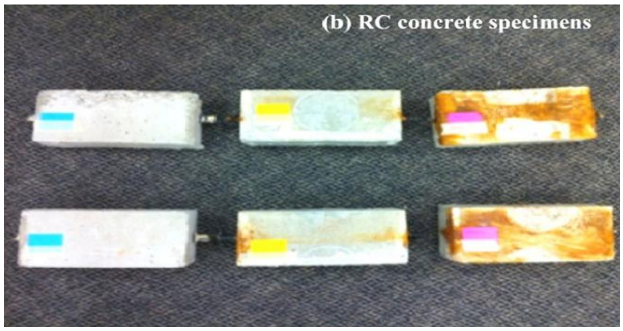

Figure2.16: Samples of corroded specimens (a) Bare rebar specimen, (b) RC specimen [24]

Impressed current method was used to induce the corrosion in the exposed and embedded bar. The steel bar was heated using inductive heater. The heat induction unit was placed on one side and the IR setup on the other side.

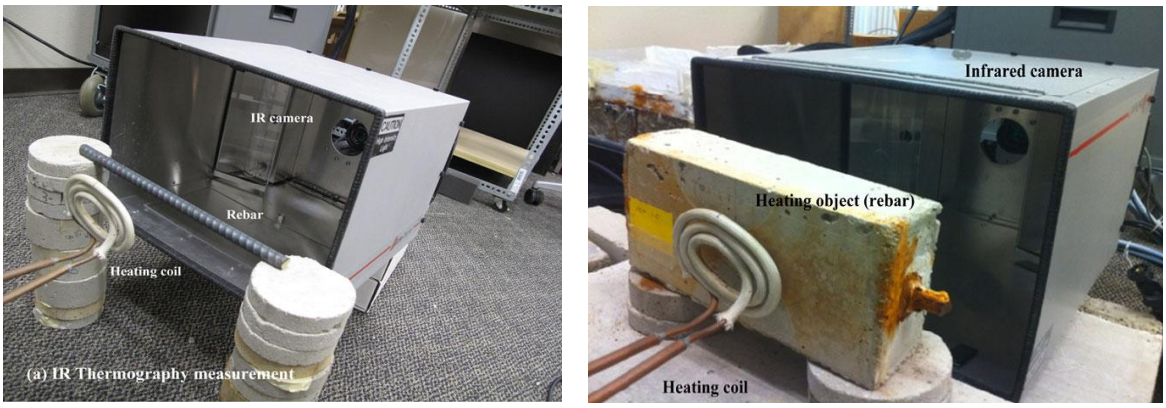

Figure 2.17: Setup for IRT for (a) Bare Bar (b) RC Specimen [24]

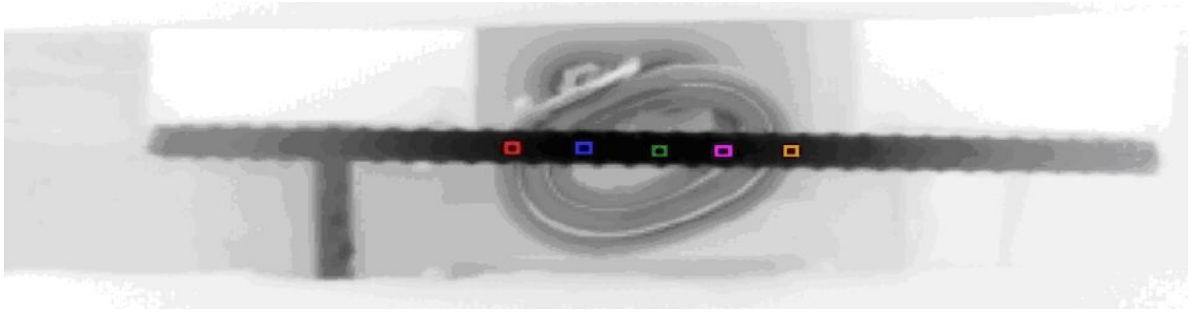

Figure 2.18: Thermal image of Bare Bar [24]

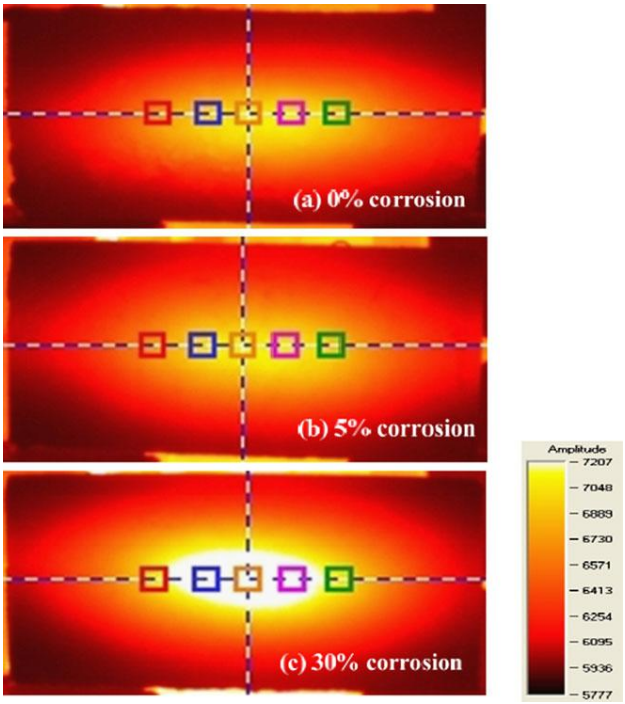

Figure 2.19: Thermal image of Embedded Bar [24]

From the results it was concluded that heating and cooling rates were directly proportional to the amount of corrosion and also on presence of rust on surface of bars. Also from the results of reinforced concrete specimens with different cover depths it was discovered that the efficiency of induction heating tends to decrease with increase in the cover depth and transfer of energy took more time to reach the surface of concrete.

Al-Hadhrami et al. (2012) [25]: This paper presented the feasibility of using infrared thermography for assessing the nature of concrete. Slab specimens 300 × 300 × 100 mm in dimensions were constructed. Shrinkage in each specimen was limited by placing mesh of 12mm steel in two directions. A total of 24 specimens were casted with three varying parameters namely: cement content (300kg/m^3 and 400kg/m^3), water to cement ratio (varying between 0.4-0.6) and consolidation efforts (25, 50, 75, and 100%). The samples were warmed to 70°C in an oven for 24 hours and afterwards set in a wooden box to capture the thermal images at interval of 10 minutes. But the thermal images after 30 minutes of initiation of cooling were used for analyses. From the thermal images it was concluded that the temperature increased with diminishing consolidity effort for the specimens with comparable composition. Additionally, it was also inferred that temperature of specimen surface is largely influenced by water cement ratio. The pore structure was also affected by the amount of cement content as demonstrated by increase in surface temperature.

Tashan et al. (2012) [26] have presented the findings of an examination of CFRP laminates and fabrics externally glued to concrete and steel specimens. Different forms of synthetic flaws were inspected in single layer and multi layer CFRP laminates and concrete interface. Particular attention was put on the use of various heating modules in this testing. Heating of the specimens was done with two lamps of maximum intensity of 2000W. IR technique used for this study is pulse thermography for period of 1-10sec and lockin thermography for long duration of 20seconds.

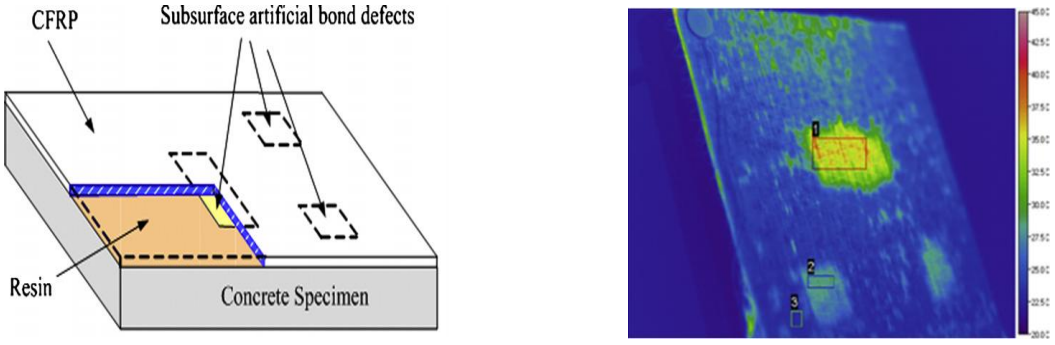

Figure2.20: Schematics and Thermograms of concrete specimens1 [26]

Processing of the thermal images was done to decode the results and study of those zones as Region of Interests. The outcomes relied on the maximal surface temperature and the thermal signal (DT). This extreme surface temperature records the area of the defect at the termination of the thermal infusion. The test results showed that the design module utilized as the part of infrared heating method significantly depend on method of heating, interval and position and directly influenced the best infrared observation ability. It was also concluded that the method helped to identify the geometry of defects with reasonable precision, depending on the quantity of CFRP layers.

Brown et al. (2013) [27]: In this research authors have examined the use of IRT as NDT method for the reinforcing system glued to concrete. 27 small concrete samples were prepared using CFRP and GFRP composites with thickness varying upto 4mm. Various wet lay-up strategies were used to soak dry fibers and the level of lattice immersion was also checked. Inspection were carried out by heating specimens for 60 seconds using the halogen lamps and each pixel in subsequent series of the thermal image was standardized to reduce the effect of non-uniform heating and to indicate the relative depth of fabricated defects w.r.t. FRP-concrete surface. The standardized temperature reaction for regions free from defects in each specimen depends on the lattice immersion levels, the absence or presence of a stiffened epoxy resin coat, and the consistency of matrix immersion.

Tashan et al. (2014) [28]: In this research authors have investigated CFRP concrete specimens having different types of false and loading cracks on the concrete surface. On the concrete specimens of size 300×300×50mm different sorts of FRP laminates and fabrics combinations were applied. A tungsten halogen lamp of capacity 2000W was employed as heating source. The thermal pulses were applied from varying angles to intensify fracture measurements. Thermograms of the specimens were taken at the rate of 0.25seconds. The results showed that the infrared thermographic method is able of detect the size and location of major cracks effectively. Also it was observed that the best thermal images were taken when pulse was applied for 5seconds and cracks at the depth of 0.8mm were monitored with accuracy.

Tashan et al. (2014) [29]: This research presented a detailed study for the identification of delaminated zones inside the bonded area of the concrete surface strengthened with single and multiple layers of CFRP. Pulse heating at various intervals was applied to the specimens using halogen lamps. The position of halogen lamp was changed to check the efficiency of technique.

For every test 600 thermal images were analyzed. Concrete specimens of size 300 x 300 x 50 mm strengthened with CF-140 CFRP fabrics and laminates were manufactured.

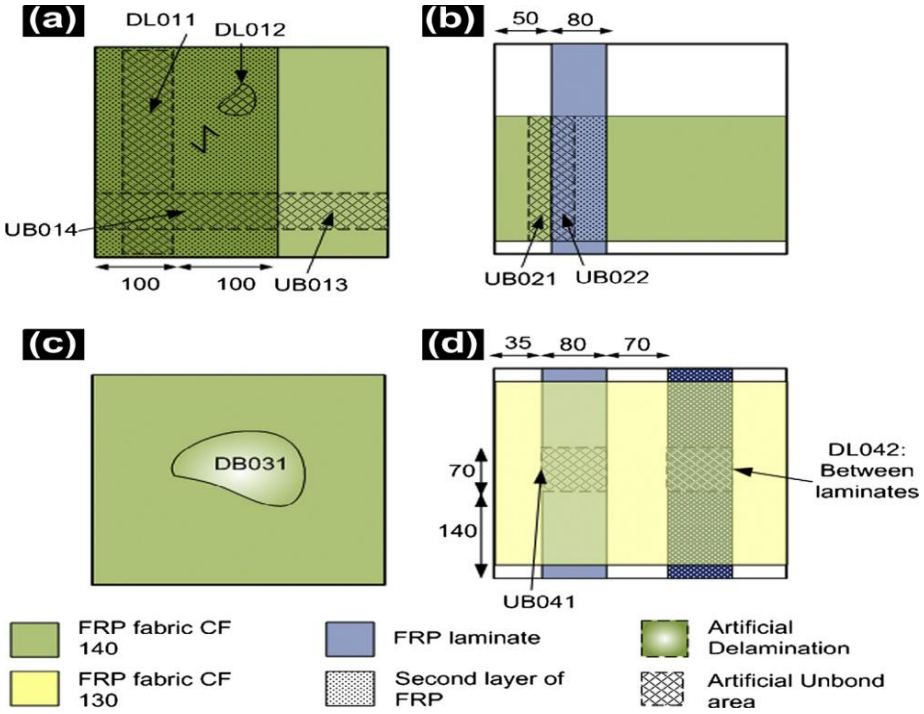

Figure2.21: Specimen details: (a) Specimen 1, (b) Specimen 2, (c) Specimen 3, (d) Specimen 4 [30]

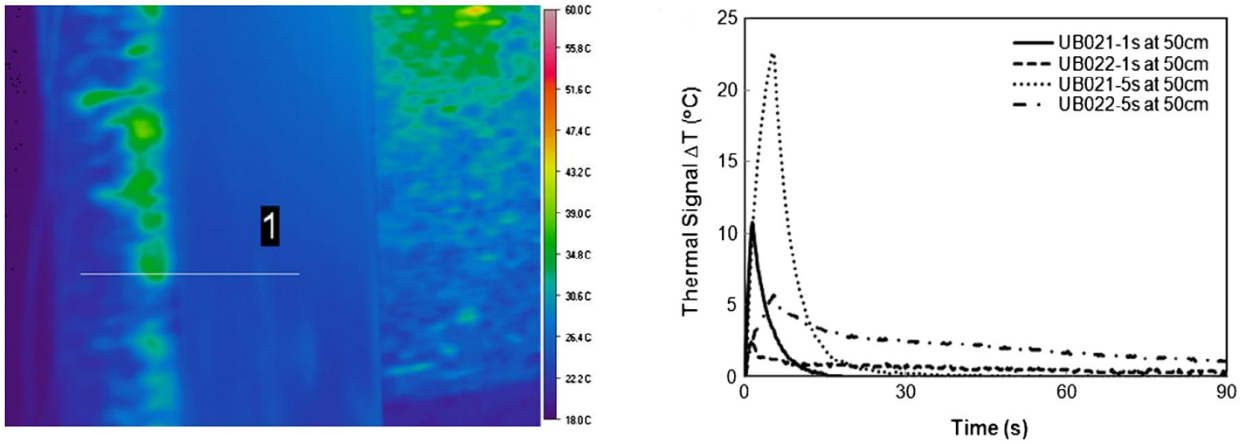

(a) Specimen 2 region of interest in a line shape (b) defects of Specimen 2 thermal signals

Figure2.22: Specimen 2 defect signals [30]

The results showed that the maximal thermal signal is related to the quantity of CFRP layers and it was to half by increasing the CFRP layers to two.

Keo et al. (2014) [31] have presented the application of infrared thermography when combined with active microwave excitation framework and an advantage of this simulation was that, there was volumetric absorption of incoming waves which leads to a great sound depth. The device generating the microwaves were made of magnetron 800W at 2.45 GHz compared to pyramidal

horn antenna. A 12mm diameter bar was placed at cover of 38mm inside the concrete specimen of size 1000 × 1000 × 65mm was detected. The heating of specimen was done for 300 seconds with power of 600Watts. An infrared camera was put on the same side as that of simulated surface and thermal images were captured at regular intervals of time. To protect the entire setup from the effect of electromagnetic radiations it was put inside an enclosure. The contrast algorithm method was employed to analyze the thermal images. The result showed a rise in temperature in the areas of steel reinforcement on the concrete surface. The use of microwaves did not affect the properties of inspected concrete.

Cotic et al. (2015) [32]: 51 artificial defects (delaminations and voids) were created in concrete and it was possible to detect them by thermal contrast method at subsurface thickness equal to or less than the size actual defect D. Preparation of four concrete test specimens was done. Three specimens measuring 50cm × 50 cm × 15cm were prepared at UL. Upto five defects of different geometry and different concrete cover were inserted artificially in these specimens, hence simulating voids. The defects have rectangular framework of D × D × s in size and were made of polystyrene. The fourth concrete test specimen of 150cm × 150cm × 30cm created at BAM had a total of 35 artificially embedded defects with varying geometry. The experiments were performed out with recording times of up to 2 hours.

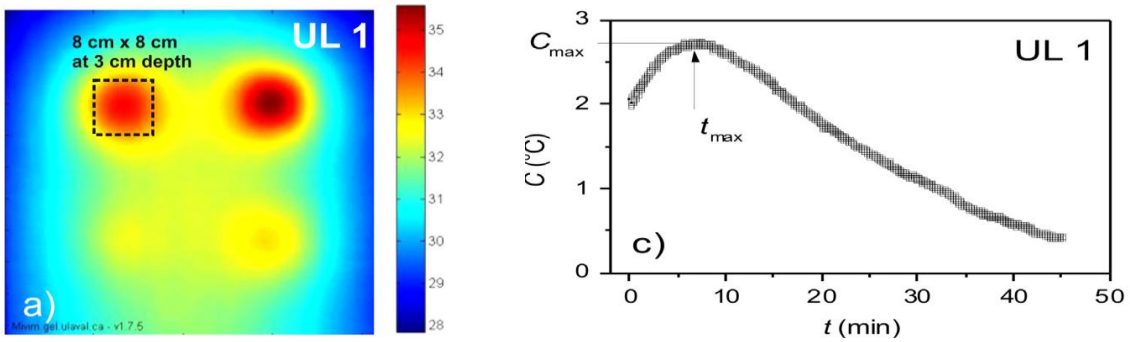

Figure2.23: The thermograms and thermal contrast image for specimen UL1 [32]

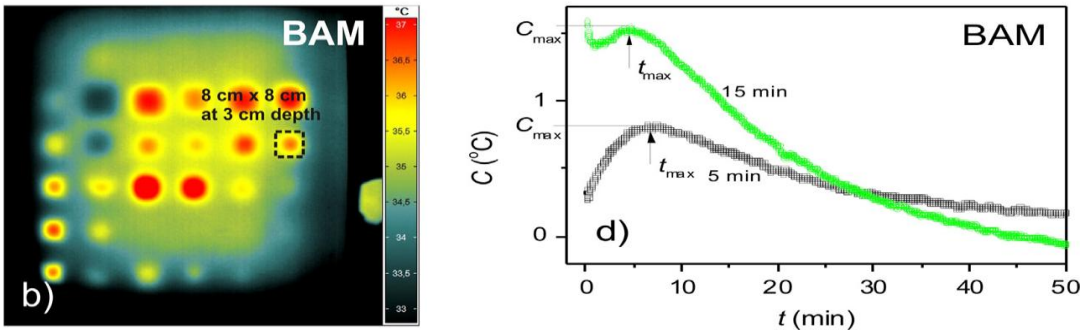

Figure 2.24: The thermograms and thermal contrast image at BAM (using a heating time of 15min) specimens at t¼tmax [32].

The important results inferred from this research were: The defects of size D embedded in concrete was detected at thickness of 0.9D or less by using thermal contrast technique and at deeper depth by phase contrast method.

Khan et al. (2015) [33] have combined experimental and numerical results for the evaluation of concrete masonry structural components. To estimate the constant and transient states of heat transference in the masonry structure 3D finite element models were formulated and executed. Three masonry specimens with known dimensions and having identical thermal properties were studied. Heat diffusion results of finite element simulations and finite difference method for one specimen were compared and were implemented on the other two specimens using IRT. The results showed a good relation between numerical and experimental values.

Alexis et al. (2015) [6]: The objective of this research was to identify the bond defect between concrete-CFRP interface and to assign those flaws a "*numerical value*". 0 was assigned to air gap and 1 to the completely glued area. Quantitative identification is performed by estimating the thermal impedance and after distinguishing the thermophysical factors of the framework through fitting the calculated impedance to a hypothetical model. A reversal procedure was performed to evaluate the unknown factors, without knowing the properties of the specimens. Authors were able to estimate precisely the quantity of glue inside a defect and the resistance of concrete to the heat.

Pastuszak (2016) [13]: He has presented the thermographic results of two types of defects presented on curved GFRP panels. The two types of defects were- (i) artificial defects that were created by placing Teflon strip during the manufacturing stage in between the laminates (ii) defects which occurred during constant load test. The specimens were prepared from 8 plies of Hexcel TVR 380 M12/R- unidirectional glass fiber prepreg layers. The specimen was cylindrical in shape with inner radius 92mm, length 300mm and thickness and thickness 2mm. The fiber volume of laminates was 60% and the thickness of ply was 0.25mm. The heating was done with halogen lamps. The results obtained from the thermograms proved the efficacy of method and the results can be effectively and easily simulated by means of FEM.

Pieper et al. (2017) [34]: This paper presented preliminary simulation and measurement results on the use of active microwave heating technique and thermography for the monitoring of corrosion on rebars in cement concrete structures. These results showed that the increased absorption of the microwave energy by corrosion leads to a measureable increase in the surface temperature of the surrounding concrete. The simulations showed that the polarization of the

incident signal can be optimized per the orientation and thickness of corrosion. Further, circular polarization was shown to perform better if prior knowledge of corrosion thickness and/or rebar orientation is not known. In addition, the presence of moisture and/or chloride ingress in concrete will lead to a higher loss tangent (and also may change the thermal properties) and therefore may also be detected using this technique.

Sultan et al. (2017) [35]: This research provided an advanced method for indicating the dependability of IRT technique and calculating the optimal thermal contrast for the recognition of flaws in concrete. Concrete slab of size 6000mm × 3000mm × 180mm was manufactured to simulate the deck of reinforced concrete bridge and artificial delaminations of 55mm thick Styrofoam sheet were embedded inside it. Thermograms of the manufactured slab were taken during the day time to take the advantage of solar loading as a source of passive thermography. Also two bridges, in service with areas of corrosion induced delaminations were also selected for test. Receiver operating characteristics in combination with image processing technique was used to analyze data from the manufactured and for the decks of bridge in service. Results from these experimental tests demonstrated the ability of IRT technique to distinguish delaminations from healthy concrete. This conclusion was reached because the non-parametric estimate of the region under the ROC curve was larger than 80% each and every group of images. They determined that the optimal thermal contrast was obtained in the range of 0.6-0.8°C. Precise explanation of real condition of the test specimens was critical to be applied for the suggested analysis method.

Hiasa et al. (2017) [36]: In this investigation, heat exchange model using finite element method for concrete blocks with false delaminations used in some past test specimen were made and examined to investigate the parameters for effective use of IRT. After the approval of these finite element models critical factors affecting the detection of delaminations such as geometry of delaminations, ambient temperature and solar irradiance conditions were examined. From the thermal images it was concluded in IRT evaluation area of delaminations matters the most than its volume and thickness. It was also expressed that the use of IRT technique did not rely on the season.

Dabous et al. (2017) [37]: In this research the delaminations in the concrete bridge were evaluated by combining two techniques namely- InfraRed Thermography and Ground Penetrating Radar (GPR) methods. A 77m^2 section was selected on the bridge located in Laval city of Canada for implementation of IRT and GPR techniques. For IRT, the section was divided into mesh of 1m^2 area thus making 77 such squares. For GPR scanning another approach was

followed by marking 24 passes at a distance of 0.3 meter. The final area of delaminations was calculated after integrating the results of IRT with GPR thus indicating that combination of multiple NDT technologies increase the reliability and accuracy the collected data.

Ghosh et al. (2017) [38]: In this study researchers had explored the combination of two techniques namely, infrared imaging and ultrasonic wave based imaging for the detection of near surface cracks in concrete slab. Thermal imaging was found to be effective in detection of fine surface breaking cracks developed as a result of accelerated corrosion of a rebar embedded in concrete slab of dimension 400 x 400 x 100 mm^3. The two 1000 W tungsten-halogen lamps were used as source of heating. The sample was kept at a distance greater than 1 meter from the heat sources to avoid heating non-uniformity. The sample was heated for a specified duration as per the required diffusion length or effective depth of penetration. After capturing the thermal images at different time intervals, amplitude and phase images were prepared using FFT.

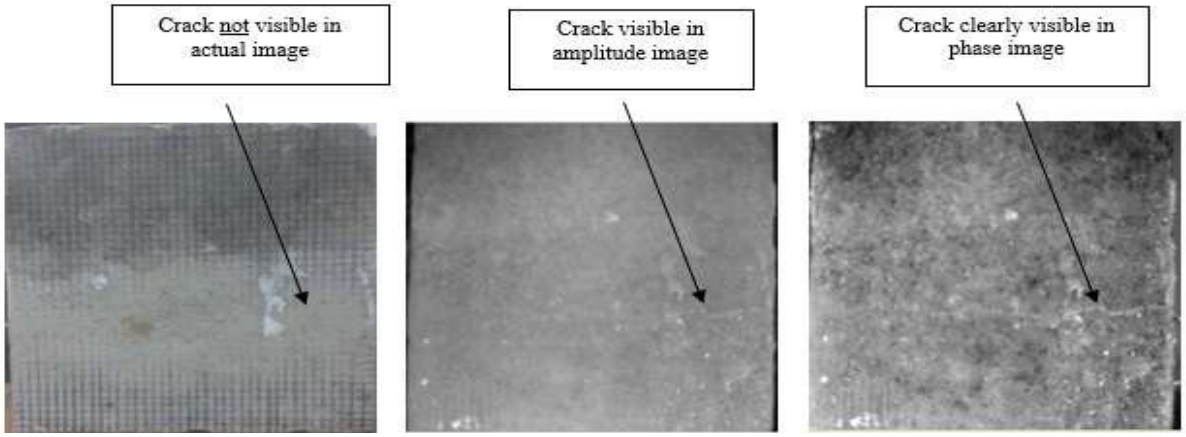

Figure2.25: Thermal Imaging: a) normal image b) amplitude image c) phase image [38]

It was evident that the crack was not visible in a photograph of the sample. However, in the thermal amplitude and phase images the crack was clearly visible, with the phase image showing a better contrast.

2.9 CLOSING REMARKS

This chapter highlights the work done by some researchers on the use of infrared thermography to detect the defects in concrete and detection of corrosion in RC structures. They have explained the different heating techniques to energize the specimens and to create the temperature differences on the surface of it. Their work predicts the depth upto defects were visible. They have also explained that the exact size and location of the defect can be known by combining it with other NDT techniques such as acoustic emission, ultrasound method, GPR, etc.

CHAPTER 3

EXPERIMENTAL INVESTIGATION AND METHODOLOGY

3.1 GENERAL

The objective of this work is to evaluate the efficiency of infrared thermographic technique to detect defects in the form of cracks, voids, delaminations, corrosion of reinforcement in civil engineering structures. Also, some destructive tests (compressive and tensile) were also conducted to identify cracks using IRT in various kinds of materials like cement mortar, concrete, bricks and interlocking tiles.

3.2 TEST PROGRAM

The test program includes:

1) Determination of fundamental properties of constituent materials i.e. cement, coarse aggregate, fine aggregate, steel bar, etc as per relevant Indian Standard Specification for casting of specimens.

2) Monitoring of Surface Defects

Different surface defects on the cement mortar cube of dimensions 70.6mm × 70.6mm × 70.6mm were captured after heating the specimen in oven.

3) ***Casting of specimens for mechanical cracks and surface defects in mortar, concrete, bricks and interlocking tiles***

- Bricks and Interlocking Tiles: Development of cracking pattern simple and plastered bricks of nominal size 230mm × 11mm× 70mm was checked in compression. Interlocking tile which are used at road pavement in minor streets was also checked in compression.
- Mortar: Casting of cement mortar cubes of dimensions 70.6mm × 70.6mm × 70.6mm for picking up the development of cracks developed under compressive testing.
- Concrete: Casting of cement concrete cubes of 150mm × 150mm× 150mm size for mechanical testing and imaging of various kinds of cracking in tension and compression.

The above specimens were heated in oven and thermal images were captured at various stages of testing to capture the crack development.

4) Detection of artificial embedded defects in concrete

Casting of concrete cubes of dimension 150mm × 150mm× 150mm with artificial embedded defects in the form of plastic piece, piece of jute, etc and steel at various cover depths to simulate defects, voids, imperfections and discontinuity in concrete . Heating of the specimens is done till the uniformity in temperature is obtained. Thermal images are captured at various stages of cooling to pick up these embedded defects.

5) Detection of delamination of GFRP sheets with concrete

A cube of 150mm × 150mm× 150mm was smoothened on the surface to avoid imaging of surface imperfections followed by application of the base coat layer of epoxy. On the concrete cube artificial debonds and delamination was simulated by placing aluminium strips before applying GFRP sheet. Thermograms were captured at various heating and cooling intervals to pick up these irregularities.

6) Detection of defects in rebars

a) Bare Bars

Imaging of plain mild steel rods both circular and square in cross-section of 12mm size and 50mm in length simulated with different kinds of surface defects like V-notches, circumferential reduction in diameter, threads and corrugations are investigated by IRT.

b) Bars embedded in concrete

- Accelerated Corrosion in embedded bar

(i) Casting of RC slab of dimensions 300mm × 300mm× 100mm with a 500mm long mild steel bar of 12mm diameter embedded in it such that 300mm of steel bar is embedded in the concrete cover with 100mm bar exposed on each side.

(ii) Subjecting the slab specimen to accelerated corrosion at a constant voltage of 10V with continuous monitoring to ensure that corrosion takes place.

(iii) Corrosion is continued for 5 days.

(iv) Thermograms of healthy and corroded specimen are taken after heating the exposed part of rod with gas welding technique after allowing sufficient time for cooling to pick up degradation due to corrosion in embedded bar.

Figure 3.1 Complete Test Program

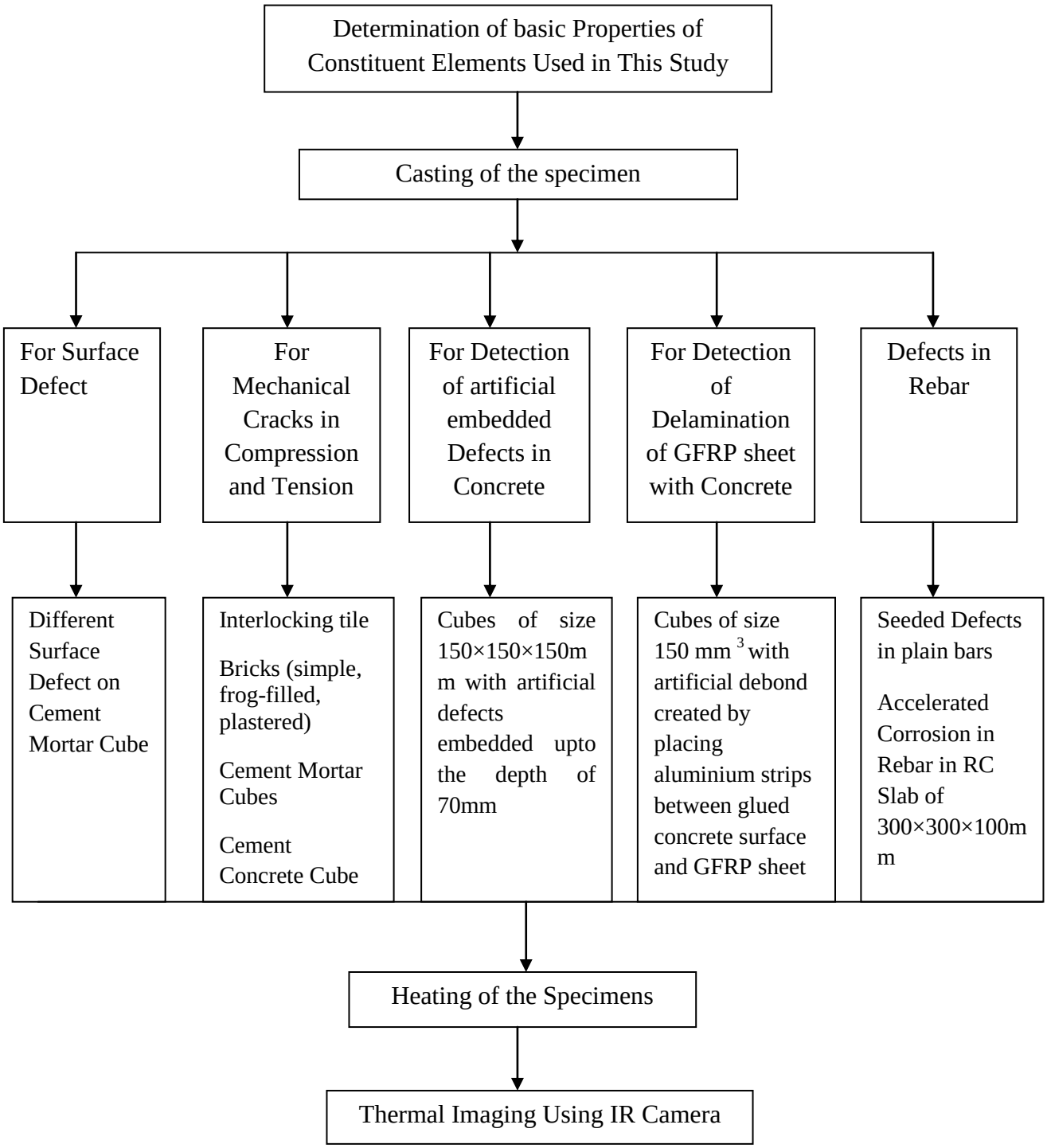

3.3 MATERIALS USED

The materials used in this study for the casting of cubes and slabs are cement, fine aggregates, coarse aggregates, water and mild steel rods as reinforcing bars. The properties and specifications of the materials are as follows:

1. ***Cement:*** Pozzolona Portland Cement (PPC) of Grade 43 is used in present experimental work. The cement used in this study was of uniform colour i.e. grey with a tint of light greenish shade and is free from any hard lumps. Various tests were conducted to determine the properties of cement as per IS codes. Summary of the tests conducted is given in **Table 3.1.**

Table 3.1 Physical Properties of Cement Used (PPC Grade 43)

S.No.	Characteristics	Experimental Values	Standard Values
1.	Normal Consistency	33%	As per **[39]**
2.	Initial setting time	50 minutes	30 minutes **[39]**
3.	Final setting time	300 minutes	600 minutes **[39]**
4.	Fineness	5%	10% **[40]**
5.	Specific gravity	2.88	2.90 **[41]**
6.	Compressive strength		
	3-days	17.2 MPa	16 MPa (Minimum) **[42]**
	7-days	24.4 MPa	22 MPa (Minimum) **[42]**
	28-days	38.6 MPa	33 MPa (Minimum) **[42]**

2. ***Fine aggregates:*** Fine aggregates (4.75 mm as maximum size) used in this experimental study were locally available and conformed to Zone II. Fine aggregates were tested as per IS recommendations given in IS: 383-1970 **[43]. Table 3.2** and **Table 3.3** shows the physical properties and sieve size analysis of the fine aggregates.

Table 3.2: Physical Properties of Fine aggregates Used

Properties	Observation
Specific Gravity	2.6
Net water absorption	0.97%
Fineness modulus	2.57

Table 3.3 Sieve Analysis for Fine Aggregates [43]

Weight of Sample taken = 2000g

S.No.	IS Sieve Designation (mm)	Weight Retained	Cumulative Weight Retained	% cumulative retained	% Passing	Limit
1.	4.75	70	70	3.5	96.5	90-100
2.	2.36	88	158	7.9	94.4	75-100
3.	1.18	262	420	21	84.8	55-90
4.	600µ	458	878	43.9	54.2	35-59
5.	300µ	797	1675	83.75	24.6	8-30
6.	150µ	277	1952	97.6	2.4	0-10
7.	PAN	48	2000	-	-	-
					Sum=257.65	

Fineness Modulus = 257.65/100 = 2.57

3. ***Coarse Aggregates:*** Crushed stone aggregates of maximum size 20mm (nominal size) were used in this work. The aggregates were cleaned thoroughly to remove dirt particles and were surface dried. Testing of aggregates was done as per IS: 383-1970 **[43]**. The results of various tests and sieve analysis is given in **Table 3.4** and **Table 3.5**

Table 3.4: Physical Properties of Coarse Aggregates Used

Properties	Observation	
	10mm	**20mm**
Type	Crushed (Angular)	Crushed (Angular)
Maximum Size	10mm	20 mm
Specific Gravity	2.68	2.65
Water Absorption	0.94%	1.01%
Fineness Modulus	6	7.02
Moisture Content	Nil	Nil

Table 3.5 Sieve Analysis of Coarse Aggregates Used (20mm) [43]

Weight of Sample taken= 2000g

S.No.	IS Sieve Designation (mm)	Weight Retained (gm)	Cumulative Weight Retained	% Cumulative retained	% Passing	Limit
1.	20	55	55	2.75	97.25	85-100
2.	10	1940	1995	99.75	0.25	0-20
3.	4.75	2.5	1997.5	99.8	0.2	0-5
4.	PAN	2.5	2000	-	-	-
				Sum= 202.3		

Fineness Modulus = (202.3 + 500)/100 =7.02

Table 3.6 Sieve Analysis of Coarse Aggregates Used (10mm) [43]

Weight of Sample taken= 2000g

S.No.	IS Sieve Designation (mm)	Weight Retained (gm)	Cumulative Weight Retained	% Cumulative retained	% Passing	Limit
1.	10	350	350	17.5	82.5	85-100
2.	4.75	1500	1850	92.5	7.5	0-20
3.	PAN	150	2000	100	0	0-5
				Sum= 100		

Fineness Modulus = (100 + 500)/100 =6

4. ***Steel Bars:*** Plain mild steel bar of 12 mm diameter with 500 mm length was used as reinforcement in slab. 300mm of rebar is embedded in concrete and 100mm bar is exposed to environment on each side, in order to use that part for electrical connections. Properties of strengthening bars used for casting of RC slab are given in **Table 3.7**.
5. ***Water:*** Clean and fresh tap water was used for casting of cubes and slabs in this experimental study. As suggested by Indian Standard the water was relatively free from oil, sugar, silt, organic matter, acidic and chloride materials.

6. ***Bricks:*** Smooth, rectangular non-modular bricks with sharp corners and uniform in colour were used in this study .The nominal size of the brick used is 230 mm× 110 mm × 70mm. Properties of Bricks are given in table 3.8

Table 3.7 Properties of Reinforcing Bars used for casting of specimens (manufacturer)

Type and size of the bar	Ultimate tensile strength (MPa)	Yield Stress (MPa)	Young's Modulus (GPa)	Percentage Elongation (%)
Mild steel, 12mm	410	240	200	23

Table 3.8: Properties of Bricks Used

S. No.	Property	Observation
1.	Water Absorption	6.8%
2.	Compressive Strength	
	Simple Brick	8MPa
	Frog-filled Brick	11 MPa
	Plastered Brick	15Mpa

7. ***Interlocking Tiles:*** Dog bone shaped concrete interlocking tiles were used in this experimental study. The thickness of the tiles used is 50 mm. The tiles are of uniform colour i.e. grey. The interlocking tiles are water resistant, impact resistant and corrosion resistant. The weight of the tiles is 4.8 kg.

3.4 MIX DESIGN

The mix design is normally carried out for a required compressive strength of concrete with sufficient workability so that the freshly made concrete can be mixed, placed and compacted properly. M25 mix design was used in this work and mix proportions were calculated as per Indian Standard IS: 10262-2009 **[44]**. **Table 3.9** shows the mix proportions for the concrete used for casting of various kinds of specimens. The compressive strength of the concrete after the curing of the specimens is given in **Table 3.10**.

Target Design Mix- M25

Maximum size of the aggregates= 20 mm

Type of exposure = Severe

Table 3.9: Mix Proportions

Unit of Batch	Water	Cement	Fine Aggregates	Coarse Aggregates
Cubic Meter Content	186 liters	380 kg	670.16 kg	1124.52 kg
Ratio of Ingredients	0.489	1	1.76	2.95

Table 3.10: Compressive Strength of Concrete

S.NO.	Days of Curing	Compressive Strength (MPa)			
					Average Strength
1.	3	15.8	16	16.8	16.2 MPa
2.	7	24	22	21.8	22.6 MPa
3.	28	42	37	41	40 MPa

3.5 EXPERIMENTAL METHODOLOGY

3.5.1 Preparation of the Specimens

1) For surface defects

- Cement mortar cubes of 70.6mm × 70.6mm × 70.6mm were casted
- Some surface defects were inflicted on the cement mortar as:
    - thumb impression,
    - V-groove with the help of shovel (8mm deep)
    - small holes 5mm in diameter and 7mm deep

The prepared specimens were heated in oven and thermal images were taken to detect the defects using its cooling stage.

2) For mechanical cracks

i. Bricks and Interlocking Tile-

Three sets locally available bricks as shown in **Figure 3.1** of nominal size 230mm × 110mm × 70mm were tested.

- Set 1- Simple brick

(a): Simple Brick

- Set 2- Brick with frog filled with cement mortar

(b): Frog filled Brick

- Set 3- Fully plastered bricks

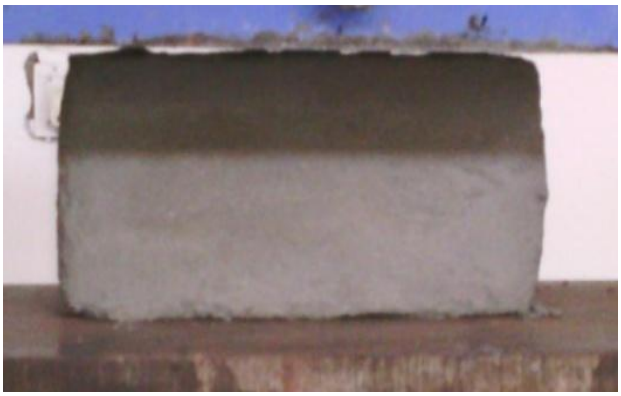

(c): Plastered Brick

- Interlocking Tiles

(d): Interlocking Tile

Figure 3.2: Bricks and Interlocking Tile Used in study

- Cement mortar (cement: sand 1:3) was used for filling the frog of brick and for plastering. Before the application of cement mortar bricks were cleaned to remove the dust particles and to make the surface smooth. The bricks were immersed in water prior the application of cement mortar.
- Thickness of the mortar for plastering the bricks was 3mm. After the application of mortar, the surface of the brick was levelled so as to give get the clean and levelled surface. Curing of set 2 and set 3 bricks were done for 7 days using the wet sack method.
- The bricks were tested after 7 days of curing under compression testing and simultaneously infrared images were captured after subjecting them to heating at regular intervals to pick up the cracking.
- Dog Bone shaped interlocking tiles are cleaned properly before compression testing. Infrared images were captured after subjecting them to heating at regular intervals to pick up the cracking.

ii. Cement Mortar and Cement Concrete-

- In this experimental work, concrete cubes of 150mm × 150mm ×150mm and cement mortar cubes of 70.6mm × 70.6mm × 70.6mm were casted. Firstly the moulds were oiled properly so as to remove the cubes from the mould easily after 24 hours. Concrete mix was poured in the mould and vibrated so as to compact the mix effectively. The vibrations were given until the mould was filled completely and there were no air gaps.

- Demoulding was done after 24 hours of casting. Cubes were cured for 7 and 28 days using an open tank method. The surface of the cube was cleaned up to remove all loose material and dirt.
- The prepared mortar and concrete cubes were tested after 7 and 28 days under compression testing and simultaneously infrared images were taken after subjecting them to heating at regular intervals to pick up the cracking.

3) For artificial embedded defects

- Eight tests were carried on the concrete cubes of 150mm × 150mm ×150mm with embedded defects simulating voids at different depths to the check the effectiveness of IRT technique to detect the sub-surface defects.
- The depth at which the defects was required to be simulated as void was marked and the defect was stationed at the levelled place with the help of thread which was tightly tied so that it does not move from its position. After the defects were set in place, concrete mix poured in mould and vibrated properly until there were no air gaps.
- The description of the different types of defect with different cover depths and the schematic diagram of the embedded defect is given in **Table 3.11** and **Figure 3.3** respectively.

Table 3.11: Description of artificial sub-surface defects embedded in concrete

Type of Defect	Depth of Defect (d in mm)	Thickness of Defect (in mm)
Wooden Piece	15	20
Plastic Bottle	20	40
Piece of Jute	25	10
Sponge	30	20
Plastic Bottle	40	45
Glass Bottle	50	35
Plastic	60	40
Steel Plate	70	15

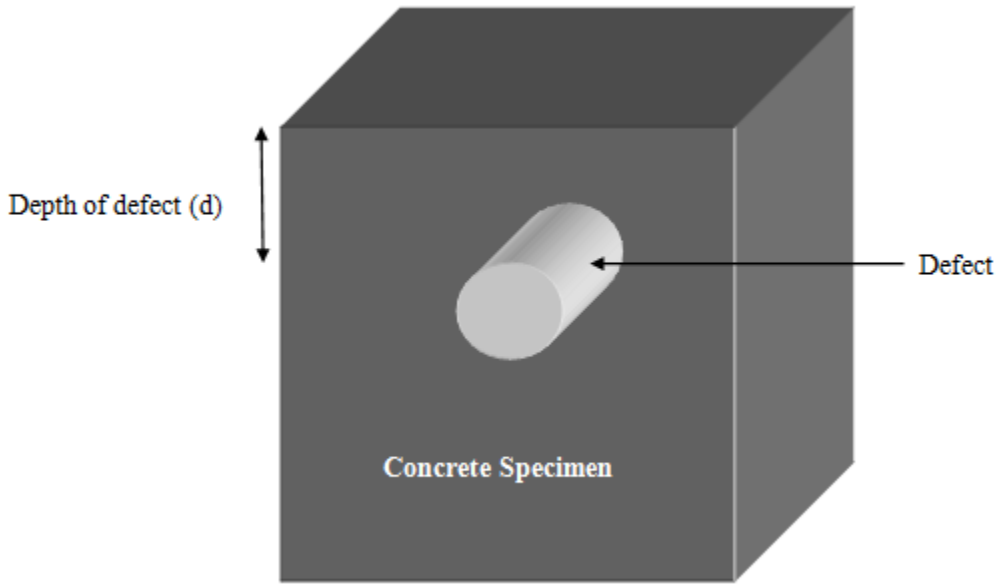

Figure 3.3: Schematic showing the embedded defect in cement concrete cube.

4) For detection of delamination for GFRP sheet

i. Casting of 150mm × 150mm ×150mm cubes was done in the same as the for the mechanical cracks. After curing the cubes for 28 days all the surface laitance was removed with the machine driven grinder to roughen the surface and to unmask the coarse aggregate.

ii. Surface was properly cleaned to remove all the dust with the help of pump. Artifical debonding between concrete and GFRP layer was created by placing 1.5 mm thick aluminium strips and pieces. The prepared MBrace saturant epoxy resin was applied onto the concrete and prior to the application of GFRP layer. After this GFRP sheet was set in position by applying some dead loads.

iii. Two types of specimens with different lengths and widths of aluminium pieces were made as detailed below in **Table 3.12** and **Figure 3.4**.

Table 3.12: Description of artificial defects to create debonds and delaminations

Specimen	No. of Aluminium Pieces to simulate delamination	Length (mm)	Width (mm)
1.	2	150, 50	30, 50
2.	2	150, 150	30, 30

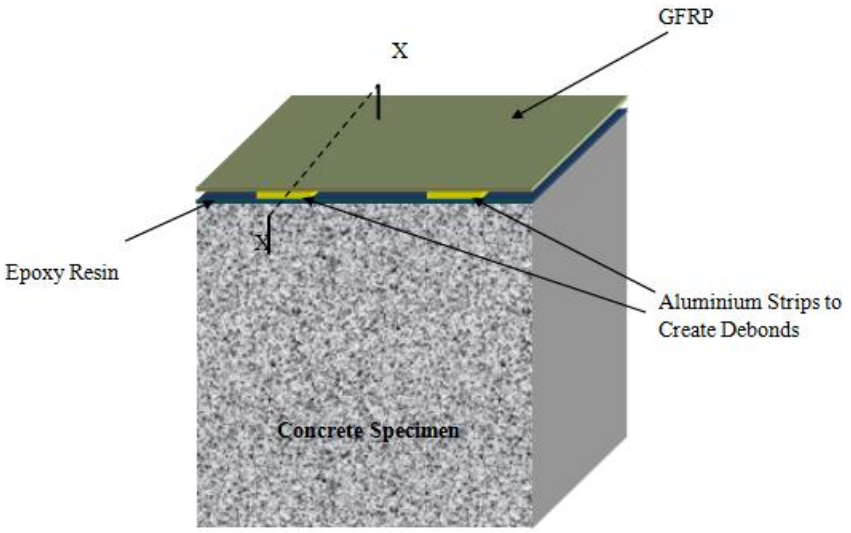

(a): Concrete specimen with artificial debond (Specimen 2).

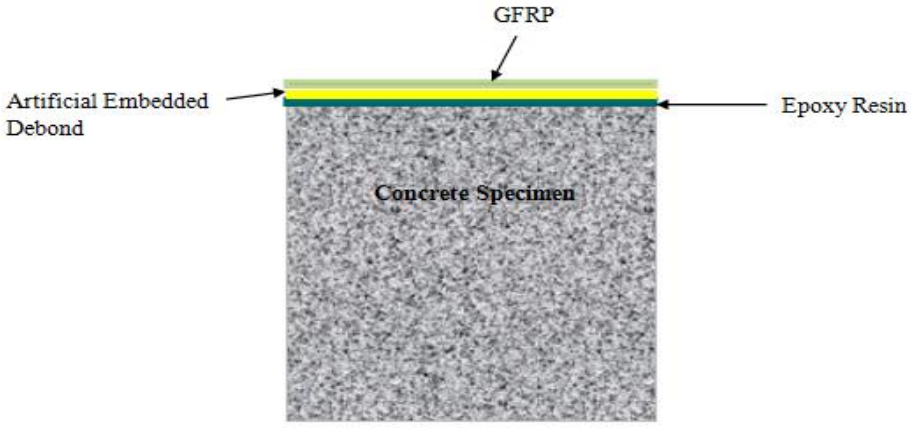

(b): View at X-X of Specimen2.

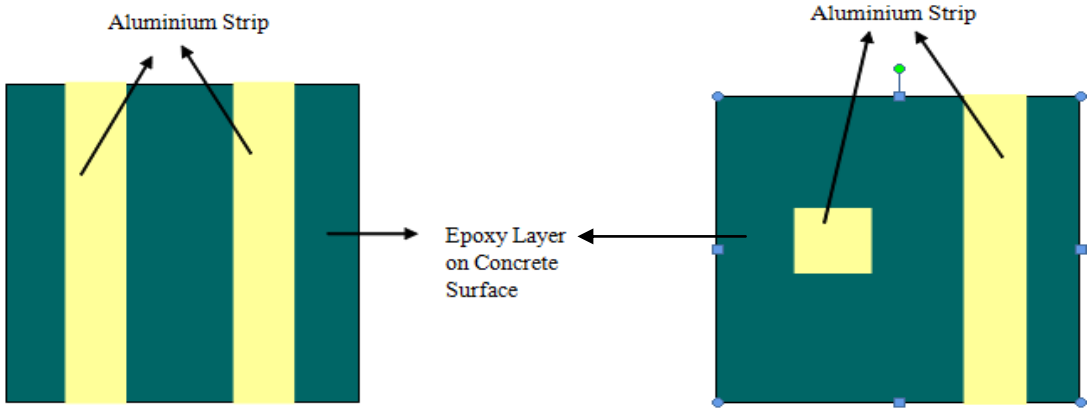

(c): Top view of concrete cube specimens showing artificial Debonds and delaminated areas

Figure 3.4: Details of simulated delamination in cubes

5) Defects in Rebars:

i. **Simulated defects in bars:** Mild steel rods both circular and square in cross-section were inflicted with various kinds of defects as detailed in **Table 3.13**. The bare rod specimen 12mm in diameter and 500mm in length of each section was wire brushed to remove the surface scales. Various defects were seeded on the surface of bar at distance of 150mm from one end.

Table 3.13: Description of surface defects on mild steel rod

S.No.	Type of Defect	Cross-section of rod	Length of defect	Detail of Defect
1.	Threads 	Circular	100mm	1.0mm deep threads were created
2.	V-Notch 	Circular	75mm	Rod was tapered to 6mm at one side
3.	Circumferential reduction in diameter 	Circular	75mm	Diameter was reduced to 8mm
4.	Square section to circular 	Square	100mm	Circular section of 8mm
5.	Corrugations 	Square	100mm	2mm deep on all four sides repeated after distance of 10mm

ii. **Specimen for embedded bar:** In this experimental work, the RC slabs of dimensions 300mm × 300mm × 100mm thick with mild steel bar of 500m length were casted with 300mm embedded in concrete and 100mm bar was projected on both sides. Initial weight of the bars was measured and oiling of the moulds was done. When the bar had been set in position, the concrete mix was poured and the concrete mix was vibrated so that mix gets properly compacted and there are no air gaps. After demoulding, the slabs were cured using wet sack method for 28 days. The slab surface was cleaned to remove dirt and loose materials. Top view of RC Slab specimen is shown in **Figure 3.5**.

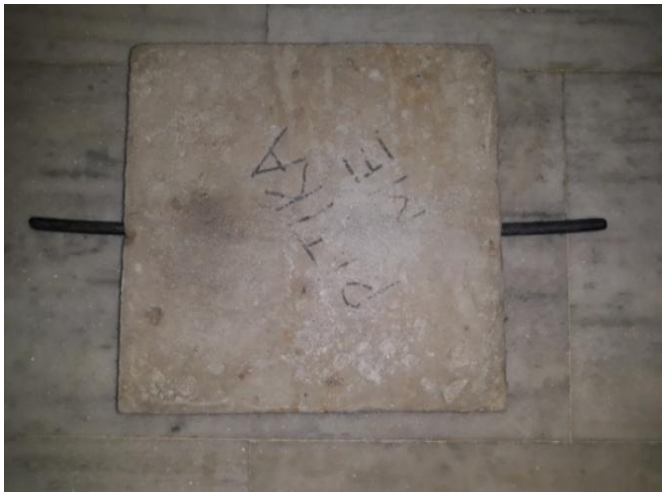

Figure 3.5: Top View of RC Slab Specimen

In this embedded bar, corrosion was induced to simulate the damage in concrete. The infrared images were taken to compare the thermograms of healthy and corroded specimens.

The methods that are generally employed for inducing the corrosion in RC specimens are salt spray method, chloride diffusion method and impressed current method **[45]**. However, the quickest of all methods for inducing corrosion in the inserted bar is by impressing an anodic current. It was done by subjecting the RC slabs to 5% NaCl salt solution dip on the specimen. Current was simultaneously impressed by making rebar as anode and a stainless steel (SS) mesh wrapped on the slab in the middle 100mm length as cathode. The Constant voltage of 10V was impressed in order to accelerate corrosion by the DC regulated power supply (APLAB Make, 64V, 0.5A). The setup for the accelerated corrosion is shown in **Figure 3.6**.

(a) Actual Setup

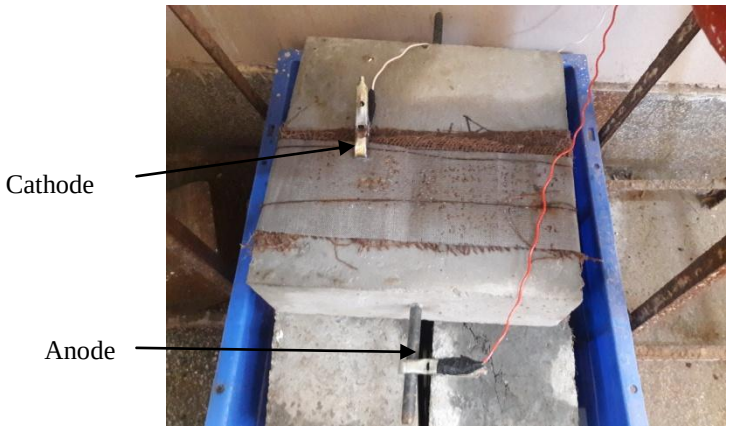

(b) Top view of Specimen **(c) Power Supply (APLAB, 64V, 0.5A)**

Figure 3.6: Accelerated Corrosion in RC Slab

3.6 INFRARED THERMOGRAPHIC SETUP

3.6.1 InfraRed Camera

The InfraRed (IR) camera used to capture thermographic images of the specimens was a **Flir T540** model with spectral range of 7.5-14 µm and sensitivity of <30Mk @ 30°C. The detailed specifications of the camera are given in **Table 2.2**. InfraRed camera was hand held and used to capture thermographic images from an approximate distance of 1m away from the specimen. The images can be digitized using a Flir Tools Professional Software (Flir Make) provided with the camera.

3.6.2 Heat Source

Two different heat sources were used as tool for active infrared thermography. There is no need to paint the surface of concrete in both techniques as the emissivity of concrete is 0.95.

i. Heating Oven

The energy source used for the heating of the cubical specimens was an oven with the operating temperature range from 10-500° C different heating time was adopted for different samples. The oven was used as source of heating because it was an easy and effective way to enduce uniform temperature in the whole specimen.

ii. Gas Welding Technique

For heating the embedded bar in concrete for monitoring the corrosion, the heating source employed was gas welding torch. Oxy-acetylene gas was used as fuel in this method. In this process the flame directly strikes the part to be heated. The temperature of the flame can be controlled by regulating the valves for each gas which control the flow of gases inside the torch. The temperature of the flash was around 300°C.

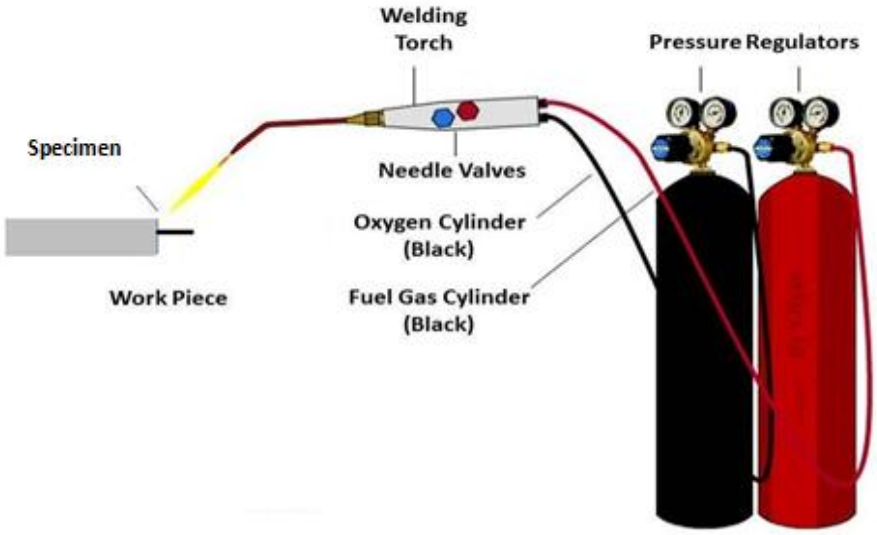

Figure 3.7: Gas Welding Setup [46]

3.7 TEST PROCEDURE

3.7.1For Surface Defects

Cement mortar cubes of 70.6mm × 70.6mm × 70.6mm with surface impressions were heated in oven for 2 hours at 90°C for uniform distribution of temperature in the whole volume. Thermal

images were taken every minute for 30min to check the change in the thermal image and temperature pattern in the cement mortar cubes at the place of the surface impression.

3.7.2For Mechanical Cracks

a) *Bricks and Interlocking Tile*: All three types of bricks were tested in compression. The bricks are placed on flat plate and compressive load is applied uniformly at the rate of 140kg/sqcm/mm till the failure of the bricks. Thermal images were taken every 30 seconds from the time the bricks were taken out from the oven to the cooling the bricks when it is completely broken under compression. Thermal image for the interlocking tiles is taken till the first crack appears on the surface.

b) *Cement Mortar:* Cement mortar cubes of 70.6mm × 70.6mm × 70.6mm and cement concrete cubes of 150mm × 150mm ×150mm were subjected to compression testing [**18**] at 7 and 28 days of curing. Before placing the specimens in UTM, the cement mortar cubes were heated in oven for 2hours and cement concrete cubes were heated for 3hours till heated at 100°C. The load is applied at the rate of 140kg/sqcm/mm. The capacity of the testing machine is 500 kN. Thermal images were taken every minute from the time the specimens were taken out from the oven to the cooling the specimen when it is completely broken under compression.

c) *Cement Concrete*: Further the cracks were also pictured during tensile testing on cement concrete cubes of 150mm × 150mm ×150mm size in the UTM diagonally. The cubes were placed on its sides between two centrally placed strips so that tensile failure occurs in a vertical plane between the places where the loads were applied. Concrete cubes were heated in oven for 3hours at 100°C before placing them in the UTM. Thermal images were taken every 20sec till the failure of the specimen. It was not possible to take the images of specimen on cooling because of the sudden failure of the specimen and splitting of it in two immediately after failure.

3.7.3 For Detecting Embedded Defects

For detecting the sub-surface defects embedded in concrete cubes, the specimens were heated in oven for 200mins to ensure uniform temperature distribution in the whole volume. Thermal images were taken from the time the when specimens were taken out from oven to the cooling time duration varying between 60 to 120 minutes for defects at different cover depths and defects. The temperature distribution was recorded every 30 sec using IR camera.

3.7.4 For Delamination of GFRP sheet

The GFRP wrapped RC cube with seeded artificial delaminations to be investigated was heated in oven for 10-30mins at 50°C. Thermal images after the heating period of 10min, 15min and 30min to the cooling of the specimens were taken. Thermal images were taken till there was no temperature difference visible on the imaging camera. The test was regulated in a way that the maximal temperature of the surface of the specimen was not greater than the temperature of the adhesive material (epoxy) used during the bonding of GFRP to the surface of cube.

3.7.5 For Defects in Rebar

- ***Simulated Defects in Bars***

Bars with different kinds of seeded defects like V-notch, threads, corrugations, etc. were heated in oven at 60°C for one hour so as to ensure uniform heating throughout the rod. Thermal images were taken by placing the rods on the white background to avoid any contrast in the image.

- ***Corrosion Damage***

Two RC slab specimens embedded with steel rebar with no corrosion and accelerated corrosion were investigated for corrosion damage using IRT. Gas welding torch was used to heat the embedded bar in slab. The flames directly used at the node from where bar was exposed to the environment. Each node was alternately heated for 1min and this process continued for 30 minutes. When heating the bar with the welding rod heat energy take time to reach the center of the bar and because of this heating process is long. Thermal images are captured from the initiation of the test to the time till the embedded bar was seen i.e. till the cooling of the specimen. The cooling period was 120minutes.

3.8 CLOSING REMARKS

Various Kinds of damages inflicted like voids, delaminations, corrosion and cracks in various kinds of material specimens like mortar, cement concrete, bricks, interlocking tiles and steel bars were monitored using InfraRed Thermographic Technique. The details of various kinds of defects are discussed in detail in IRT technique and the principle of same are detailed in the chapter.

CHAPTER 4

RESULTS AND DISCUSSION

4.1 INTRODUCTION

In this work, the application of active infrared thermography to detect the various kinds of defects in various civil engineering applications is studied. The efficiency of the technique to detect the defects at different cover depth was also checked to ensure the sensitivity of the technique. The effectiveness of the technique to observe the surface, subsurface, delamination and defects and corrosion was investigated in detail and the results are presented below:

4.2 MONITORING OF THE SURFACE DEFECTS

The thermal images of some surface defects inflicted on the cement mortar were captured

Images were taken after heating the cubes in oven for 2 hours at 90°C.

- thumb impression,
- V-groove with the help of shovel (8mm deep)
- small holes 5mm in diameter and 7mm deep

(a) Actual image of cement mortar cube with 7mm deep holes

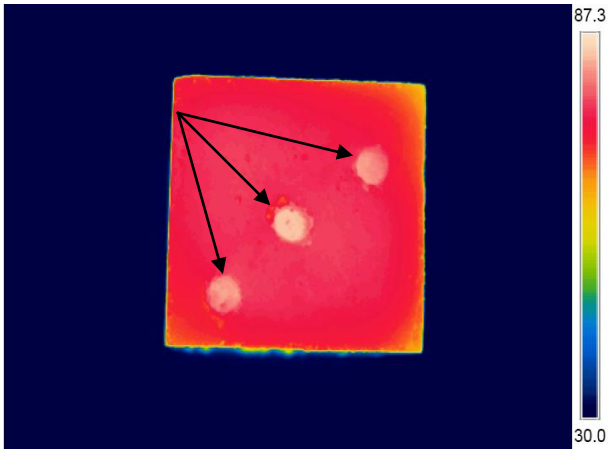

(b) Thermal image of cement mortar cube with 7mm deep holes

(c) Actual image of cement mortar cube with 8mm deep V-groove

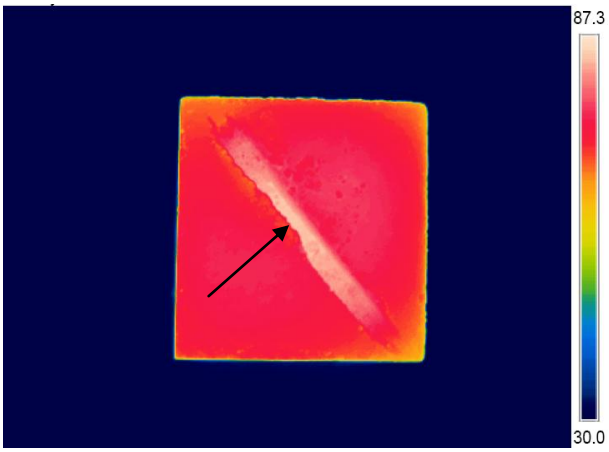

(d) Thermal image of cement mortar cube with 8mm deep V-groove

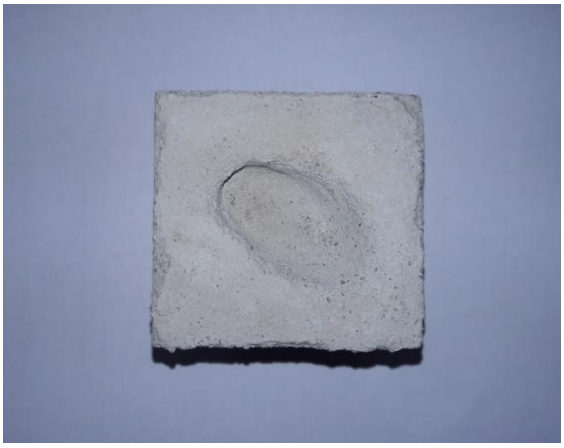

(e) Actual image of cement mortar cube with a thumb impression

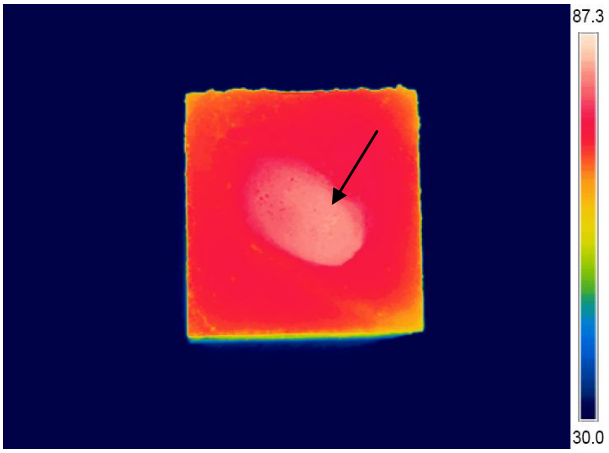

(f) Thermal image of cement mortar cube with a thumb impression

Figure 4.1 : Actual and Thermal image of cement mortar cube with surface defects

The following observations are made from the thermal images of cement concrete cubes inflicted with surface defects:

- The surface defect appears as the hot spot in the thermal image **Figure 4.10 (b), (d) and (f)**. It is because of retention of the heat energy by these shallow defects.
- These surface defects simulate the actual construction defects that can occur during the construction period of the structures.
- InfraRed Thermography helps to capture these defects easily by creating the colour contrast due to the temperature change and can easily pick up the surface damages.

4.3 MONITORING OF THE MECHANICAL CRACKS

The process of cracking in solids i.e. mortar, concrete, rock, etc is accompanied by the loss of energy that dissipates through different forms. The elastic strain energy that is initially stored in these solids contributes to three great mechanical losses that occur during the process of fracture. The three major losses are surface energy loss which is due to the loss of atomic bonds at the moving crack tip, loss due to the conversion of strain energy into kinetic energy and the loss by the plastic deformation in the crack tip i.e. plastic energy. This dissipation of energy occurs through heat exchange. IRT is used to discover the heat generated at the tip of the crack when the crack is propagating.

4.3.1 Cracks under Compression

a. *Bricks and Interlocking tile:* Bricks and interlocking tile under compression testing and simultaneously infrared images were taken after subjecting them to heating at regular intervals to pick up the cracking.

- Simple Brick

(a) Actual Image at initiation of test

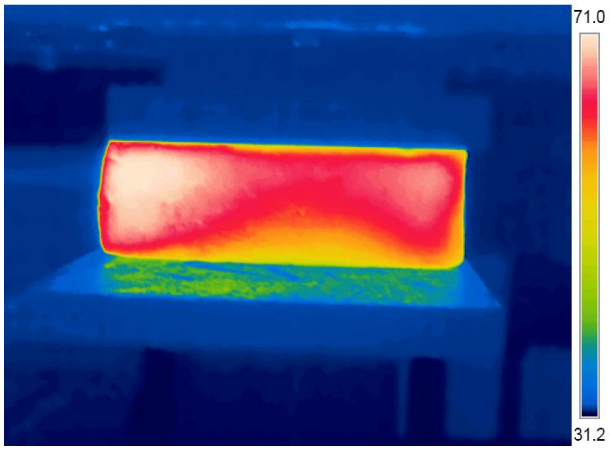

(b) Thermal image at initiation of test

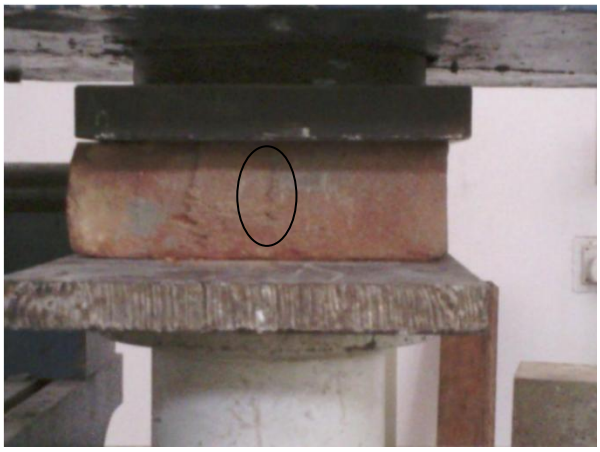

(c) Actual Image at first major crack

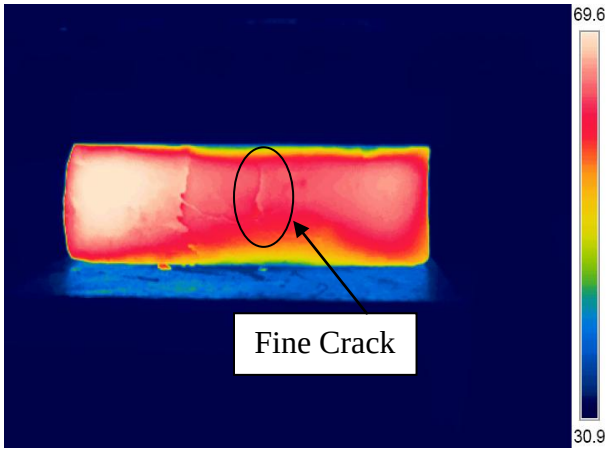

(d) Thermal image at first major crack

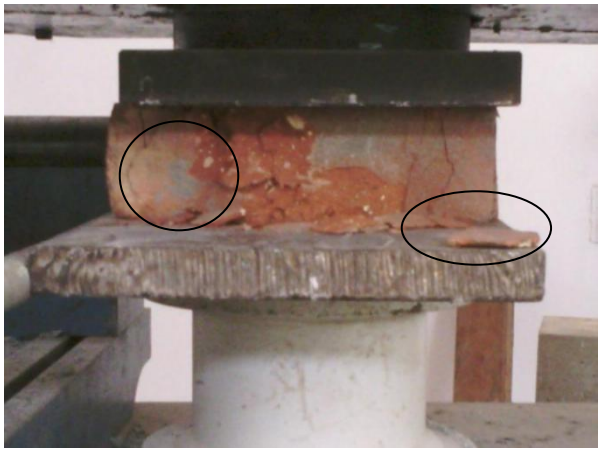

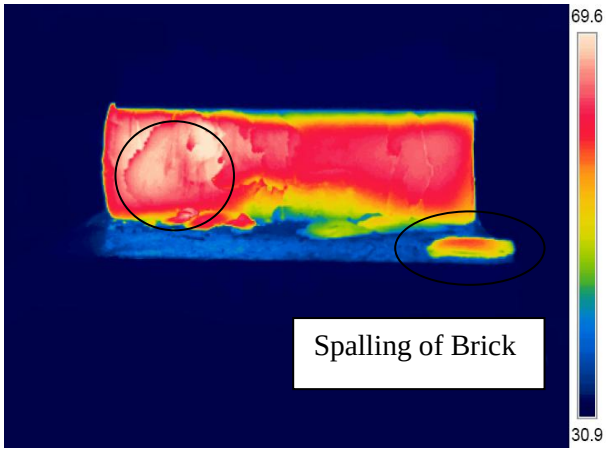

(e) Actual Image at ultimate load **(f) Thermal image at ultimate load**

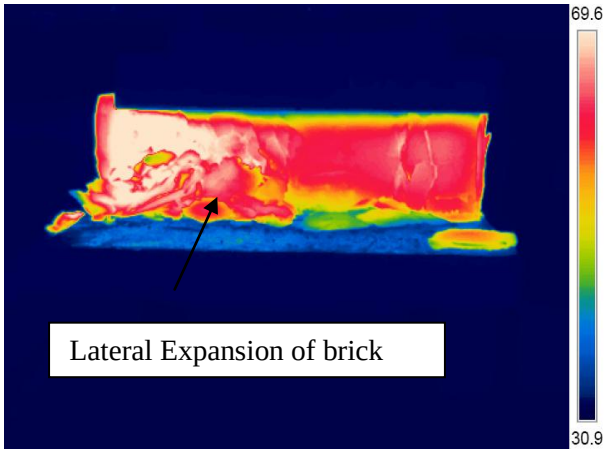

(g) Actual Image at failure **(h) Thermal image at failure**

Figure 4.2: Actual and Thermal image of simple brick

- Frog- Filled Brick

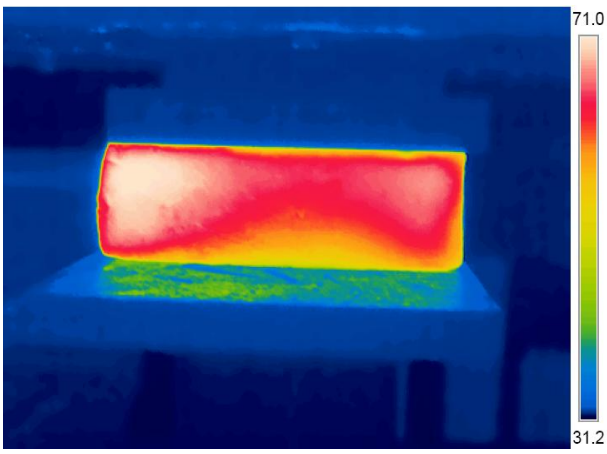

(a) Actual image at initiation of test **(b) Thermal image at initiation of test**

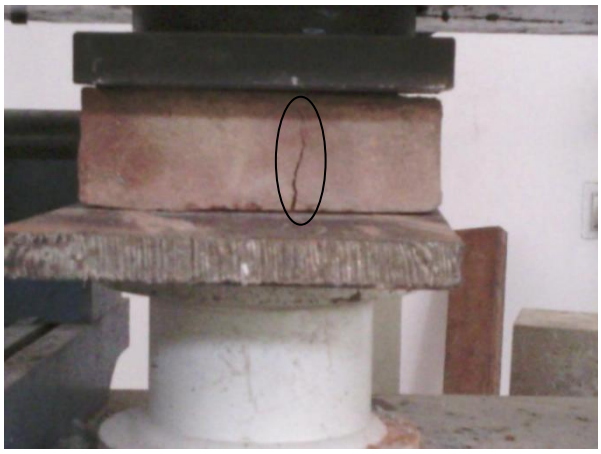

(c) Actual image at first crack

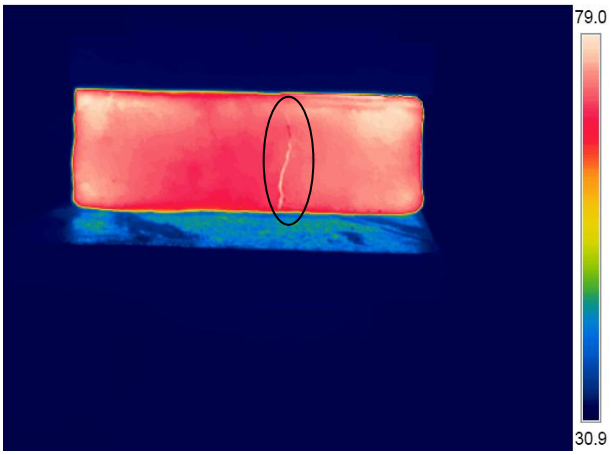

(d) Thermal image at first crack

(e) Actual image at ultimate load

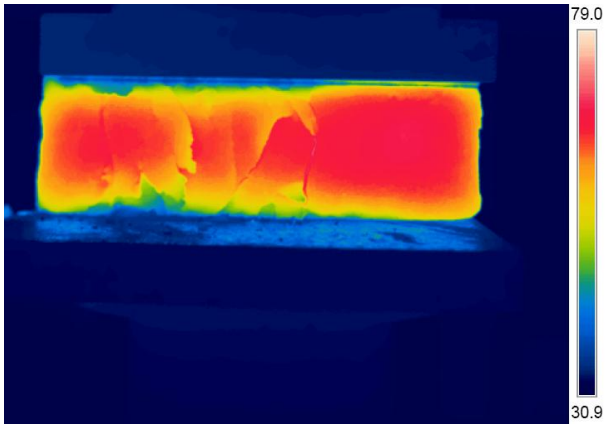

(f) Thermal image at ultimate load

(g) Actual

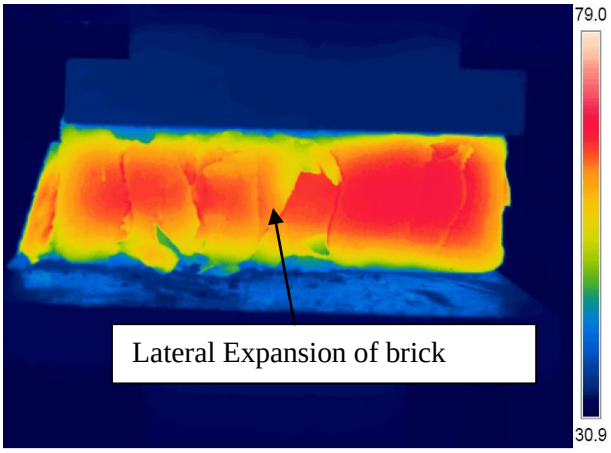

(h) Thermal image at failure

Figure 4.3: Actual and Thermal image of frog filled brick

- Plastered Brick

(a) Actual image at initiation of test

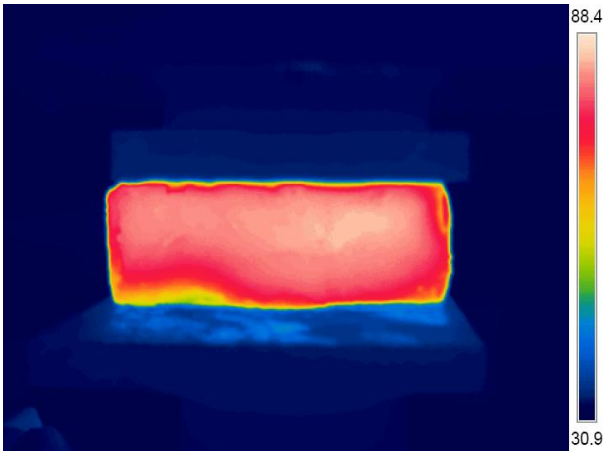

(b) thermal image at initiation of test

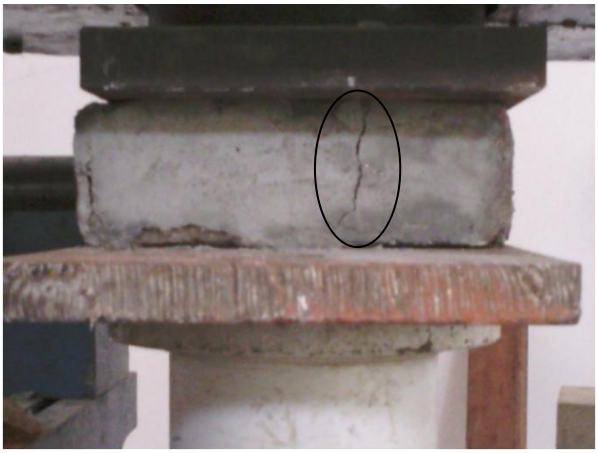

(c) Actual image at first major crack

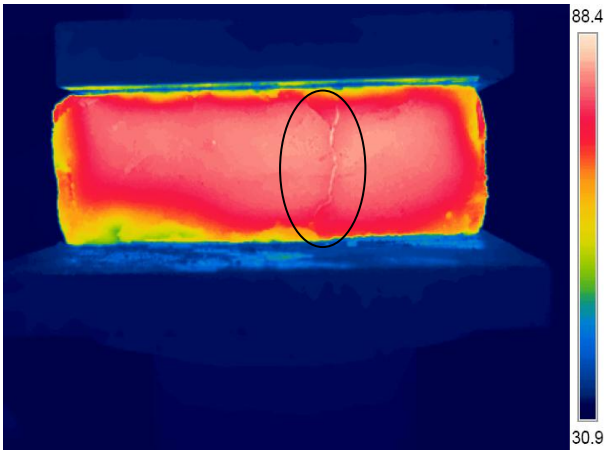

(d) Thermal image at first major crack

(e) Actual image at plaster detachment at the place of crack

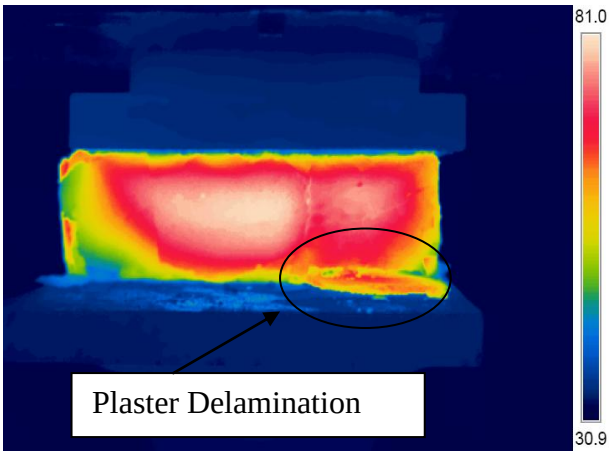

(f) thermal image at plaster detachment at the place of crack

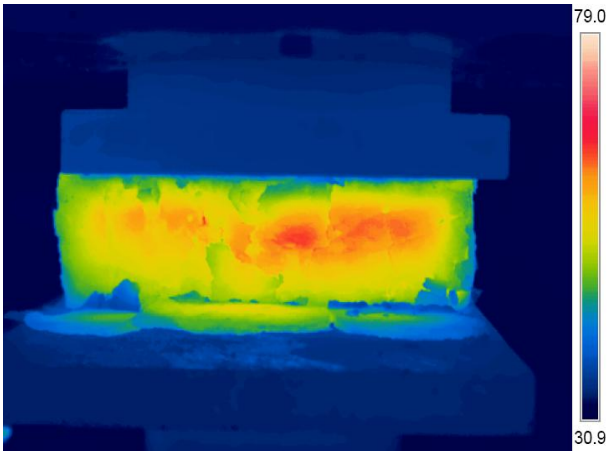

(g) Actual image at failure **(h) Thermal image at failure**

Figure 4.4:Actual and Thermal image of plastered brick

- Interlocking Tiles

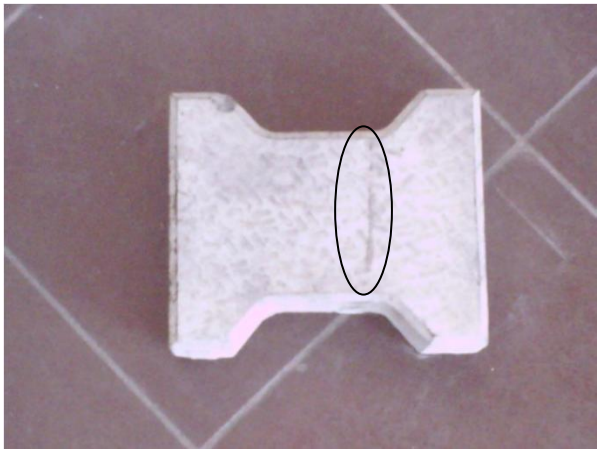

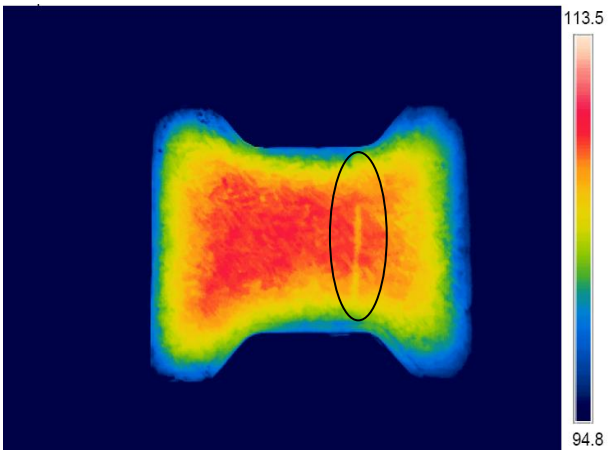

(a) Actual Image at first crack **(b) Thermal image at first crack**

Figure 4.5: Actual Image and Thermal image of interlocking tile

The following key points observed from the thermal images of bricks and interlocking tiles in compression testing are:

- The crack pattern of the simple brick is **Figure 4.2 (d)** not well defined as compared to the frog-filled brick and plastered brick [**Figure 4.3 (d)** and **Figure 4.4 (d)]** respectively.
- Even the finest crack in each of these brick can be captured effectively as there is release of hot air from the crack which is captured by the camera very efficiently.
- Under the increasing load, spalling from the bricks can be seen easily and picked up in case of simple brick **Figure 4.2 (f)** and frog-filled brick **Figure 4.3 (f)** . Lateral expansion and spalling is observed in both simple and frog filled bricks [**Figure 4.2(h)** and **Figure**

4.4 (h)] much before the actual failure from the temperature difference in the thermal image.

- In plastered brick first cracking and spalling is observed in the cement mortar and clearly first major crack is successfully picked up by the IR image **Figure 4.4 (d)**. **Figure 4.4 (e) and (f)** shows the actual and thermal image of the detachment of the mortar piece from the brick during cracking and failure.

  This is because the strength of the plastered brick depends on the strength of the cement mortar and also in this case lateral expansion of the brick is confined by frictional forces at the interface of brick and mortar.

  Due to this greater resistance is offered by cement mortar to the load transfer and this can be the reason for increase in strength for plastered brick.
- IR Thermography also successfully picks up the finest crack in the interlocking tile under compression loading **Figure 4.5 (b)**.
- The IR thermography is able to successfully pick up initiation, progression and ultimate failures and fracture of all types of bricks (simple, frog-filled and plastered) and interlocking tiles.

b. *Cement Mortar:* The mortar cubes were tested after 7 and 28 days under compression testing and simultaneously infrared images were taken after subjecting them to heating at regular intervals to pick up the cracking.

(a) Actual Image at the initiation of test

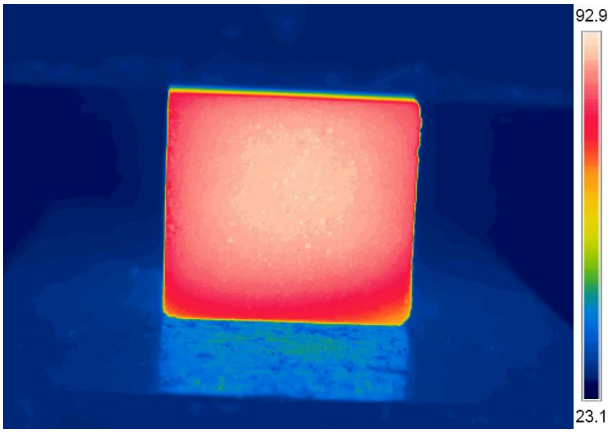

(b) Thermal Image at the initiation of test

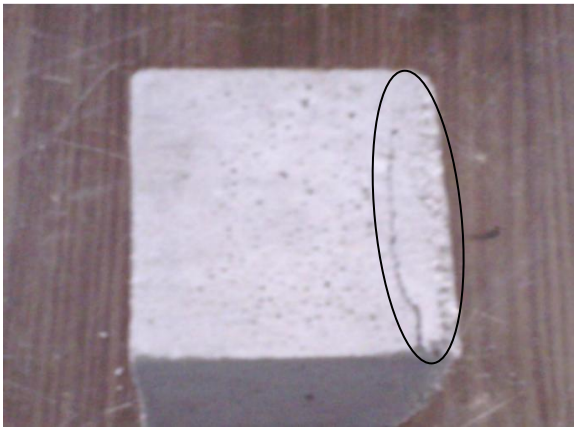

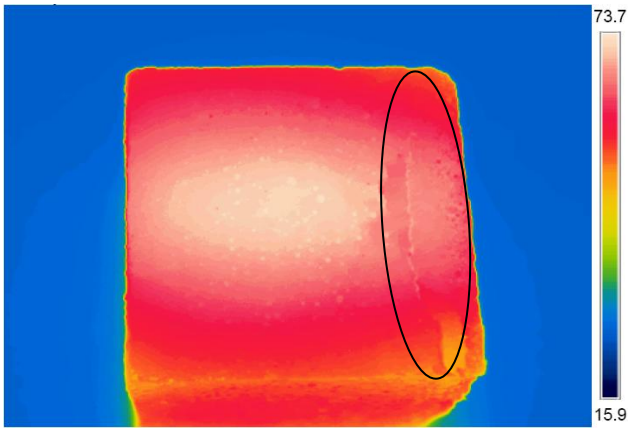

(c) Actual Image at failure **(d) Thermal Image at failure**

Figure 4.6: Actual Image and Thermal Image of Cement Mortar Cube at 7 days curing

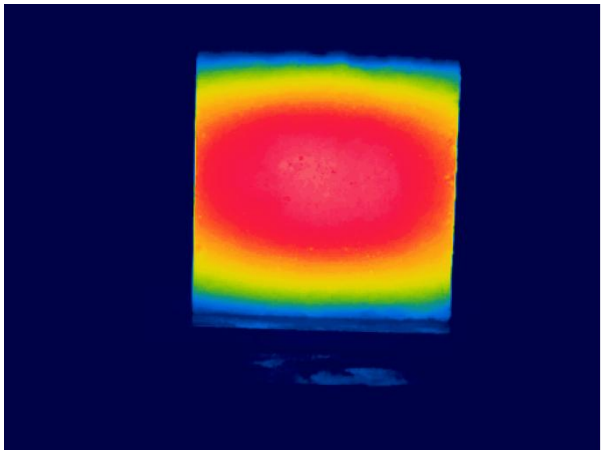

(a) Actual Image at the initiation of test **(b) Thermal Image at the initiation of test**

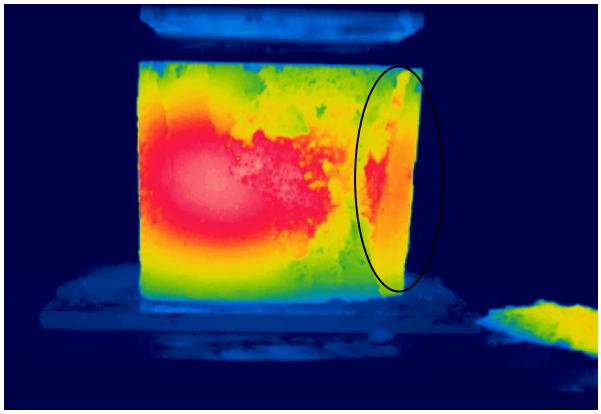

(c) Actual Image at failure **(d) Thermal Image at failure**

Figure 4.7: Actual Image and Thermal Image of Cement Mortar Cube at 28 days curing.

From the actual and IRT images of cement mortar cube at 7 and 28 days of curing in **Figure 4.6and 4.7**, the following observations are made:

- There is slight change in temperature near the centre of the specimen and is affected by thermoelastic stress to the small extent in the centre, resulting that the compressive stresses causing the initiation of the crack are concentrated near the center and not near to the contacts.

  Mortar is a brittle material but instead of using the brittle term quasi brittle is used to describe the initiation of crack and its propagation. During the loading of a mortar specimen, failure is preceded by subcritical cracking. This nucleation of the microcracks is caused by the separation process at the cement sand interface and is known as micro plasticity. For every microcarck, the plastic zone at the tip cannot develop completely. The energy presented in this zone is dispersed on reaching a sand molecule, and the separation of grains stops the microcracks. Grains that are effectively larger or weaker may break, allowing the crack to advance. At the macrocrack level, a damage zone develops ahead of the crack, which results in more microcracks that will eventually link up with each other and with the pre-existing microcracks, and allow microcarck extension. Due to this reason slight temperature change was observed in the mortar specimens.
- Also, from the images of cement mortar specimens after 7 and 28 days of curing in **Figure 4.6 (c) and 4.7 (c)** it is also seen that crack pattern is clearly visible in cubes after 28 days of curing.
- The cracks in the failed cement mortar cubes under compression and the one captured by IRT as shown in **Figure 4.6 and 4.7 (c)** show a close and clear match. This shows that the IRT can clearly pick up the fracture in the cement mortar under compression and can be used as a monitoring tool for cement mortar also like bricks and interlocking tiles.

c. *Cement Concrete:* The study was further extended to monitoring the failure and crack pattern in cement concrete cubes. Thermal images from the beginning of the test to failure of the concrete specimen after 7 and 28 days of curing are shown in **Figure 4.8 and 4.9** respectively.

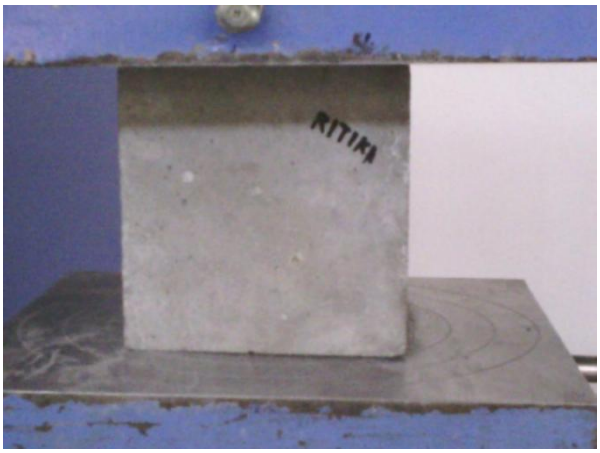

(a)) Actual image at the initiation of test

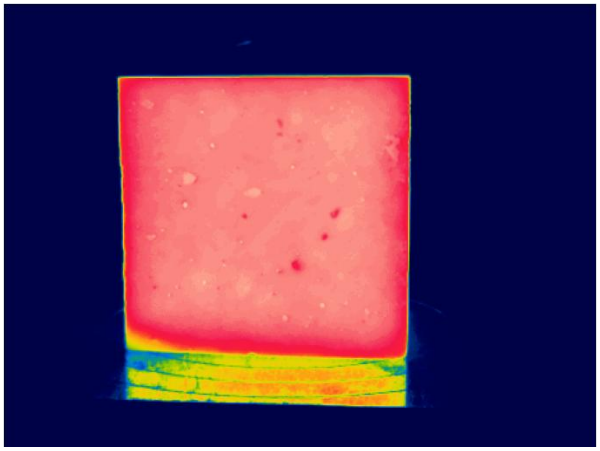

(b) Thermal image at the initiation of test

(c) Actual image at first major crack

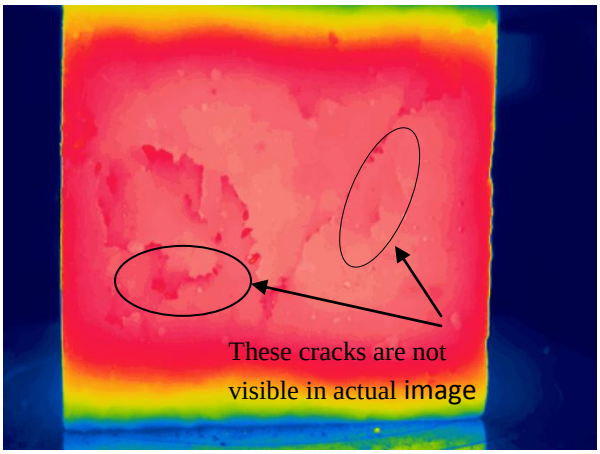

(d) Thermal image at first major crack

(e) Actual image at failure

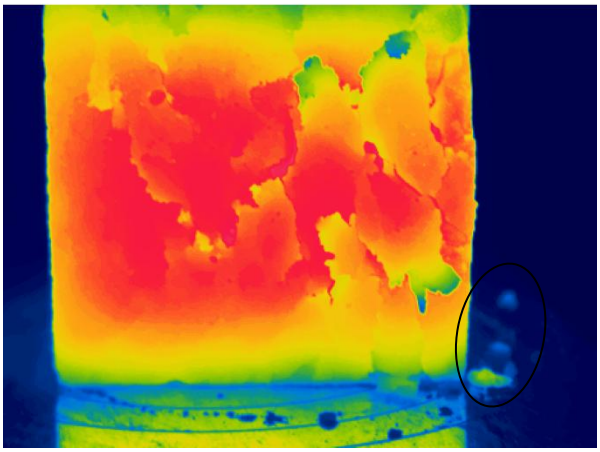

(f) Thermal image at failure

Figure 4.8: Actual and Thermal image of cement concrete cube at 7 days curing

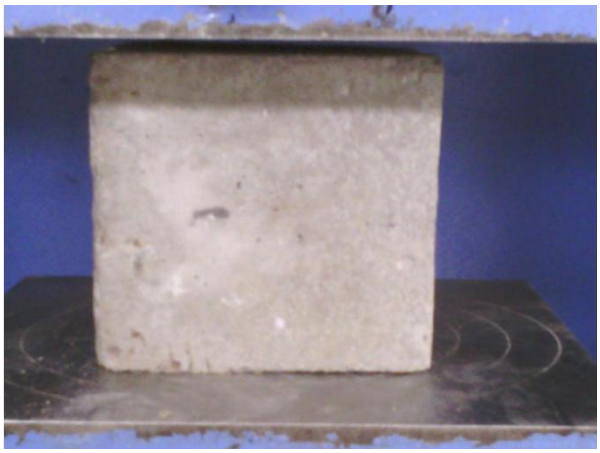

(a) Actual image at the initiation of test

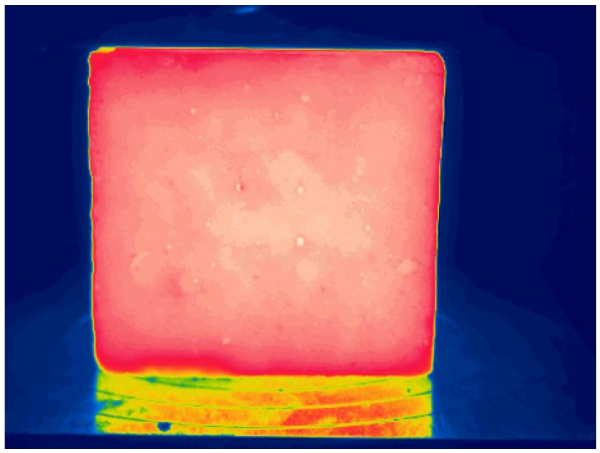

(b) Thermal image at the initiation of test

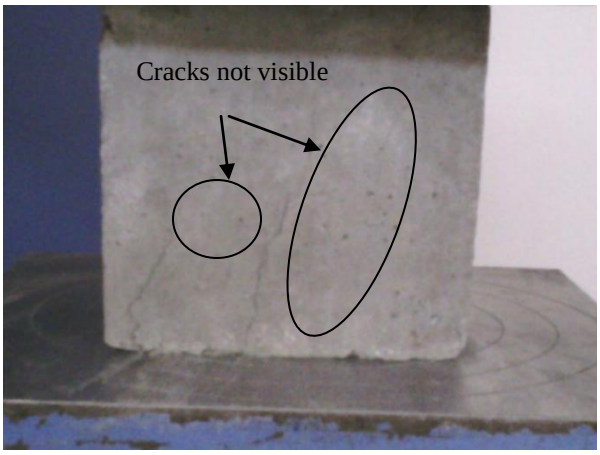

(c) Actual image at first major crack

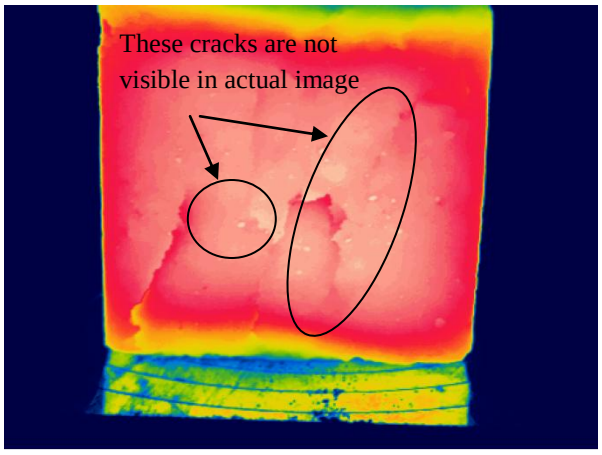

(d) Thermal image at first major crack

(e) Actual image at failure

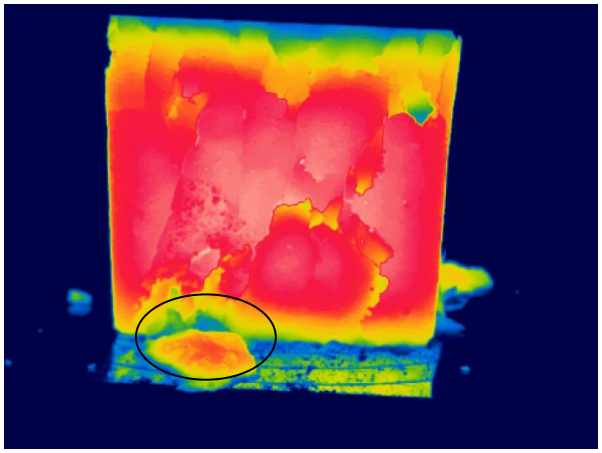

(f) Thermal image at failure

Figure 4.9: Actual and Thermal image of cement concrete cube at 28 days curing

The following observations are made:

- The cracking starts at the two contacts of cube and propagates towards the center of the specimen.

- The cracking at 7 days initially is picked up by IRT though it is not visible with naked eye. It shows the excellent capability of IRT to pick up cracking much before it is visible to naked eye.
- The failed actual cube and the IRT image at failure shows an excellent match **[Figure 4.8 and 4.9 (e) & (f)].**
- The mechanism of failure in cement concrete can be explained as, under the load application the concrete deforms completely despite of the negligible inconsistency between the aggregates and the matrix which stimulate further breakdown. This failure appears as the microcracking and possibly as the slip at the aggregate- mortar interfaces. At macroscopic level, this disintegration is convoyed by both loss in stiffness and agglomeration of unrecoverable deformations. But before the beginning of the crack, thermomechanical heat exchange occurs when the material is in an elastic phase.

  Plastic deformation creates permanent changes where microcracking and slip occurs. These minute cracks which are not visible in the real image of the specimen can be seen in infrared image as these minute cracks show some temperature difference.

  It is very clear from the thermal image of cement concrete specimens in **Figure 4.8 and 4.9(d)** at 7 and 28 days the small cracks accompanying the major crack are not visible in the actual image of the specimen **Figure 4.8 and 4.9 (c)** (encircled in the image).

- It is seen from **Figure 4.9 (d) and 4.9 (f)** the crack patterns is distinctly visible in the cube specimen tested at 28 days of curing as compared to the specimen tested at 7 days of curing. It is because the concrete acquired the sufficient strength after 28 days i.e. 80-90% of the desired strength. The slip of the aggregates the failure load can be clearly seen in **Figure 4.9(d)** as compared to **Figure 4.8 (d)**.
- Most of the energy required to cause this plastic deformation is dissipated as heat. This development of heat is easily observed when it is produced in a fixed location. Under the uniaxial loading there is increase of the surface temperature where the crack occurs. There is no yielding and the final failure is brittle and followed by little sound.

  Also when the concrete specimens are tested in compression the cracks occurs more abruptly and the thermal images are disturbed by fragments detaching from the surface and flying around as in **Figure 4.8 and 4.9(f)**.

4.3.2 Cracks in Tension

a) Cement Concrete: The study was further extended to monitoring the failure and crack pattern in cement concrete cubes in tension.

(a) Actual image at beginning of test

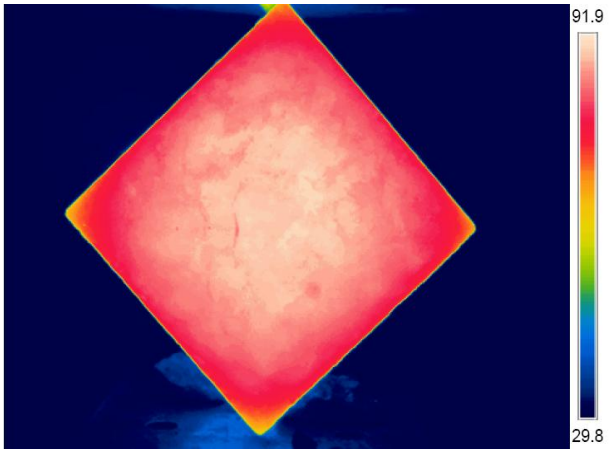

(b) Thermal image at beginning of test

(c) Actual image at initiation of fracture

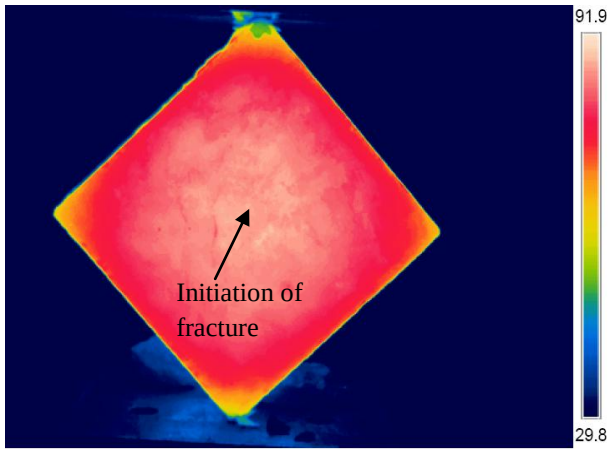

(d) Thermal image at initiation of fracture

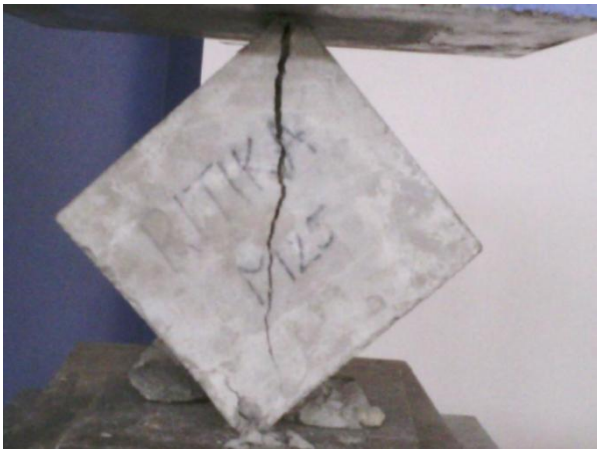

(e) Actual image after 10sec of fracture initiation

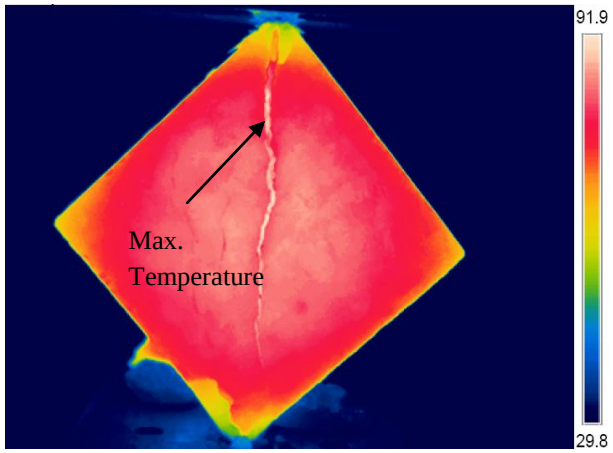

(f) Thermal image after 10sec of fracture initiation

Figure 4.10: Actual and Thermal images under tensile loading at 7 days curing

(a) Actual image at beginning of test

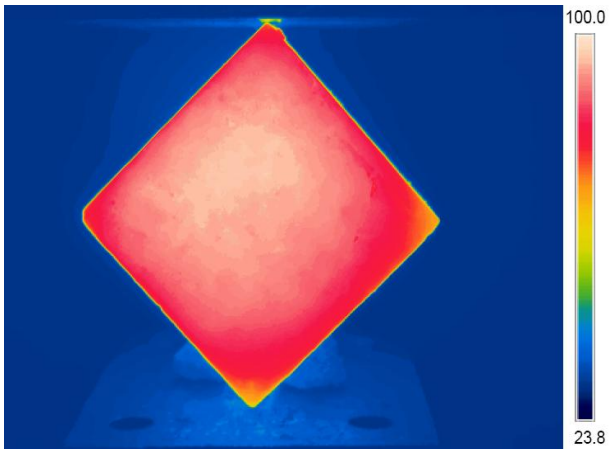

(b) Thermal image at beginning of test

(c) Actual image at initiation of fracture

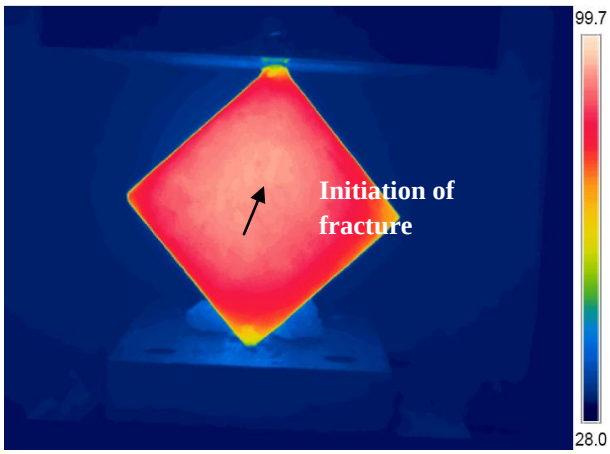

(d) Thermal image at initiation of fracture

(e) Actual image after 20sec of fracture initiation

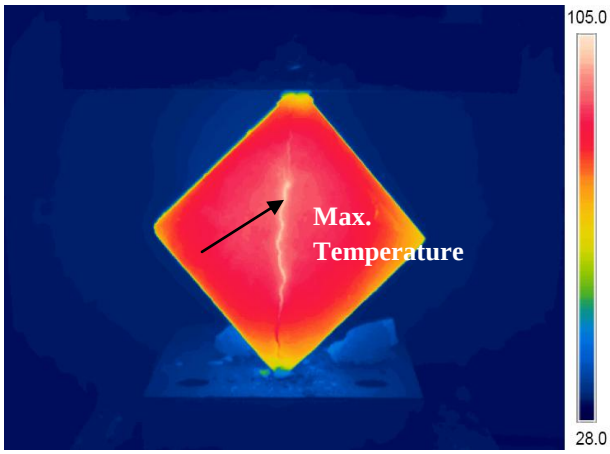

(f) Thermal image after 20sec of fracture initiation

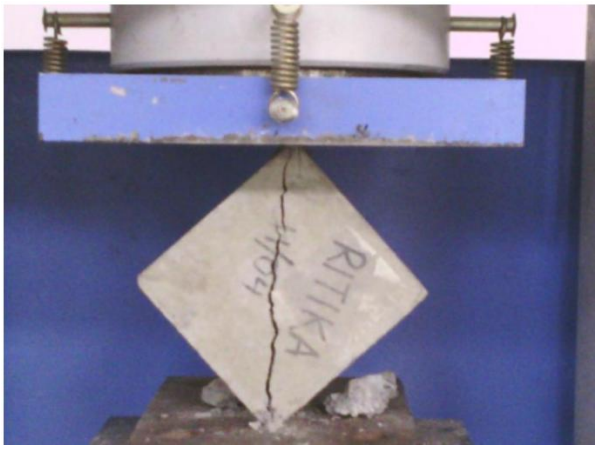

(g) Actual image after 10sec of crack showing that the flanks of crack moving away

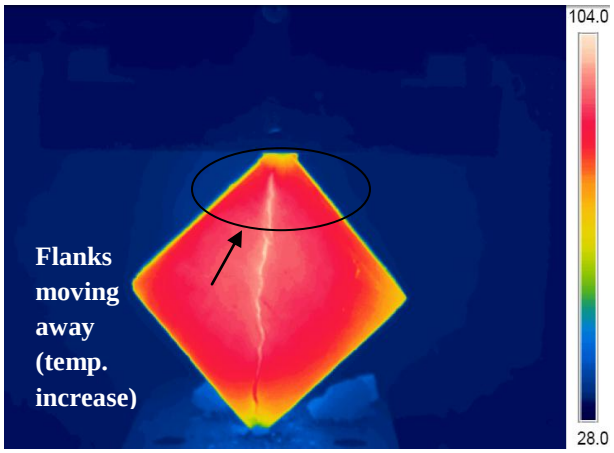

(h) Thermal image after 10sec of crack showing that the flanks of crack moving away

Figure 4.11: Actual and Thermal images under tensile loading at 28 days curing

The followings observations are made from the actual and IRT images of the cement concrete cubes subjected to split tension:

- The propagation of the crack is distinctly visible in the image of **Figure 4.10 and 4.11 (d)** of the specimens after 7 and 28 days of curing. The small area at the centre of the specimens is at high temperature than the surrounding concrete. It is specified that the propagating crack started near the contact before moving to the centre of the specimen and thermographic images were taken simultaneously.
- When flanks of the crack move away, much higher temperature was noticed developing in the location of the crack surface. The thermographic images suggest that the tensile stresses causing the initiation fracture are not concentrated near the centre but at the contacts (**Figure 4.10 and 4.11 (c) & (d)**).

4.4 ARTIFICIAL EMBEDDED DEFECTS IN CONCRETE

a) The cement concrete cube with artificial defects embedded at different cover depths are analyzed after cooling of the heated concrete sample taken out from an external source of heating i.e. oven.

b) Thermograms of the heated samples were taken upto 120 minutes depending on the depth of embedded defects. The details of the defects are given in **Table 3.9**. The thermal

images of all the eight specimens with embedded defects were taken from top during their cooling stage.

a) Wooden Piece at 15mm cover

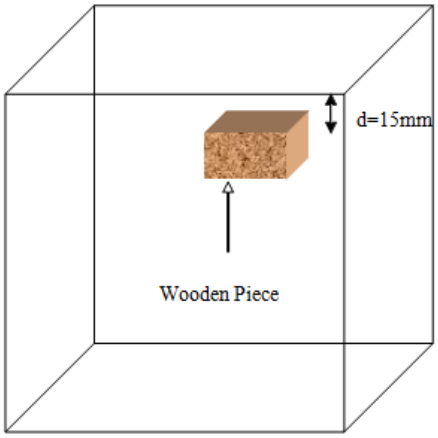

(a) Schematic showing embedded wooden piece

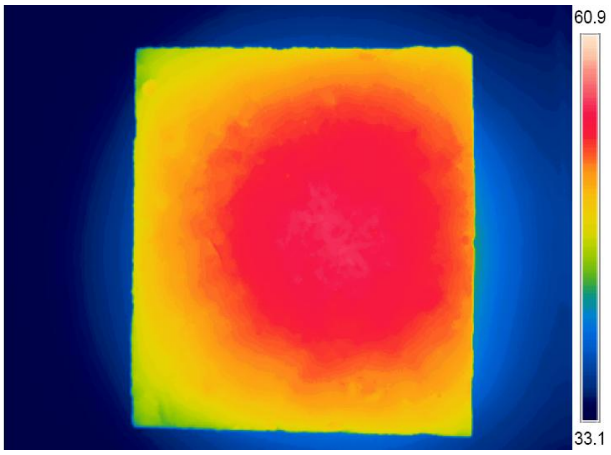

(b) Thermal image after 15minutes

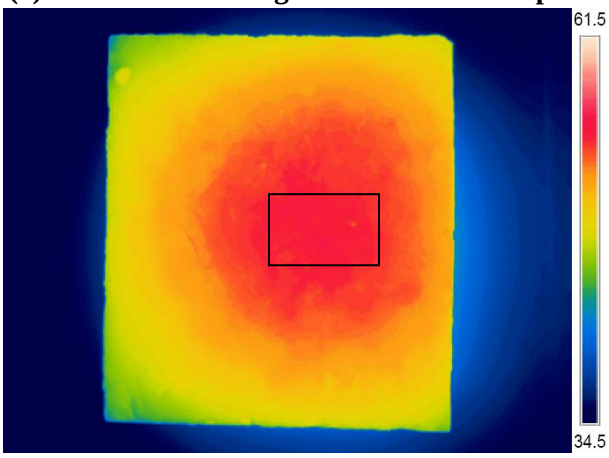

(c) Thermal image after 30 minutes

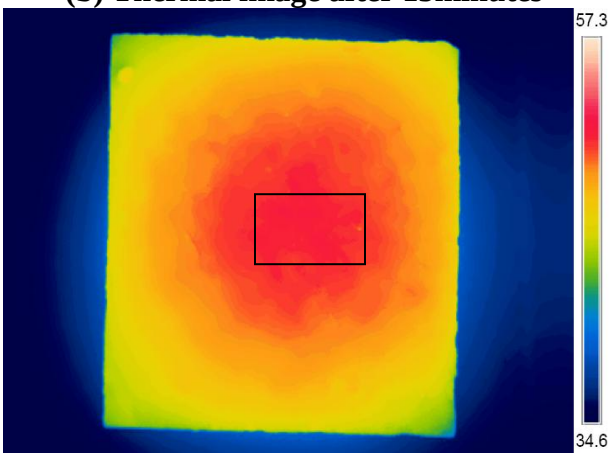

(d) Thermal image after 35minutes

Figure 4.12: Images with wooden piece at d= 15mm

b) Plastic piece at 20mm cover

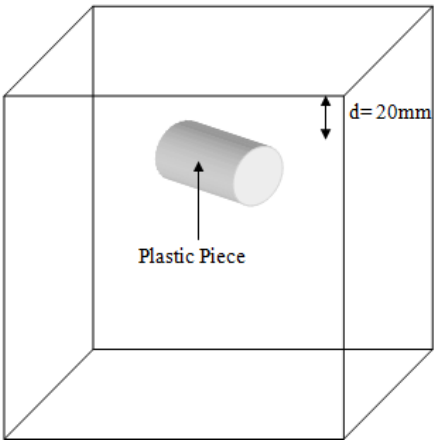

(a) Schematic showing embedded plastic

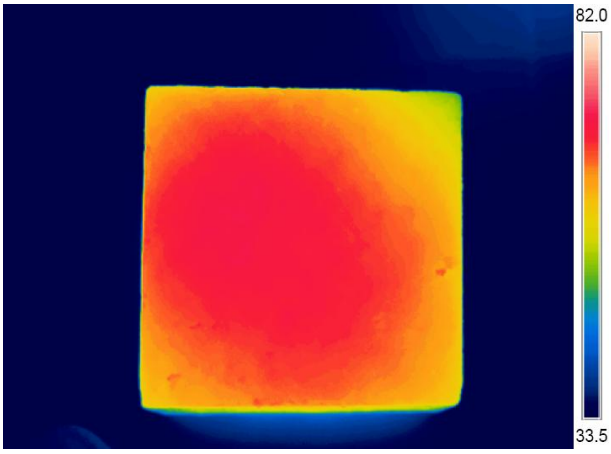

(b) Thermal image after 20 minutes

piece

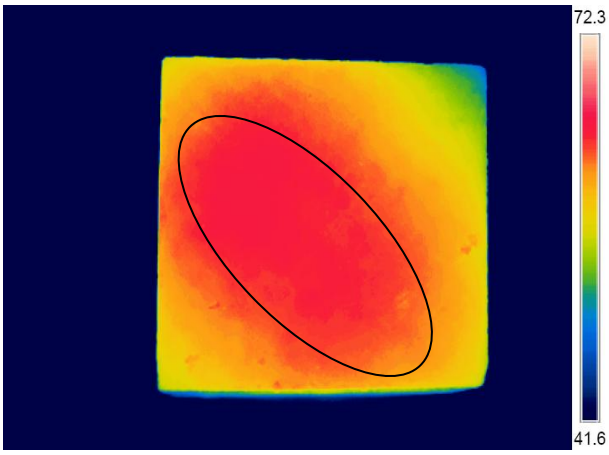

(c) Thermal image after 35 minutes

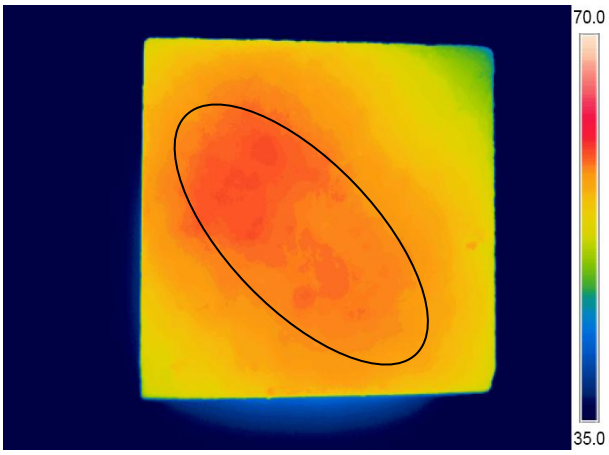

(d) Thermal image after 45 minutes

Figure 4.13: Images with a plastic piece at d= 20mm

c) Piece of Jute at 25mm cover

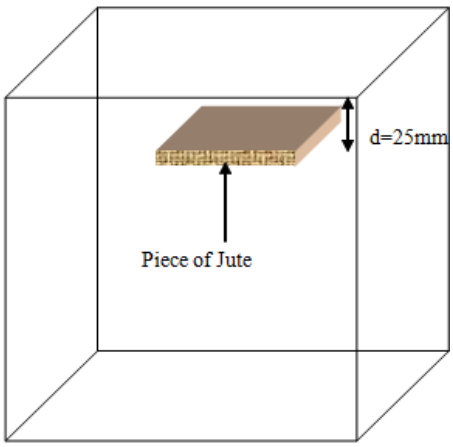

(a) Schematic showing embedded piece of jute

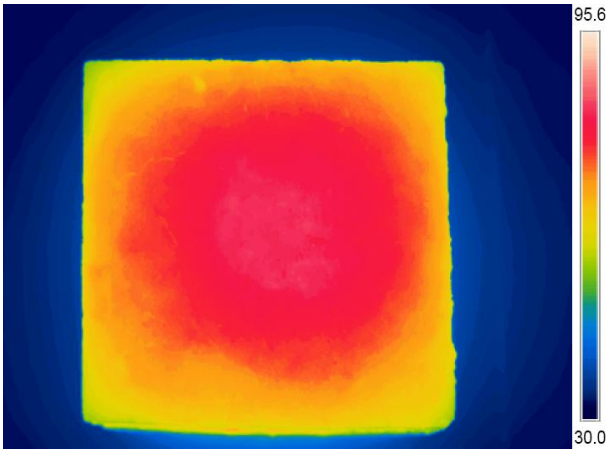

(b) Thermal image after 25 minutes

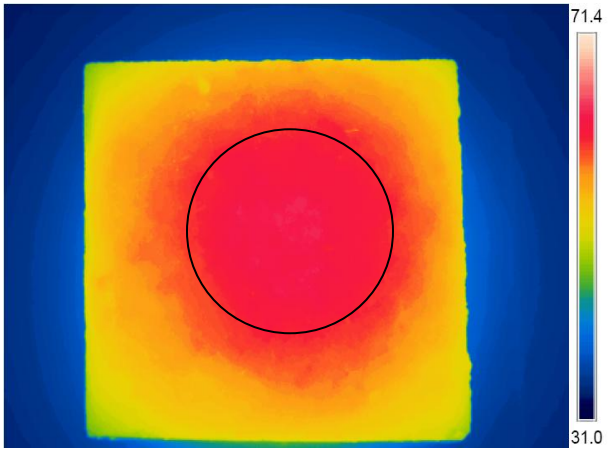

(c) Thermal image after 40 minutes

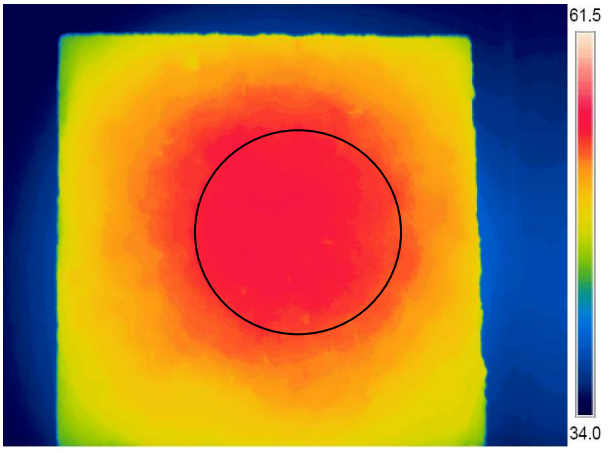

(d) Thermal image after 50 minutes

Figure 4.14: Images with piece of jute at d= 25mm

d) Sponge at 30mm cover

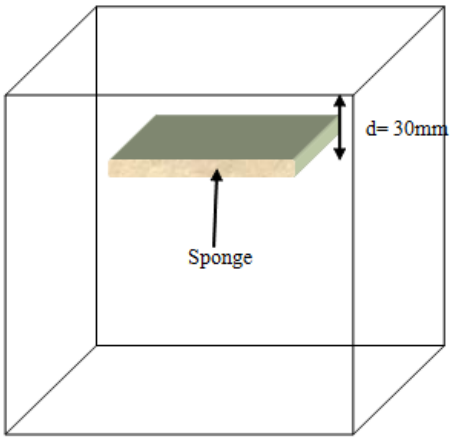

(a) Schematic showing embedded sponge

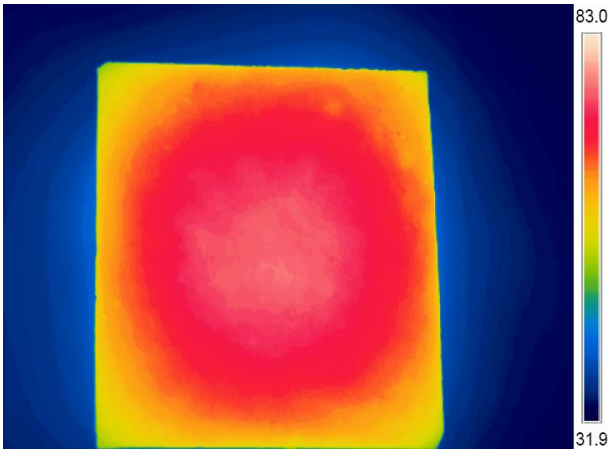

(b) Thermal image after 30 minutes

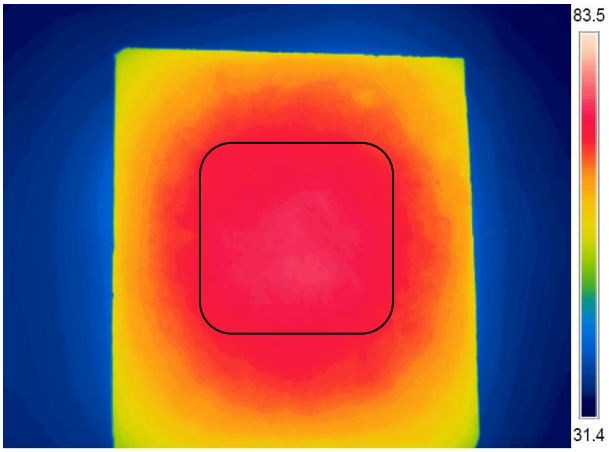

(c) Thermal image after 45 minutes

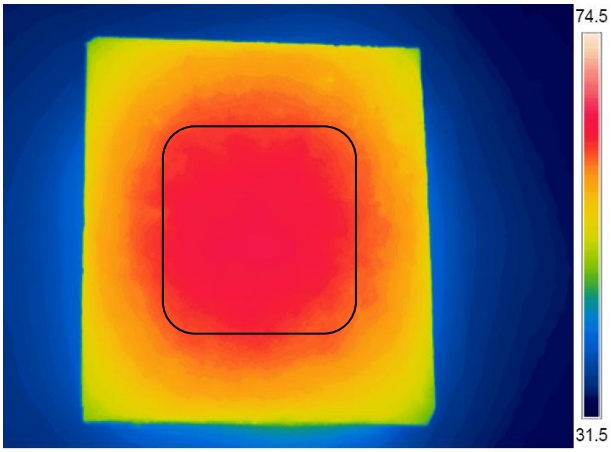

(d) Thermal image after 50 minutes

Figure 4.15: Images with sponge at d= 30mm

c) Plastic Piece at 40mm cover

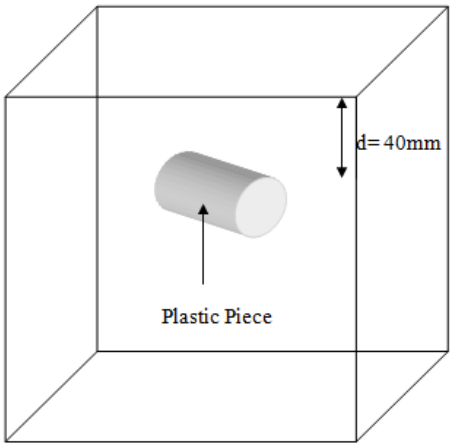

(a) Schematic showing embedded plastic piece

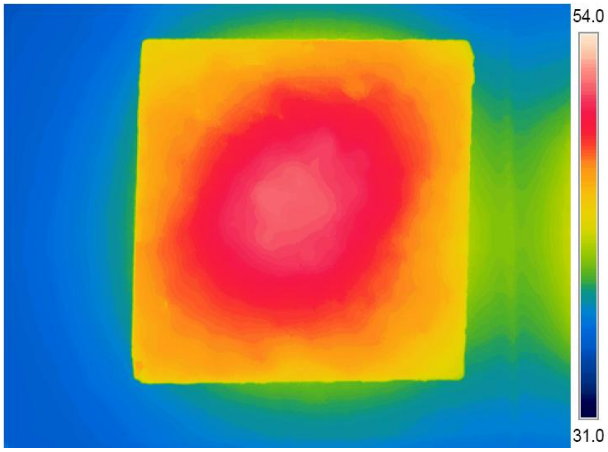

(b) Thermal image after 35 minutes

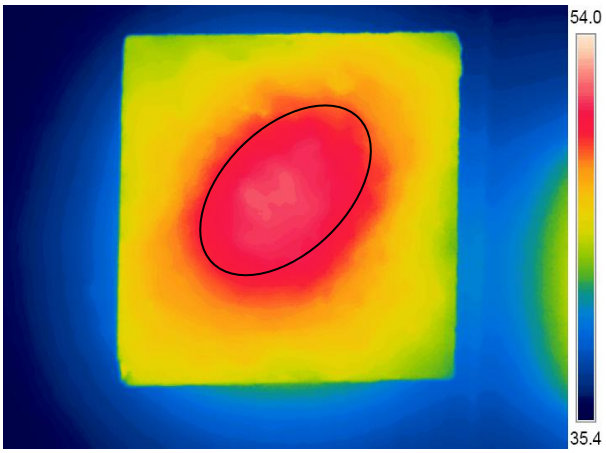

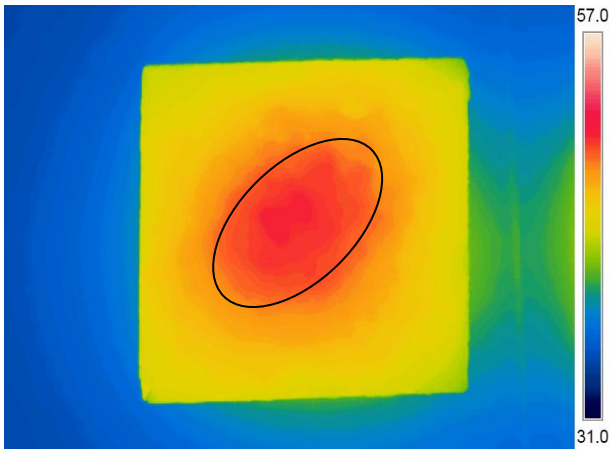

(c) Thermal image after 50 minutes **(d) Thermal image after 70 minutes**

Figure 4.16: Images with plastic piece at d=40mm

d) Glass Piece at 50mm cover

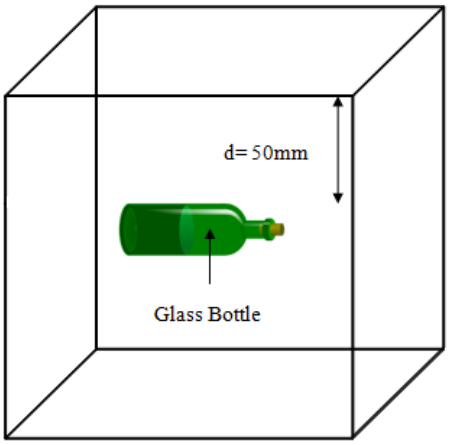

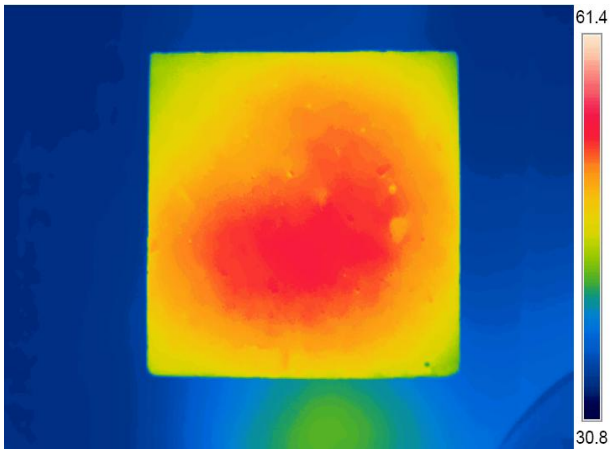

(a) Schematic showing embedded glass piece **(b) Thermal image after 40 minutes**

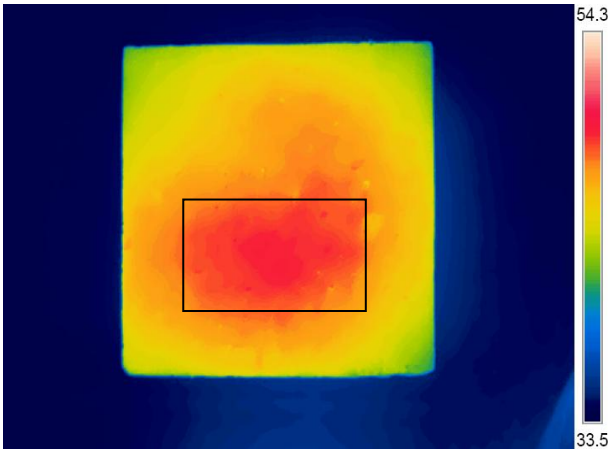

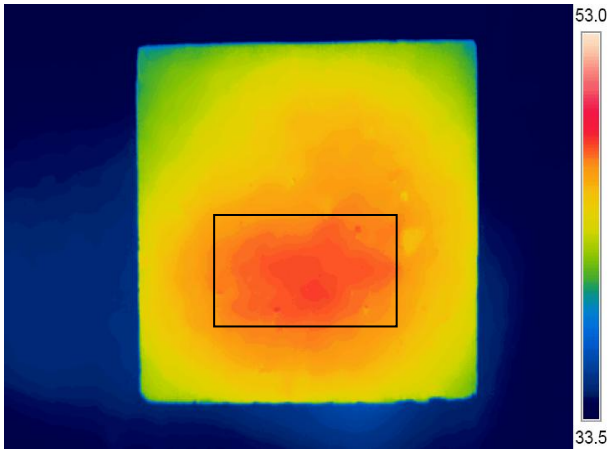

(c) Thermal image after 60 minutes **(d) Thermal image after 75 minutes**

Figure 4.17: Images with glass piece at d= 50mm

e) Plastic box at 60mm cover

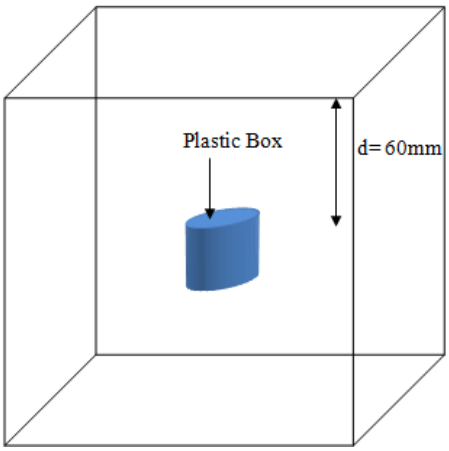

(a) Schematic showing embedded plastic box

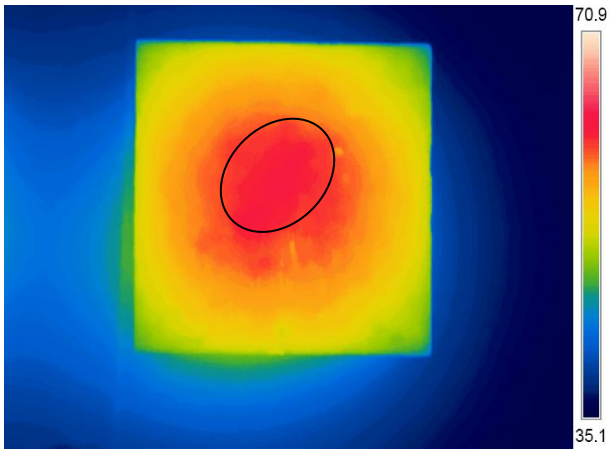

(b) Thermal image after 55 minutes

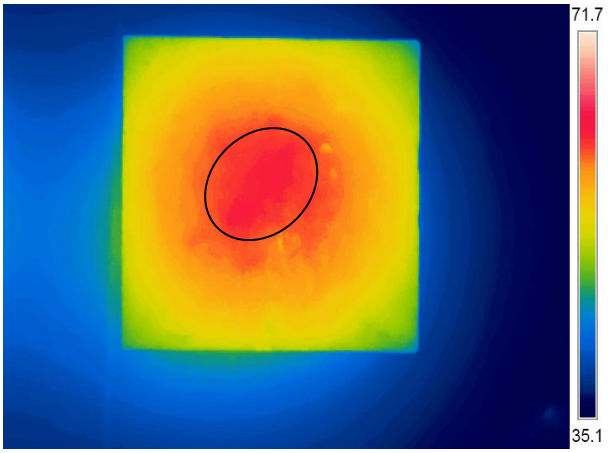

(c) Thermal image after 70 minutes

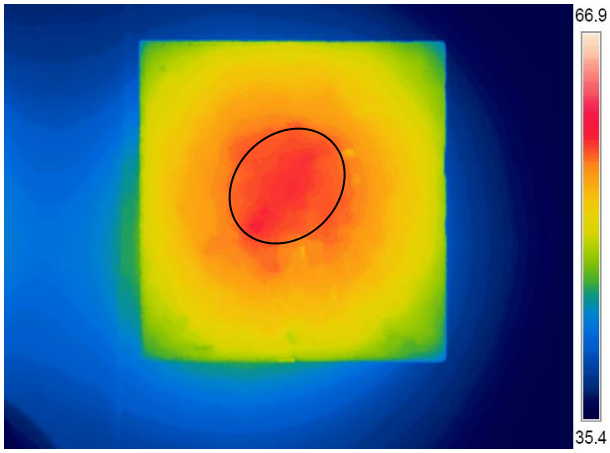

(d) Thermal image after 95 minutes

Figure 4.18: Images with plastic box at d= 60mm

f) Plate at 70mm cover

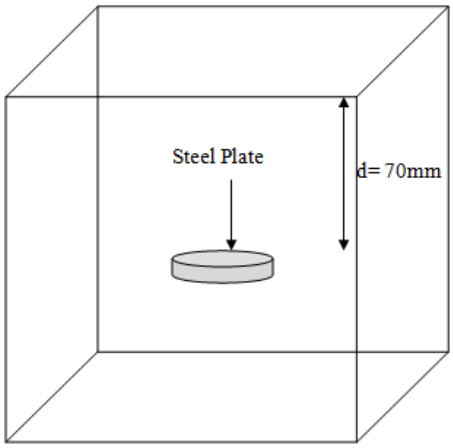

(a) Schematic showing embedded plate

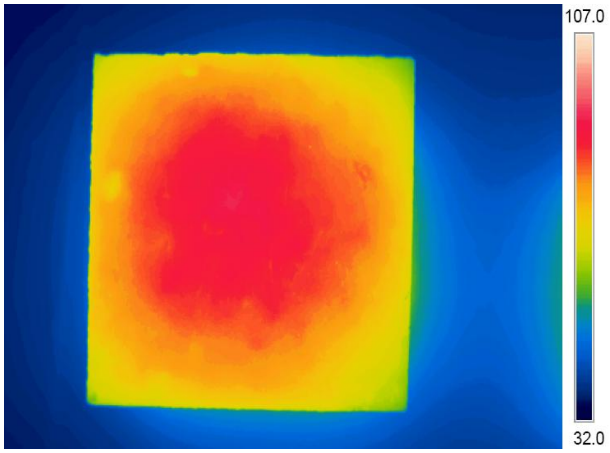

(b) Thermal image after 70 minutes

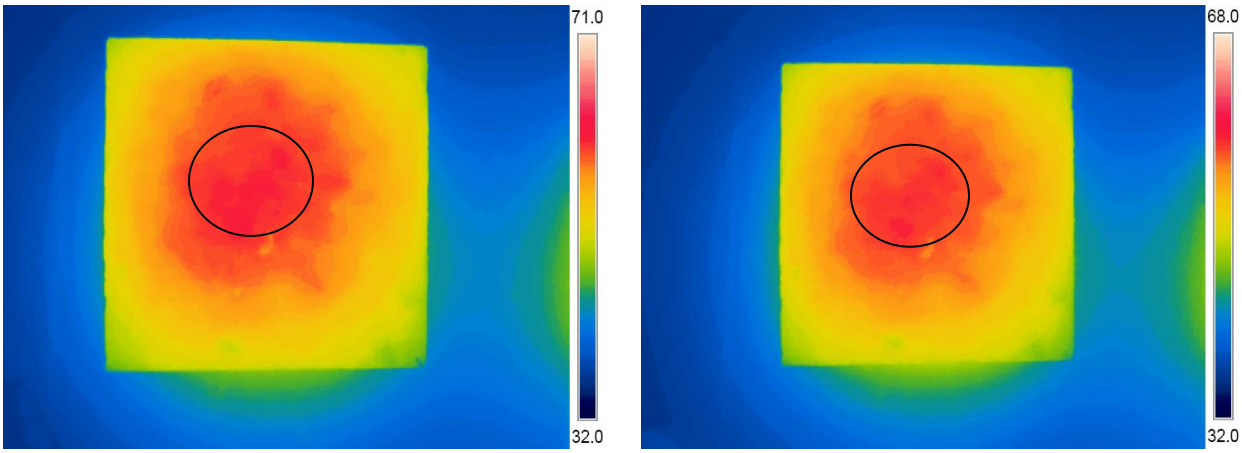

(c) Thermal image after 95 minutes **(d) Thermal image after 115 minutes**

Figure 4.19: Images with plate at d= 70mm

The following observations are made from the thermal images for the artificial embedded defects at different cover depths in cement concrete cubes:

- This study highlights and investigates the capability of IRT technique to pick up defects at different depths of embedment.
- The minimum recording time at which maximum thermal contrast is obtained depends on the depth of the defect '**d**'.
- Shallow as well as deep defects upto 70 mm i.e. middle of the cube was picked up.
- The defects at shallow depth upto 30mm have good contrast after short cooling period while defects at deeper depth appear after waiting for long time. Deeper defects require more cooling time to show a good contrast.
- Cooling time is important for detecting the shape and depth of defect in concrete. Surface of the concrete cube shows a uniform distribution when temperature decreases as in **Figure 4.12 to 4.19 (c)**.
- Weak but still detectable defect was seen at depth of 70mm.

4.5 DELAMINATIONS OF GFRP SHEEET WITH CONCRETE

The GFRP wrapped RC cube with seeded artificial delaminations to be investigated was heated in oven for 10-30 minutes at 50°C. Thermal images after the heating period of 10min, 15min and 30min to the cooling of the specimens are shown in **Figure 4.20 and 4.21**.

a) Specimen 1

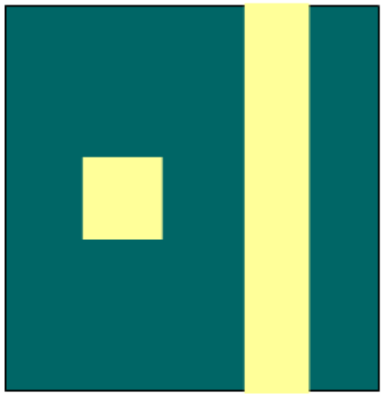

(a) Top View of Speciemn 1

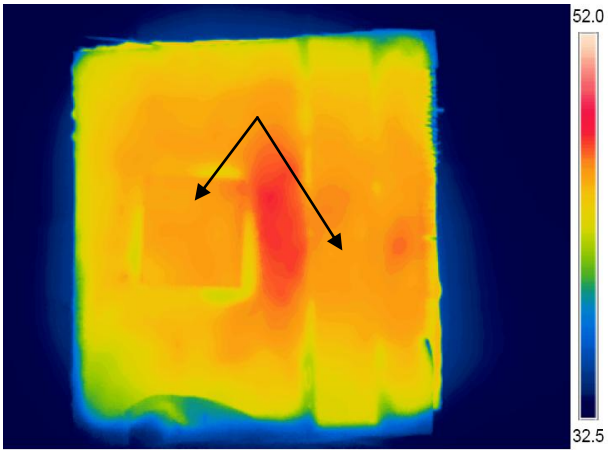

(b) Thermal image after 10 min of heating

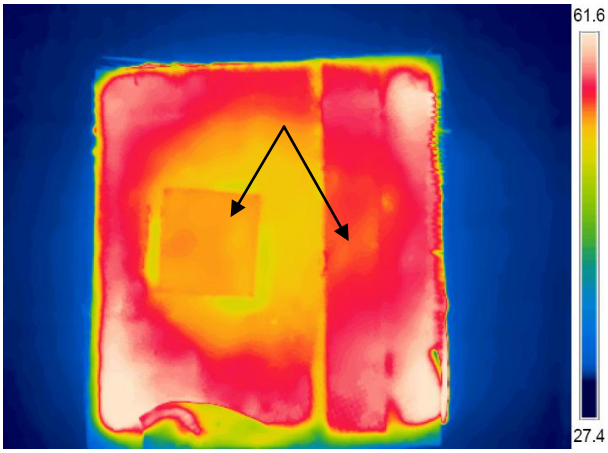

(c) Thermal image after 15 min of heating

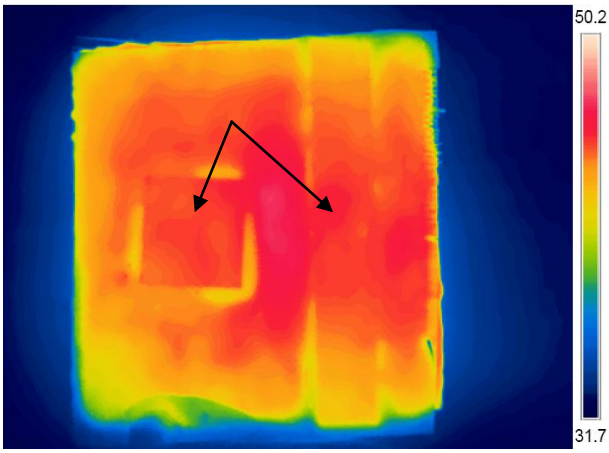

(d) Thermal image of after 30 min of heating

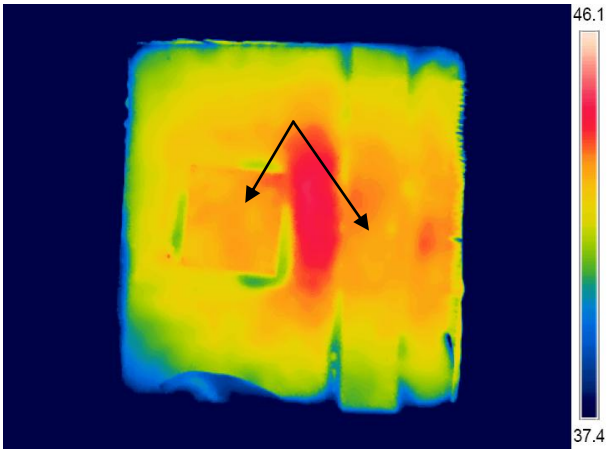

(e) Thermal image during cooling

Figure 4.20: Schematic and thermal images of Specimen 1 from top

b) Specimen 2

(a) Top View of Speciemn 2

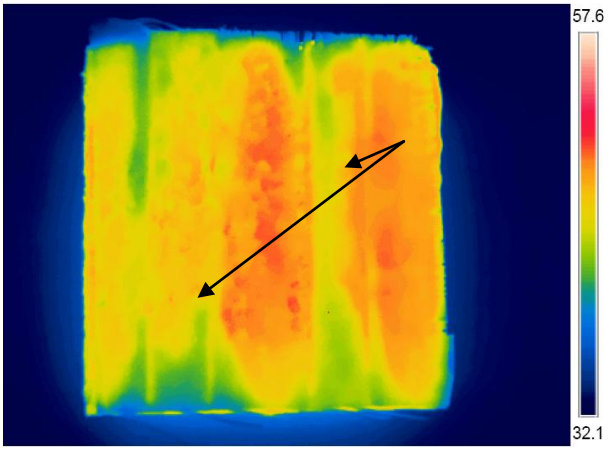

(b) Thermal image after 10 min of heating

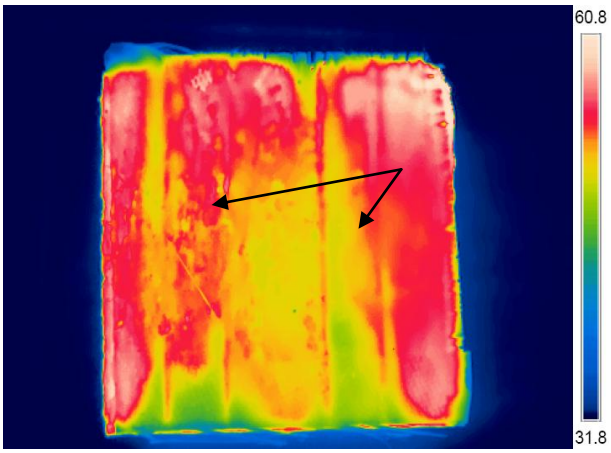

(c) Thermal image after 15 min of heating

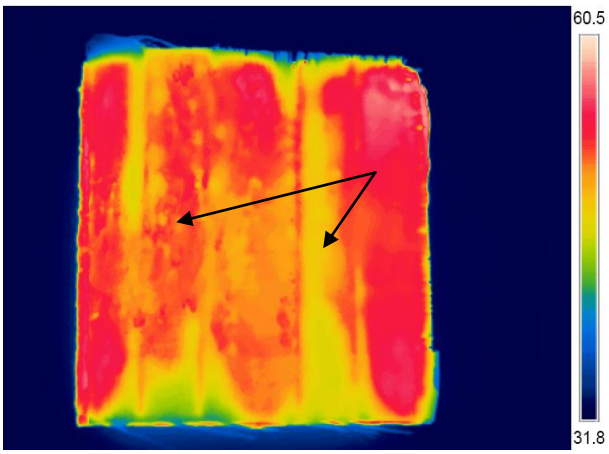

(d) Thermal image after 30 min of heating

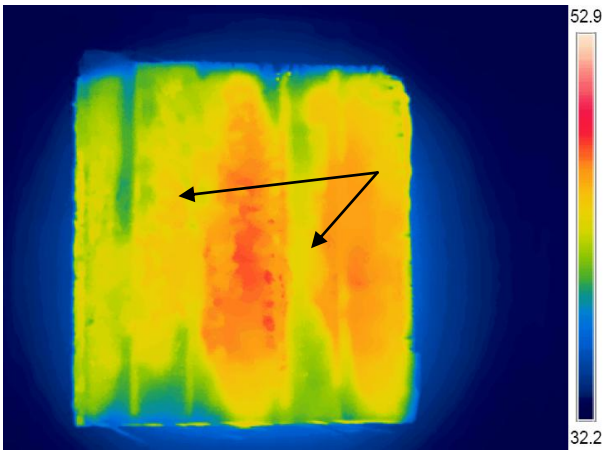

(e) Thermal image during cooling

Figure 4.21: Schematic and thermal images of Specimen 2 from top

- IRT can be successfully implemented not only for picking up fracture, cracking and damages in concrete, bricks, tiles, cement mortar but also debonding failure of FRP repaired or strengthened concrete structures.
- From the thermal images in **Figure 4.20 and 4.21 (b) & (c)** it was seen that simulated debonding and delamination of GFRP from the surrounding concrete can be easily picked up by IRT after 10 minutes of heating and the long strip is visible after the heating of 15 minutes.
- Hot spots appear with the temperature increasing slowly towards the center of the delaminations. The temperatures contrasts are induced to a difference in the thermal properties of the composite material and the inserted artificial debond.
- The thermal conductivity of the artificial delamination is very low which require extra time for the external thermal wave infusion to generate heat wave within the specimen to enable detection.

4.6 DEFECTS IN REBARS

4.6.1 Monitoring of Bars with different surface defects

Thermal images of bars with the seeded defects are shown below:

a) Threads

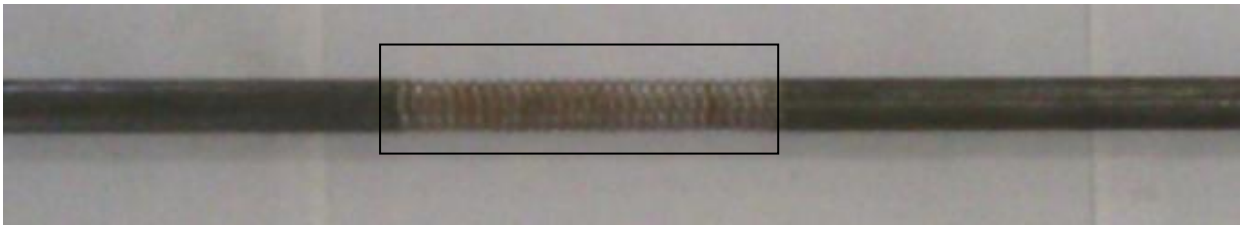

(a) Actual image

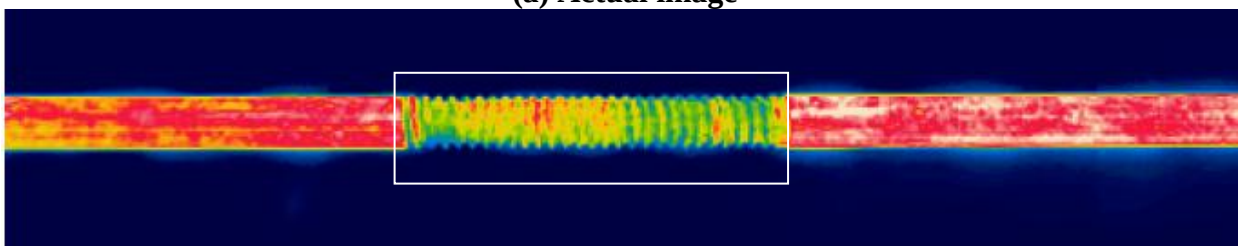

(b) Thermal image

Figure 4.22: Actual and Thermal image of a bar with threads

b) V-notch

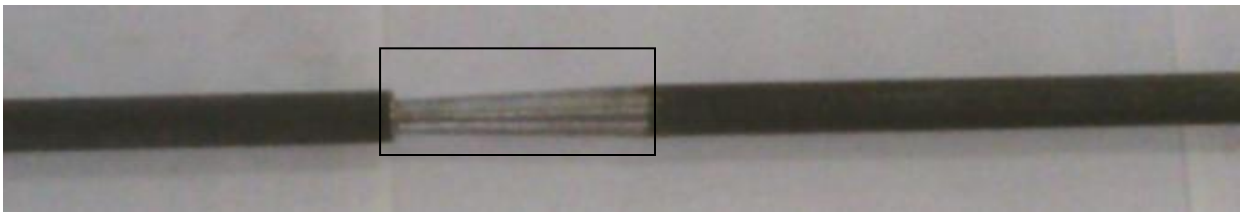

(a) Actual image

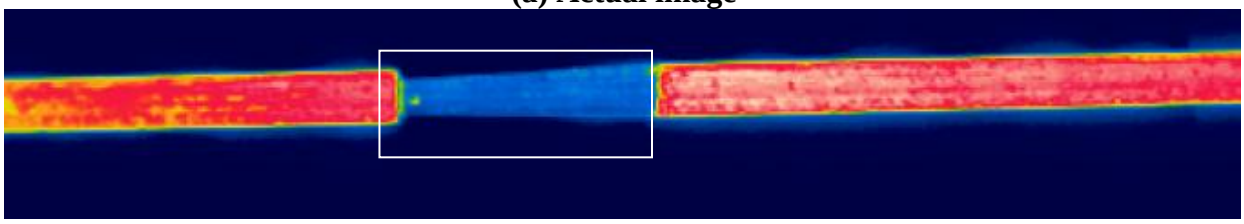

(b) Thermal image

Figure 4.23: Actual and Thermal image of a bar with V-notch

b) Circumferential Reduction in Diameter

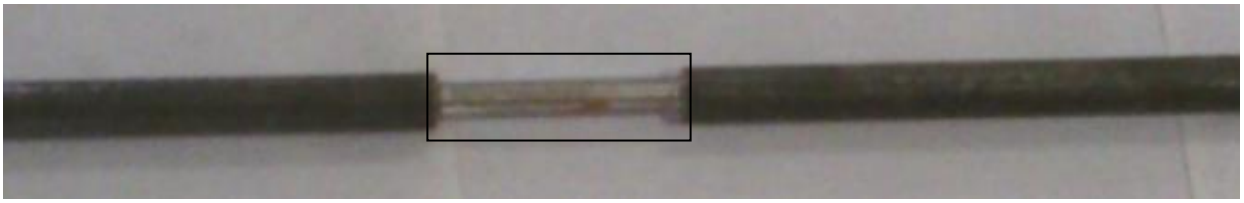

(a) Actual image

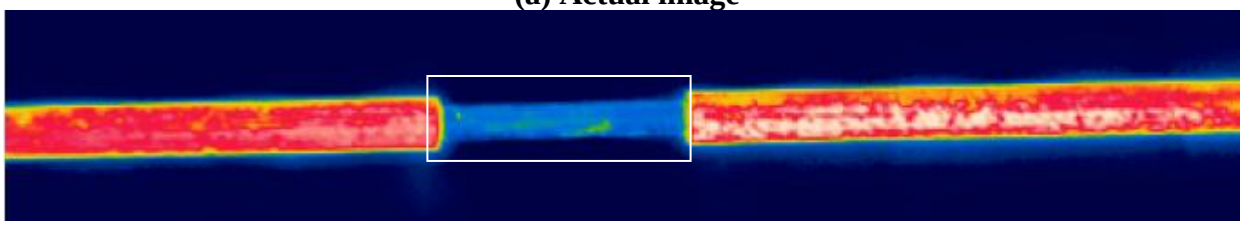

(b) Thermal image

Figure 4.24: Actual and Thermal image of a bar with circumferential reduction in diameter

c) Square Section to Circular

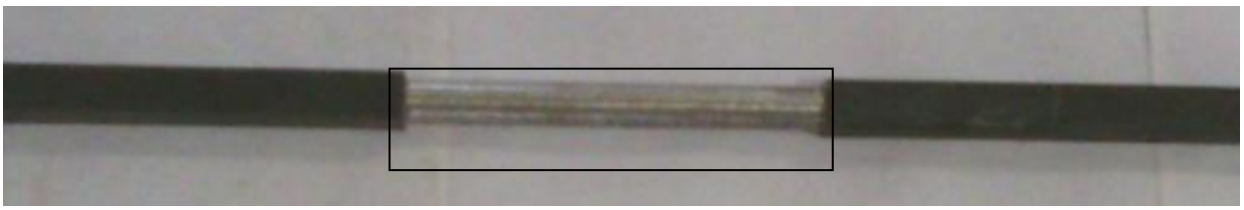

(a) Actual image

(b) Thermal image

Figure 4.25: Actual and Thermal image of a bar with square section reduced to circular.

e) Corrugations

(a) Actual image

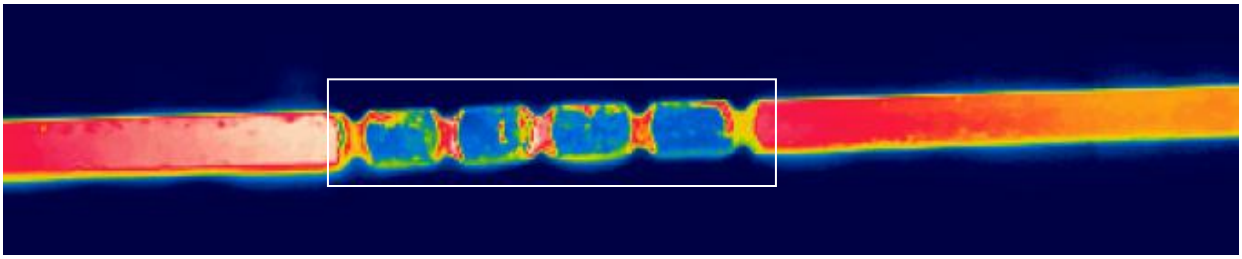

(b) Thermal image

Figure 4.26: Actual and Thermal image of a bar with corrugations

- The seeded defects simulate the damage, imperfections, irregularities, area reduction due to corrosion that can occur due to accidents during the manufacturing of the steel bars as well as during usage of structure.
- Even the shallowest defect (threads) 1mm deep **Figure 4.22 (b)** can be captured effectively in the thermal image.
- The decrease in temperature at the place of defect is due reduction in the diameter of the bar **Figure 4.22-4.26 (b)** as the steel bar with less diameter tends to cool faster. As the size of the bar changes at the place of defect its thermal conductivity changes because the homogeneity of the bar is altered with the seeded defects and hence a thermal contrast is obtained **Figure 4.22-4.26 (b)**.
- Due to uneven heating and cooling of the bar with threads **Figure 4.22 (b**) and corrugation **Figure 4.26 (b)**, the surface temperature distribution is not normal and there is retention of heat in between the defects.

4.6.2 Monitoring of the embedded bar

Two RC slab specimens embedded with steel rebar with no corrosion and accelerated corrosion were investigated for corrosion damage using IRT. Gas welding torch was used to heat the embedded bar in slab. The flames directly used at the node from where bar was exposed to the environment.

a) Healthy specimen

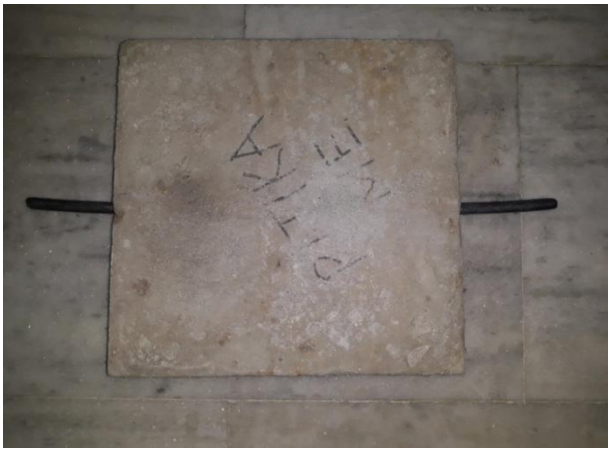

(a) Actual image

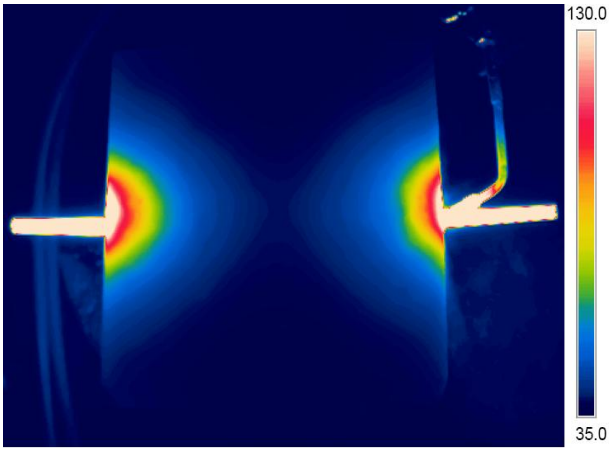

(b) Thermal image at beginning of heating

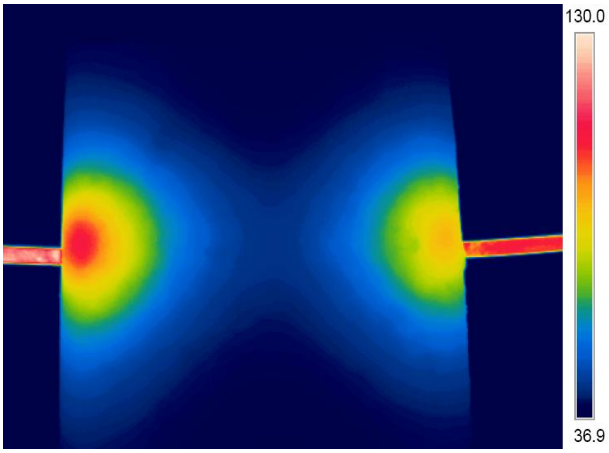

(c) Thermal image at end of heating

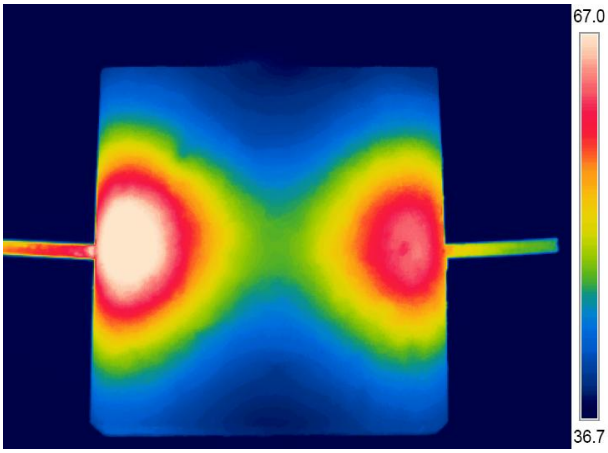

(d) Thermal image after 30 minutes during cooling

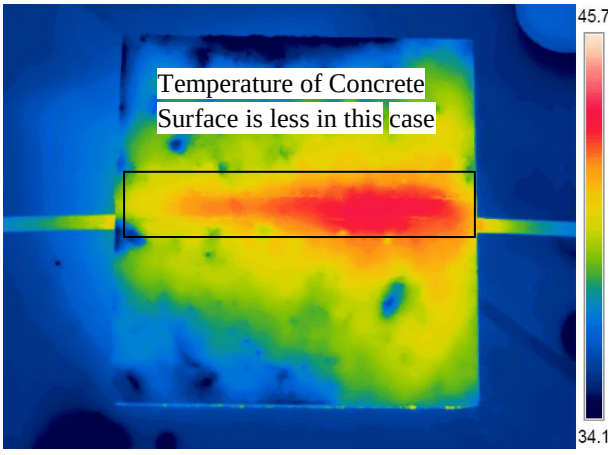

(e) Thermal image when bar is visible after 70 minutes during cooling

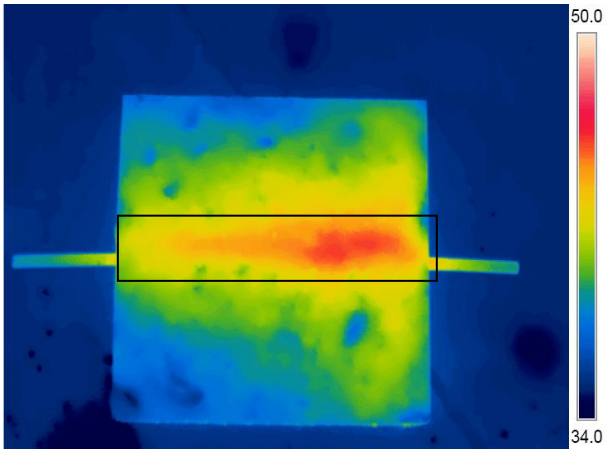

(f) Thermal image after 85 minutes during cooling

Figure 4.27: Actual and Thermal image of Healthy bar RC Slab

b) Corroded specimen

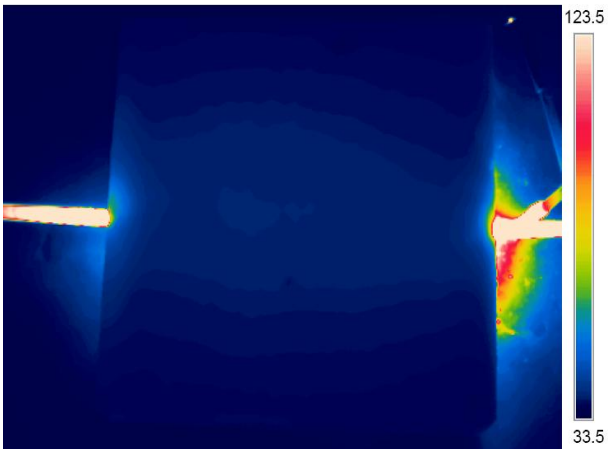

(a) Thermal image at beginning of heating

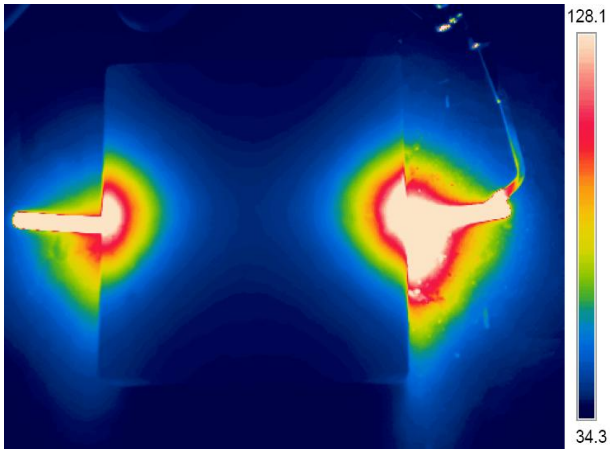

(b) Thermal image at end of heating

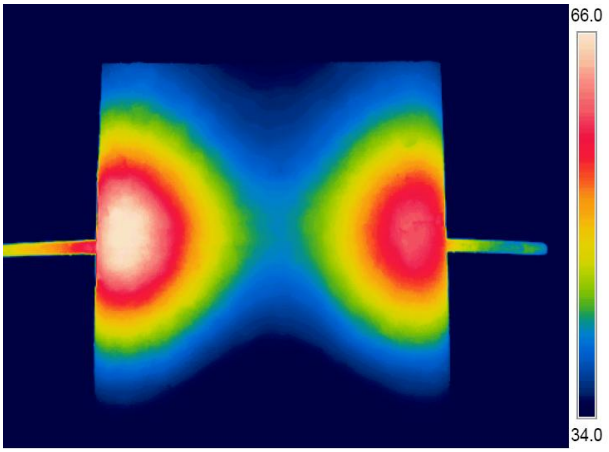

(c) Thermal image after 20 minutes during cooling

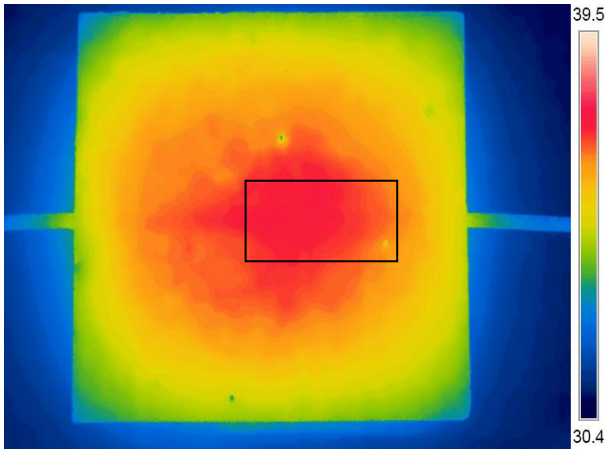

(d) Thermal image after 80 minutes during cooling

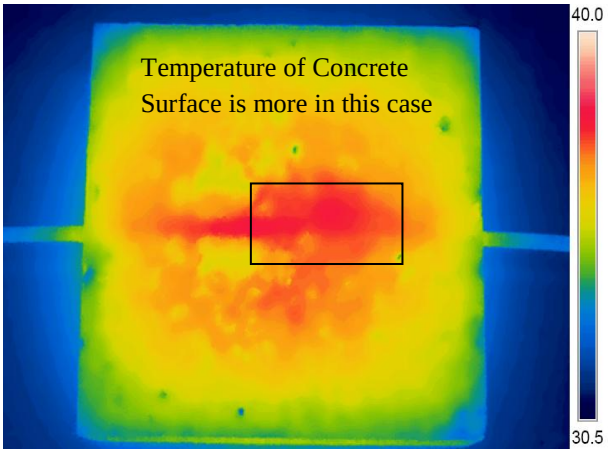

(e) Thermal image after 100 minutes

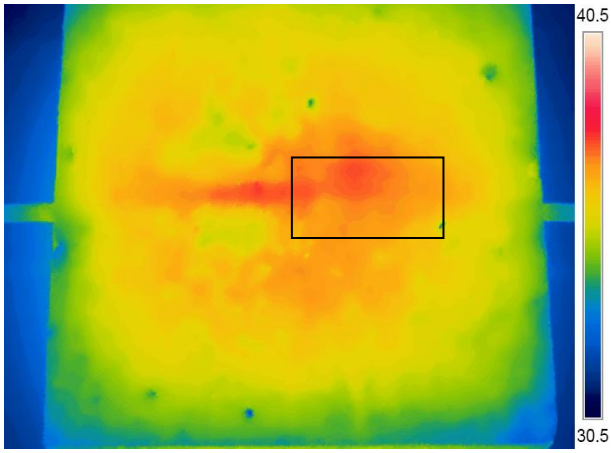

(f) Thermal image after 130 minutes at the end of cooling period.

Figure 4.28: Thermal of images of Corroded Bar RC slab

From the thermal images of the embedded bars in concrete and corrosion induced bar in concrete following observations can be made:

- From the thermal images of the embedded bar it is seen that the healthy bar is visible after 70 minutes **Figure 4.27 (c)** during the cooling whereas the corroded bar is visible after 60 minutes **Figure 4.28 (c)**.
- As corrosion occurs there is reduction in net area of steel due to which there is difference in the infrared emission on application of external thermal source.
- The infrared intensity is highest in the specimen with the corroded bar **Figure 4.28 (d) and (e)**.
- Large difference in the temperature at the termination of the heating, results in large cooling period for corroded sample but the reduced conductivity because of the generation of the air gaps between the rebar and concrete builds the thermal resistance for conduction of heat.
- The thermal image in **Figure 4.28 (e) and (f)** shows the increase in the temperature of the surrounding concrete surface due to absorption of the heat energy by corroded bar as compared to the bar with no corrosion **Figure 4.27 (e) and (f)**.
- Actual accelerated corrosion damage in rebar in concrete is picked up successfully by IRT technique and shows the capability of the thermographic technique to real time corrosion monitoring in structures.

4.7 CLOSING REMARKS

This chapter highlights the results obtained from the experiments done during the thesis work. It shows the results of concrete specimens with various defects such as cracks, debonds, voids and corrosion when detected with infrared thermographic technique.

The thermal images showed a difference in the temperature at the place of the defects and flaws. The minor cracks in concrete under compression and tension can be detected much before the actual failure at aggregate cement interface.

Defects embedded in concrete simulating voids at the known depths were detected due to the difference in the thermal properties of those defects and this difference was obtained quickly when depth at which defect is embedded is small. Also, it was able to detect known areas of debonds when concrete is strengthened with GFRP.

Corrosion in embedded reinforcing bar without damaging the surrounding concrete can also be monitored using IRT technique due to the difference in the temperature obtained at the end of heating period and difference in thermal conductivity.

CHAPTER 5

CONCLUSIONS

The application of active InfraRed Thermography to evaluate the various kinds of defects in various civil engineering applications is studied. The technique is found to be effective in observing the subsurface, surface defects effectively. Following conclusions are drawn from this experimental work:

1. **For Surface Defects**
    - The surface defect appears as the hot spot in the thermal image**)**. It is because of retention of the heat energy by these shallow defects.
    - These surface defects simulate the actual construction defects that can occur during the construction period of the structures.
    - The smallest air void can be can be captured by this method
2. **For the Mechanical Cracks and Surface Defects**
    - In this experimental work the process of generation of heat that accompanied the cracks in bricks, mortar and cement concrete under the axial compressive and tensile load was investigated. High rise in the temperature was observed in brick and cement concrete specimens along the crack but only slight change was observed in cement mortar specimens.
    - The IR thermography is able to successfully pick up initiation, progression and ultimate failures and fracture of all types of bricks (simple, frog-filled and plastered) and interlocking tiles.
    - Under the compressive load microstructure the bricks and cement mortar plays an key role in the process of propagation of crack and in generation of temperature rise. In concrete, this propagation of cracks also depends on the slip at aggregate cement interface. The location of minute cracks which is not visible in real image at this slip is captured by the InfraRed camera as they show temperature difference. Also, it was seen that compressive stress causing the fracture are concentrated near the center.
    - Under the tensile load the heat dissipation at the crack tip shows the accumulation of the tensile stresses and thermographic images suggest that these tensile stresses

causing the initiation of fracture are concentrated near the contacts. From thermal images the maximum temperature in fractured zone is recorded near the tip of crack.

3. **For Artificial Embedded Defects**
    - It is observed that under the similar conditions of heating, the maximum difference in temperature obtained on the surface of the specimen depends on the geometry of the embedded defects. The difference in the temperature is attained quickly when the depth of the defect is small and vice versa. The thermal images clearly mark the presence of the embedded defects.
    - This study highlights and investigates the capability of IRT technique to pick up defects at different depths of embedment.
    - Shallow as well as deep defects upto 70 mm i.e. middle of the cube was picked up.
    - IRT proved to be a very useful tool for detection of embedded defects upto the depth of 70mm. The defect at 70mm was weak but still detectable.
4. **For Delamination of GFRP Sheet**
    - The technique is quite effective in fast and efficient location of debond under the GFRP sheet applied to the concrete.
    - IRT can be successfully implemented not only for picking up fracture, cracking and damages in concrete, bricks, tiles, cement mortar but also debonding failure of FRP repaired or strengthened concrete structures.
    - The best InfraRed thermal images inspection depends on the method and time interval adopted for heating the specimen. The results revealed that different shapes and sizes can be evaluated with reasonable fairness depending on the thermal properties of the defect.
5. **For Detection of Defects in Rebar**
    a) **Bare Bars**
        - The seeded defects simulate the impact that can occur due to accidents during the manufacturing of the steel bars. Even the shallowest defect (threads) 1mm deep is captured easily in the thermal image.
        - The temperature distribution depends on the geometry and type of the defect and also depends on the thermal conductivity of the bar with seeded defects.

- IRT can pick up damage, imperfections, irregularities, area reduction due to corrosion in steel bars easily and hence the technique was extended to investigate the bars in concrete in healthy and corrosion damaged state.

b) Bars Embedded in Concrete

- Corrosion in bar embedded in concrete without any damage to the concrete was monitored using IRT technique. The thermal images of the healthy and corroded bar are compared. From the thermal images it was observed that temperature increases much faster in the corroded specimen indicating that the presence of corrosion in the reinforcing steel affects the infrared emission is affected by corrosion.
- Large difference in the temperature at the termination of the heating results in large cooling period for corroded sample but the reduced conductivity because of the generation of the air gaps between the rebar and concrete builds the thermal resistance for conduction of heat.
- Also, the temperature of the reinforcing steel bar affects the temperature of the surrounding concrete and concrete in case of corroded bar is warmer than the healthy bar.

Further Scope of Work

The work must be proceeded towards of increasing sensitivity of the technique for detection of smaller and deeper defects, and on to check the large specimens by combining this method with other NDT method.

- Capability of IR thermography to pick up progressive deterioration in buildings like bricks and tiles is successfully demonstrated and established. IR Thermography as a real time and in-situ NDT tool for monitoring damage and fracture growth in civil engineering materials.
- The technique can be extended to pick up degradation of FRP repaired concrete structures under actual loading condition in real time and in-situ in field.
- Capability of IRT for sensitivity of imaging of surface defects can be employed.
- This was a pilot test and further more extensive research needs to be carried out pick up initiation and progression of damage in RC structures.

CHAPTER 6

REFRENCES

1. Sultan, A.A. & Washer, G. A pixel by pixel reliability analysis of infrared thermography (IRT) for the detection of subsurface delamination. NDT & E International, 92, 177-186.
2. Li, Z., Leung, C. & Xi, Y. Structural Renovation in Concrete. Technology and Engineering. CRC Press.
3. Cheng, C.C., Cheng, T.M. & Chiang, C.H. (2008). Defect detection of concrete structures using both infrared thermography and elastic waves. Automation in Construction, 18, 87-92.
4. Usamentiaga, R., Venegas, P., Guerediaga, J., Vega, L., Molleda, J. & Bulnes, F.G. (2014). InfraRed Thermography for temperature measurement and Non-destructive testing. Sensors, 12305-12348.
5. Verma, A.K. Validation of Active Thermography technique for local paper thermal property measurement. Master of Technology, Indian Institute of Technology, Roorkee, 2008.
6. Vollmer, M. & Mollmann KP. Infrared Thermal Imaging: Fundamentals, Research and Applications, John Wiley & Sons, 2011.
7. Meola, C. Infrared Thermography Recent Advances and Future Trends, Bentham Science Publishers, Technology & Engineering, 2012.
8. Maldague, X. (2001). Theory and practice of infrared technology for non destructive testing. John-Wiley & Sons.
9. Ways to transfer thermal energy. Available at http://coolcosmos.ipac.caltech.edu/cosmic_classroom/light_lessons/thermal/transfer.html. Accessed on 25th April 2018.
10. Bolleni, NK. Environmental Effects on Subsurface Defects Detection in Concrete Structures using InfraRed Thermography. Master of Science. University of Missouri-Columbia, 2009.
11. Pastuszak, P.D. (2016). Characterization of defects in curved composite structures using active infrared thermography. IX International Conference on Computational Heat and Mass Transfer, ICCHMT 2016, 157, 325-332.
12. Thermographic Camera. Available at https://en.wikipedia.org/wiki/Thermographic_camera. Accessed on 25th April 2018.

13. Flir T540 Camera. Available at https://www.flir-direct.com/product/flir-t540-14-42-thermal-imaging-camera-with-14-degree-and-42-degree-lens. Assessed on 20th April 2018.
14. Applications of IRT. Available at https://bin95.com/infrared-thermography-applications.html. Assessed on 15th April 2018.
15. Maierhofer, Ch., Brink, A., Rollig, M. & Wiggenhauser, H. (2002). Transient thermography for structural investigation of concrete and composites near surface region. Infrared Physics and Technology, 43, 271-278.
16. Clark, M.R., McCann, D.M. & Forde, M.C. (2003). Application of infrared thermography to the non-destructive testing of concrete and masonry bridges. NDT&E International, 36, 265-275.
17. Chung, L., Paik, I.K., Cho, S.H. & Roh Y.S. (2006). Infrared thermographic Technique to measure corrosion in reinforcing bar. Key Engineering Materials, 321-323, 821-824. Trans Tech Publication, Switzerland.
18. Galietti, U., Luprano, V., Nenna, S., Spagnola, L. & Tundo, A. (2007). Non-destructive defect characterization of concrete structures reinforced by means of FRP. Infrared Physics & Technology, 49, 218-223.
19. Barreira, E. & Freitas, V.P (2007). Evaluation of building materials using infrared thermography. Construction and Building Materials, 21, 218-224.
20. Aggelis, D.G., Kardatos, E.Z., Soulioti, D.V. & Matikas, T.E. (2010). Combined use of thermography and ultrasound for characterization of subsurface cracks in concrete. Construction and Building Materials,24, 1888-897.
21. Lai, W.L., Kou, S.C., Poon, C.S., Tsang, W.F. & Lai, C.C. (2010). Characterization of the deterioration of externally bonded CFRP-concrete composites using quantitative infrared thermography. Cement & Concrete Composites, 32, 740-746.
22. Taillade, F., Quiertant, M., Benzarti, K. & Aubagnac, C. (2011). Shearography and pulsed stimulated infrared thermography applied to a nondestructive evaluation of FRP strengthening systems bonded on concrete structures. Construction and Building Materials, 25, 568-574.
23. Aggelis, D.G., Kardatos, E.Z., Strantza, M., Soulioti, D.V. & Matikas, T.E. (2011). NDT approach for characterization of subsurface cracks in concrete. Construction and Building Materials, 25, 3089-3097.

24. Beak, S., Xue, W., Feng, M.Q. & Kwon, S. (2012). Nondestructive corrosion detection in RC through integrated heat induction and IR thermography. Journal of Nondestructive Evaluation, 31, 181-190.
25. Tashan, J. & Al-Mahaidi, R. (2012). Investigation of the parameters that influence the accuracy of bond detection in CFRP bonded specimens using IR thermography. Composite Structures, 94, 519-531.
26. Al-Hadhrami, L.M., Maslehuddin, M., Shameem, M. & Ali, M.R. (2012). Assessing concrete density using infrared thermographic images. Infrared Physics & Technlogy, 55, 442-448.
27. Tashan, J. & Al-Mahaidi, R. (2012). Investigation of the parameters that influence the accuracy of bond detection in CFRP bonded specimens using IR thermography. Composite Structures, 94, 519-531.
28. Brown, J.R. & Hamilton, H.R. (2013). Quantitative infrared thermography inspection for FRP applied to concrete using single pixel analysis. Construction and Building Materials, 38, 1292-1302.
29. Tashan, J. & Al-Mahaidi, R. (2014). Detection of cracks in concrete strengthened with CFRP system using infrared thermography. Composites: Part B, 64, 116-125.
30. Tashan, J. & Al-Mahaidi, R. (2014). Bond defect detection using PTT IRT in concrete structures strengthened with different CFRP systems. Composite structures, 111, 13-19.
31. Keo, S.A., Brachelet, F., Breaban, F. & Defer, D. (2014). Steel detection in reinforced concrete wall by microwave infrared thermography, 62, 172-177.
32. Cotic, P., Kolaric, D., Bosiljkov, V.K. & Bosiljkov, V. (2015). Determination of the applicability and limits of voids and delamination detection in concrete structure using infrared thermography. NDT&E International, 74, 87-93.
33. Khan, F., Bolhassani, M., Kontsos, A., Hamid, A. & Bartoli, I. (2015). Modeling and experimental implementation of infrared thermography of concrete masonry structures. Infrared Physics & Technology, 69, 228-237.
34. Alexis, C., Frank, B., Didier, D., Emmanuel, A. & Hangseok, C. (2015). Evaluation of gluing of CFRP onto concrete structures by infrared thermography coupled with thermal impedance. Composite: Part B, 69, 350-358
35. Pieper, D., Donnell, K.M., Ghasr, M.T. & Kinzel E.C. (2017). Integration of microwave and thermographic NDT methods for corrosion detection.

36. Hiasa, S., Birgul, R. & Catbas, N. (2017). Investigation of effective utilization of infared thermography (IRT) through advanced finite element modeling. Construction and Building Materials, 150, 295-309.
37. Dabous, S.A., Yaghi, S., Alkass, S. & Moselhi, O. (2017). Concrete bridge deck condition assessment using IR thermography and Ground Penetrating Radar technologies. Automation in Construction, 811, 340-354.
38. Ghosh, D., Rahul, Roy, D., Ganguli, A., Tuli, S. & Mukherjee, A. (2017). Combination of thermal and elastic wave imaging technique for detection of subsurface defects in concrete. NDE 2017 Conference & Exhibition of the Indian Society for NDT (ISNT) [Chennai, India: 2017], 1-11
39. IS: 4031 (Part 5)-1988 METHODS OF PHYSICAL TESTS FOR HYDRAULIC CEMENT METHODS OF PHYSICAL TESTS FOR HYDRAULIC CEMENT
40. IS: 4031 (Part 3)-1988 METHODS OF PHYSICAL TESTS FOR HYDRAULIC CEMENT
41. IS: 2720 (Part 3)-1980 Determination of specific gravity of fine, medium & coarse grained soil.
42. IS: 1489 (Part 1)-1991 PORTLAND-POZZOLANACEMENTSPECIPICATION
43. IS: 383-1970 Specifications for Coarse and Fine Aggregates From Natural Source for Concrete.
44. IS: 10262-2009 concrete mix proportioning- guidelines
45. IS: 516- 1959 Methods for Tests for Strength of Concrete.
46. Gas Welding. Available at http://www.mech4study.com/2017/04/gas-welding-principle-working-equipment.html. (Accessed on 20th June 2018).